2015

Selective Synthesis and Characterization of Single-Site Hy Zeolite-supported Rhodium Complexes and their use as Catalysts for Ethylene Hydrogenation and Dimerization

Konstantin Khivantsev
University of South Carolina

SELECTIVE SYNTHESIS AND CHARACTERIZATION OF SINGLE-SITE HY ZEOLITE-SUPPORTED RHODIUM COMPLEXES AND THEIR USE AS CATALYSTS FOR ETHYLENE HYDROGENATION AND DIMERIZATION

by

Konstantin Khivantsev

Bachelor of Science
Lomonosov Moscow State University, 2009

Master of Science
Lomonosov Moscow State University, 2009

Submitted in Partial Fulfillment of the Requirements

For the Degree of Doctor of Philosophy in

Chemical Engineering

College of Engineering and Computing

University of South Carolina

2015

Accepted by:

Michael D. Amiridis, Major Professor

Oleg S. Alexeev, Committee Member

Donna A. Chen, Committee Member

Christopher T. Williams, Committee Member

John W. Weidner, Committee Member

Lacy Ford, Senior Vice Provost and Dean of Graduate Studies

DEDICATION

You know who You are. Thank you for everything. I love You.

ACKNOWLEDGEMENTS

First of all, I would like to thank my advisor Dr. Michael D. Amiridis for the opportunity to do the most unusual and interesting research I have ever done, and his continuous support and encouragement throughout the years. Thank you for everything.

Secondly, I would like to thank Dr. Oleg S. Alexeev for constantly pushing the envelope of my scientific research. It was a very unusual research project, and quite a few times I felt that I was not going to get out of it with my sanity and health intact. Yet I did.

My committee members deserve an extra special thanks: Dr. Donna A. Chen's class was one of the best I have ever taken; it was also instrumental in helping me understand the most important concepts of surface science!

Dr. Williams is one of the most optimistic people at the department, and his expertise in catalysis was very helpful on many occasions! Also, whenever I needed to use some special equipment that belongs to Dr. Williams group, I always had a green light.

Dr. Weidner is the head of the department and obviously extremely busy, yet he has always remembered to ask me about my research and encouraged me to continue and never give up!

A big and very special thanks goes to Dr. John Monnier for being an extraordinary scientist and person. You are a true inspiration! Thanks a million for everything, including your groundbreaking and inspiring research!

ABSTRACT

Single-site $Rh(CO)_2$, $Rh(C_2H_4)_2$ and $Rh(NO)_2$ complexes anchored on various dealuminated HY zeolites can be used as precursors for the selective surface mediated synthesis of well-defined site-isolated Rh(CO)(H)x complexes. DFT calculations and D_2 isotope exchange experiments provide strong evidence for the formation of a family of site isolated mononuclear rhodium carbonyl hydride complexes (including the first examples of RhH complexes with undissociated H_2 ligands): $Rh(CO)(H_2)$, $Rh(CO)(H)_2$, and Rh(CO)(H). The fraction of each individual complex formed varies significantly with the Si/Al ratio of the zeolite and the nature of the precursor used.

HY zeolite-supported mononuclear $Rh(CO)_2$ complexes are remarkably active in ethylene hydrogenation and ethylene dimerization under ambient conditions. There is strong evidence for the cooperation mechanism between mononuclear rhodium complexes and Bronsted acid sites of the zeolite support in C-C bond formation process, as well as ethane formation. Finally, it is shown that the dimerization pathway selectivity can be progressively tuned (and completely switched off) by modifying the number of Bronsted acid sites on the zeolite surface.

HY zeolite-supported mononuclear $Rh(NO)_2$ complexes can be selectively formed upon exposure of $Rh(CO)_2$/HY to the gas phase NO/He. They are structurally similar to $Rh(CO)_2$/HY with Rh(I) retaining square planar geometry and nitrosyl ligands adopting a linear configuration. $Rh(NO)_2$/HY30 is active in ethylene hydrogenation and ethylene

dimerization under ambient conditions. This is the first unprecedented example of a supported transition-metal nitrosyl complex capable of performing a catalytic reaction. Moreover, this is the first example of a site-isolated Rh complex with ligands other than ethylene or carbonyl, which can catalyze both ethylene hydrogenation and dimerization. Unlike its dicarbonyl counterpart, dinitrosyl rhodium complex has a uniquely different reactivity towards ethylene and hydrogen.

The mononuclear site-isolated nature of the Rh species on both HY-supported $Rh(CO)_2$ and $Rh(NO)_2$ is preserved after 20 hours of continuous catalysis as evidenced by FTIR data and HAADF-STEM images of the used catalyst.

The comparison of catalytic results for $Rh(CO)_2$/HY30 and $Rh(NO)_2$/HY30 is the first successful example of the precise manipulation of the ligand environment (CO and NO) around the single metal atom anchored to the solid support (on the single atom scale) and the opportunity to observe how it affects reactivity and catalytic activity, using catalytic ethylene hydrogenation and dimerization as a model reaction. This opens up a new chapter in the chemistry of supported single-site materials and demonstrates there is a pathway to truly and selectively tune the catalytic activity by changing the electron density on the metal center (as well as ligand environment).

TABLE OF CONTENTS

LIST OF TABLES

LIST OF FIGURES

CHAPTER 1. THE EFFECT OF SI/AL RATIO AND RH PRECURSOR USED ON THE SYNTHESIS OF HY ZEOLITE-SUPPORTED RHODIUM CARBONYL HYDRIDE COMPLEXES

1.1 Introduction

In the 1960s, Wilkinson and co-workers demonstrated that various molecular organometallic complexes of rhodium can catalyze liquid phase hydroformylation and hydrogenation reactions due to their ability to activate hydrogen and form metal hydride species, which are believed to be the key intermediates in these reactions [1-3]. Since this discovery, substantial research efforts have been focused on the synthesis of transition metal hydride complexes, their chemical reactivity, and catalytic applications[4.] As a result, many such complexes are used today as important homogeneous catalysts [5-9]. However, the commercial use of such catalysts is limited due to difficulties associated with their separation from the reaction products. A surface organometallic chemistry approach has been used in the past to prepare solid catalytic materials that consist of well-defined metal complexes attached to surfaces of solid supports [10-13]. Literature examples available for Ti, Zr, Hf, Ta, and W clearly demonstrate that this preparation route allows for the creation of heterogeneous analogs for free standing molecular complexes of these transition metals, in which both the molecular nature of the supported metal complexes and the reactivity of the ligands attached to the metal sites remain

preserved [12, 14-18]. Moreover, it has been shown that when SiO_2-supported complexes of these metals are exposed to H_2 at elevated temperatures, stable surface hydride complexes can be formed [15-18]. The single-site nature of hydride complexes thus formed was confirmed spectroscopically and they were found to be active for the metathesis and hydrogenolysis of alkanes, as well as for the hydrogenation and polymerization of alkenes [18-21].

Few reports related to the synthesis of supported hydride complexes of group VIII metals exist in literature. For example, Schwartz et al.[22] have reported that the exposure of SiO_2-supported $Rh(C_3H_5)_3$ complexes to H_2 at 25°C yields Si-O-$Rh(H)_2$ species with characteristic ν_{RhH} bands at 2038 and 1812 cm^{-1}. These species were found to be active for the hydrogenation of alkenes and naphthalenes at room temperature. In contrast, Foley [23] reported that the treatment of $Rh(C_3H_5)_2/SiO_2$ with H_2 at 25°C resulted in the formation of Rh nanoparticles with sizes in the 1-3 nm range. Since such Rh nanoparticles were also found to be active for the hydrogenation of alkenes [23], it remains uncertain whether the SiO_2-supported Rh hydride complexes presumably formed from the same precursor in earlier reports were actually stable under reaction conditions and therefore responsible for the hydrogenation activity observed.

More recently, SiO_2-supported rhodium phosphine hydride complexes have been prepared using $Rh(C_3H_5)_2/SiO_2$ as the starting material [24]. In this case, the treatment of $Rh(C_3H_5)_2/SiO_2$ with P^iPr_3 tris(isopropyl)phosphine yields $Rh(P^iPr_3)_2$ species on the silica surface, and subsequent exposure to H_2 at 25°C leads to the formation of stable $Rh(H)_2(P^iPr_3)_2$ complexes with characteristic $_{RhH}$ bands at 2162 and 2043 cm^{-1}. Unfortunately, no data on the catalytic properties of these complexes is available.

It has also been shown [25] that the dihydride pincer complex [IrH_2(POCOP)] reacts with the surface silanol groups of mesoporous SBA-15 silica to give the coordinatively unsaturated but stable hydridesiloxo Ir(III) species [IrH(O-SBA-15)(POCOP)]. These silica-grafted complexes were found to be active for the hydrogenation of alkenes without prior activation, indicating that such metal hydride complexes are indeed catalytically active species.

Finally, the formation of MgO-, TiO_2-, SiO_2-, and γ-Al_2O_3-supported $Rh(CO)H_x$ complexes among other Rh surface species has been postulated in several literature reports when the corresponding supported Rh samples were exposed to CO_2/H_2 mixtures at elevated temperatures [26,27]. However, such species were never formed with high yields, and their FTIR fingerprints were weak, suggesting that the inherent nonuniformity of these supports substantially affects the nature of the surface species formed. In this respect, highly crystalline supports such as zeolites provide a better alternative. For example, it has been shown that $Rh(C_2H_4)_2$(acac) and $Rh(CO)_2$(acac) complexes react with the surface of dealuminated HY zeolite to yield site-isolated and well-defined $Rh(C_2H_4)_2$ and $Rh(CO)_2$ species anchored to the zeolite framework [28-31].

More recently, the structure and reactivity of the faujasite-supported $Rh(C_2H_4)_2$ complexes have been investigated by computational methods [32]. Moreover, we have shown that $Rh(CO)_2$/HY30 samples incorporate two types of $Rh(CO)_2$ species with characteristic ν_{CO} bands at 2117/2053 (~83 %) and 2113/2048 cm^{-1} (~17 %), and our DFT calculations suggest that differences in the nature of the binding sites in the dealuminated zeolite are responsible for their formation [33]. Furthermore, carbonyl ligands in both types of the $Rh(CO)_2$ complexes can react with gas phase C_2H_4 to form

$Rh(CO)(C_2H_4)$ species. When the latter are exposed to H_2 at 25°C, well-defined $Rh(CO)(H)_x$ species are formed with a high yield [34]. These $Rh(CO)(H)_x$ species are site-isolated, mononuclear, bound to oxygen atoms of the zeolite framework (as evidenced by EXAFS), and are characterized by a set of well-defined ν_{CO} and ν_{RhH} (and/or ν_{HH}) bands in their FTIR spectra. We have also proposed that zeolite-supported $Rh(CO)(H)_x$ species thus formed have a pseudo-trigonal bipyramidal or even octahedral geometry, with several structural isomers being formed. The formation of these isomers may be responsible for the complex structure of the infrared bands in the ν_{CO} and ν_{RhH} vibration regions.

The goal of this work was to determine how the Si/Al ratio in HY zeolites affects the synthetic pathway described above, and to examine if HY zeolite-supported $Rh(CO)(H)_x$ species can be formed from zeolite-supported $Rh(C_2H_4)_2$ and $Rh(NO)_2$ complexes. We have also conducted DFT calculations that clarified the nature of the $Rh(CO)(H)_x$ surface species formed, and show that the ν_{CO} and ν_{RhH} bands experimentally observed correspond to complexes with dissociated and intact H_2 molecules attached to the zeolite framework at different locations.

1.2 Experimental Methods

1.2.1 Reagents and Materials

Dicarbonyl(acetylacetonato) rhodium (I) $Rh(CO)_2(acac)$ and diethylene(acetylacetonato) rhodium (I) $Rh(C_2H_4)_2(acac)$ (acac = $C_5H_7O_2$) (Strem, 98% purity) precursors were used as supplied. *n*-Pentane (Aldrich, 99% purity) was refluxed

under N_2 in the presence of Na/benzophenone ketyl to remove traces of moisture and deoxygenated by sparging of dry N_2 prior to use. All glassware used in preparation steps was previously dried at 120°C. H_2, He, CO, NO, and C_2H_4 (Airgas, all UHP grade) were additionally purified prior to their use by passage through oxygen/moisture traps (Agilent) capable of removing traces of O_2 and water to 15 and 25 ppb, respectively. CBV760, CBV720, and CBV600 dealuminated HY zeolites (Zeolyst International) with Si/Al atomic ratios of 30, 15, and 2.6, respectively, were calcined in O_2 at 300°C for 3 h, evacuated at 10^{-3} Torr and 300°C for 16 h, and stored in a glovebox (MBraun) filled with N_2 prior to use. The residual water and O_2 concentrations in the glovebox were kept below 0.1 ppm. For simplicity, these supports are further denoted as HY30, HY15, and HY2.6, respectively.

1.2.2 Preparation of Supported Samples

All syntheses and sample transfer procedures were performed with exclusion of air and moisture on a double-manifold Schlenk line and in a N_2-filled MBraun glovebox. Zeolite-supported samples were prepared by slurrying $Rh(CO)_2(acac)$ or $Rh(C_2H_4)_2(acac)$ precursors in appropriate amounts with the powder support in *n*-pentane under N_2 for 24 h at room temperature, followed by overnight evacuation at 25°C to remove the solvent and yield samples containing 1 wt.% Rh. The Rh weight loading was verified by inductively coupled plasma-mass spectrometry (ICP-MS) analysis (Galbraith Laboratories Inc.). The prepared samples were stored and handled in a glovebox filled with N_2 to prevent possible decomposition of supported species.

1.2.3 FTIR Spectroscopy

A Nicolet Nexus 470 spectrometer equipped with a MCT-B detector cooled by liquid nitrogen was used to collect spectra with a resolution of 2 cm^{-1}, averaging 64 scans per spectrum. Each powder sample was pressed into a self-supported wafer with a density of approximately 20 mg/cm^2 and mounted in a home-made cell connected to a gas distribution manifold. The cell design allowed for the treatment of samples at different temperatures, while various gases flowing through the cell.

1.2.4 Mass Spectrometry Measurements

Mass spectrometry (MS) measurements were used to monitor ligand exchange reactions between surface species and different gases, and to identify the products released during such reactions. In a typical experiment, approximately 100 mg of the sample was loaded into a plug-flow micro reactor in a glovebox, and the reactor was sealed to avoid air exposure. The reactor was subsequently connected to a gas distribution system equipped with mass flow controllers and an online Inficon Transpector 2 residual gas analyzer operating in a multi-ion detection mode. Before each experiment, the reactor was purged with He (100 ml/min) at 25°C and atmospheric pressure for 1 h to stabilize the baseline MS signal. When this procedure was completed, various feeds (as specified in the text) were introduced into the reactor at 25°C and a flow rate of 100 ml/min. The feed and effluent compositions were routinely monitored to detect species such as CO (m/z = 28) and NO (m/z = 30).

1.2.5 Computational Method and Models

Periodic DFT calculations were performed with the PW91 exchange-correlation functional [35] using a Vienna *ab initio* simulation package (VASP) [36,37]. Ultrasoft pseudopotentials [38, 39] were used as implemented in the VASP package. Due to the large size of the unit cell (see below), the Brillouin zone was sampled using only the Γ point [40]. The valence wave functions were expanded in a plane-wave basis with a cutoff energy of 400 eV.

The cubic unit cell of the zeolite framework was optimized for the pure silicate structure with dimensions a = b = c = 24.345 Å [41]. To simulate the structure of a highly dealuminated HY zeolite, one Si atom in the unit cell was replaced with Al. The negative charge around the Al site was compensated by the Rh^+ ion or its complexes. During the geometry optimization procedure, all the zeolite atoms and the adsorbate species were allowed to relax until the force on each atom was less than 5×10^{-4} eV/pm.

The binding energy (BE) of the CO and other adsorbates (when applicable) was determined as:

$$BE[Rh(CO)(X)^+/Zeo] = E[Rh(CO)(X)^+/Zeo] - E[Rh^+/Zeo] - E[CO] - E[X],$$

where $E[Rh(CO)(X)^+/Zeo]$ is the energy of the zeolite system together with the metal cation and adsorbed CO and X molecules in the optimized geometry, E[CO] and E[X] are the energies of the adsorbates in the gas phase, $E[Rh^+/Zeo]$ is the energy of the initial zeolite system containing a bare Rh^+ cation, and X= CO, N_2, H_2, C_2H_4, or $1/2H_2$. Consistent with this definition, negative values of BE imply a favorable interaction.

The vibrational frequencies for periodic models were obtained from a normal mode

analysis where the elements of the Hessian were approximated as finite differences of gradients, displacing each atomic center by 1.5 pm either way along each Cartesian direction. All calculated C-O and N-N vibrational frequencies were shifted by the difference of the calculated harmonic frequency of the free CO and N_2 molecules obtained with the same computational approach and the experimentally measured (anharmonic) frequency of CO and N_2 in the gas phase (i.e., 2143 and 2331 cm^{-1}, respectively) [42]:

$$\nu(C\text{-}O)^{calc} = \nu_{calculated} - \nu_{calculated}(CO\text{-}gas) + 2143$$

$$\nu(N\text{-}N)^{calc} = \nu_{calculated} - \nu_{calculated}(N_2\text{-}gas) + 2331$$

In this case, the calculated ν_{CO} and ν_{NN} frequencies are corrected for both the anharmonicity (which is 39 and 17 cm^{-1} for gas phase CO and N_2, respectively) and the systematic error of the computational method.

1.3 Results and Discussion

FTIR data reported elsewhere[33,34] for $Rh(CO)_2$/HY30 prepared from the $Rh(CO)_2$(acac) precursor indicate that the $Rh(CO)_2$ surface species initially formed in this material do not react with H_2 in the 25-300°C temperature range, as no new features were observed in the spectra. With increasing temperature, however, the intensity of the ν_{CO} bands at 2117 and 2053 cm^{-1} - assigned to zeolite-supported $Rh(CO)_2$ complexes - declines and the bands eventually disappear from the spectra at approximately 300°C, indicating the complete decarbonylation of the $Rh(CO)_2$ species under these conditions [33, 34]. This result was further confirmed by EXAFS, as no Rh−CO contributions were detected in spectra of the $Rh(CO)_2$/HY30 sample treated in H_2 at 300°C. EXAFS data

further show that the site-isolated Rh cations initially present in $Rh(CO)_2$/HY30 undergo aggregation in H_2 at elevated temperatures. For example, the first-shell Rh-Rh coordination number was found to be 4.0 at a distance of 2.67 Å after H_2 treatment at 300°C [33,34]. Since no higher Rh-Rh shells were detected in the EXAFS spectra, one can assume that small Rh_6 clusters were formed. These results clearly show that zeolite-supported $Rh(CO)_2$ complexes do not react with H_2 to form Rh carbonyl hydride species. In contrast, the thermal treatment of $Rh(CO)_2$/HY30 in H_2 facilitates decarbonylation of the surface species and subsequent aggregation of Rh.

The lack of hydrogen activation by $Rh(CO)_2$/HY30 can be understood better by examining parallel examples in solution chemistry. For example, the majority of d^8 metal hydride complexes formed in solution incorporate various phosphine, amine, alkene, and arene ligands, all of which exhibit relatively strong electron-donor properties [43]. Hence, one can conclude that the basicity of the metal site, and therefore, its ability to weaken the H-H bond via donation of the electrons into the antibonding orbital of molecular hydrogen, governs the formation of metal hydride complexes in solution. Since CO is a far stronger back-bonding ligand, the presence of two such ligands on Rh sites in the $Rh(CO)_2$/HY30 sample makes the Rh sites more electron deficient and less basic. In addition, a comparison of the ν_{CO} band positions and Rh 3d binding energies provided elsewhere[33] for zeolite-bound $Rh(CO)_2$ species and $Rh(CO)_2$(acac) molecular complexes strongly suggests that the zeolite itself acts as a macroligand for the supported $Rh(CO)_2$ species with relatively strong electron withdrawing properties. Therefore, lack of the required basicity on Rh sites could at least partially explain the inability of $Rh(CO)_2$/HY30 to participate in oxidative addition of H_2. Some literature reports also

indicate that the oxidative addition of H_2 to $Rh(CO)_2$ complexes is a thermodynamically unfavorable process due to the presence of the initial substitution step during which the strong Rh–CO bond must be broken and only a weak Rh-(η^2-H_2) bond is formed [44]. Regardless of the case, one can assume that the ligand environment of Rh sites in $Rh(CO)_2$/HY30 must be modified in order to facilitate activation of H_2 species.

1.3.1 Pathway to Zeolite-Supported $Rh(CO)(H)_x$ Complexes

To verify this hypothesis, the reactivity of carbonyl ligands in zeolite-supported $Rh(CO)_2$ complexes was examined. For this purpose, a $Rh(CO)_2$/HY30 sample prepared from the $Rh(CO)_2$(acac) precursor was exposed to C_2H_4 pulses at room temperature and atmospheric pressure, while FTIR and MS spectra were collected to monitor changes in both the surface and gas phase species formed. As we reported elsewhere [33,34], the results of these experiments provide compelling evidence that the carbonyl ligands of the $Rh(CO)_2$ surface species react with C_2H_4 under ambient conditions to yield $Rh(CO)(C_2H_4)$ complexes on the zeolite surface and CO in the gas phase. The $Rh(CO)(C_2H_4)$ complexes thus formed have characteristic infrared bands at 3094 (ν_{CH}), 3070 (ν_{CH}), 3021 (ν_{CH}), 2986 (ν_{CH}), 2053 (ν_{CO}), 1536 ($\nu_{C=C}$/ν_{CH2}), and 1438 (ν_{CH2}) cm^{-1} and are stable for an extended period of time under He flow.

The structure of these complexes was further confirmed by EXAFS. More specifically, the Rh *K* edge EXAFS data characterizing the surface species formed after exposure of $Rh(CO)_2$/HY30 to C_2H_4 show the presence of Rh–C and Rh–O* contributions from carbonyl ligands with average coordination numbers of 1.0 and 1.1 at average distances of 1.83 and 2.97 Å, respectively. In addition, it was found that the first

coordination shell of Rh also includes Rh−C and Rh-O contributions with average coordination numbers of 2.1 and 2.5 at average distances of 2.15 and 2.21 Å, respectively. Since the Rh-C distance of 2.15 Å is typical for alkenes π-bound to cationic Rh sites in molecular complexes[45], the presence of such contribution in the EXAFS spectrum of the C_2H_4-treated sample provides strong evidence for the π-bonding of C_2H_4 to the Rh sites. Finally, based on the EXAFS parameters (i.e., coordination numbers and bond distances) obtained for the surface species formed in the C_2H_4-treated $Rh(CO)_2$/HY30 sample, we can confidently conclude that approximately one CO and one C_2H_4 ligand are coordinated to each Rh atom in the surface species formed. These $Rh(CO)(C_2H_4)$ surface complexes are site-isolated (no Rh−Rh contributions were observed) and strongly bound to two oxygen atoms of the zeolite framework, as evidenced by the presence of Rh−O contributions.

In contrast to $Rh(CO)_2$/HY30, the Rh sites of $Rh(CO)(C_2H_4)$/HY30 are expected to be less electropositive since the replacement of one CO ligand by C_2H_4 brings more electron density on the Rh sites. While we cannot provide spectroscopic data to confirm this expectation, we have shown that the $Rh(CO)(C_2H_4)$/HY30 sample indeed exhibits different chemical properties with respect to H_2. For example, the treatment of $Rh(CO)(C_2H_4)$/HY30 with H_2 at 25°C for 30 min completely removes the infrared signature of the $Rh(CO)(C_2H_4)$ surface species. Changes observed in the FTIR spectra were accompanied by the appearance of C_2H_6 in a gas phase, consistent with the hydrogenation of C_2H_4 ligands under such treatment conditions. The Rh *K* edge EXAFS data reported elsewhere[34], for the $Rh(CO)(C_2H_4)$/HY30 sample treated in H_2 at 25°C show a complete absence of Rh−C contributions at a distance of 2.15 Å from π-bound

C_2H_4 ligands, confirming complete removal of the C_2H_4 ligands from the surface species. In contrast, both Rh–C and Rh–O^* contributions (originating from carbonyl ligands) with average coordination numbers of 0.9 and 1.0 at average distances of 1.84 and 2.96 Å, respectively, remain in the EXAFS spectrum[34], suggesting that one carbonyl ligand remains intact on each Rh atom in the surface species thus formed. These species are site-isolated and mononuclear in nature, as the EXAFS spectra lack any Rh–Rh contributions. Consistent with these structural data and FTIR results collected previously for the Rh(^{13}CO)(C_2H_4)/HY30 sample during H_2 exposure,[34] the spectral region shown in Fig. 1.1 is assigned with confidence to the ν_{CO} vibrations of a CO ligand in the new surface species formed from Rh(CO)(C_2H_4) after H_2 treatment.

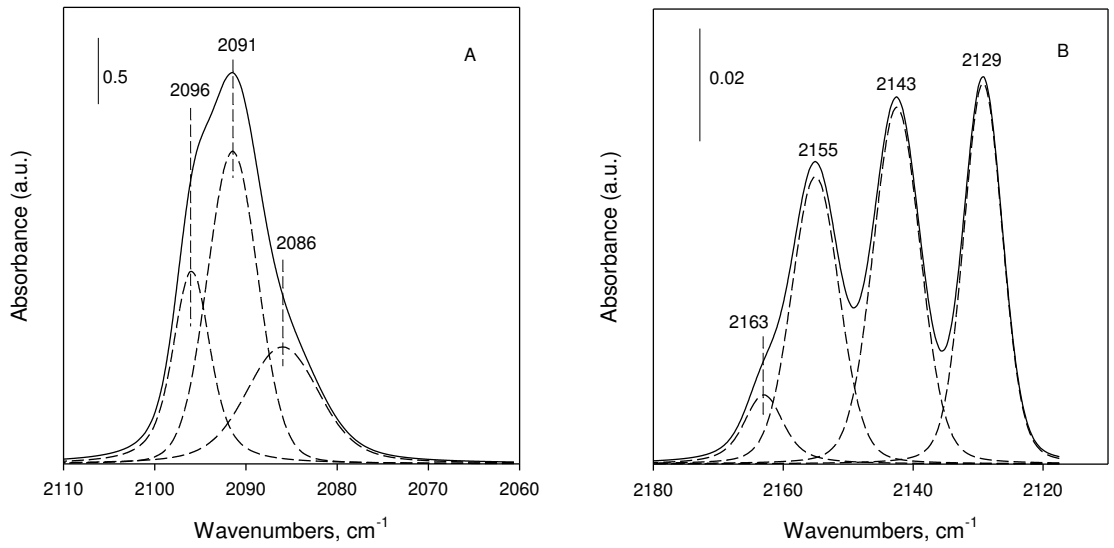

Fig. 1.1 FTIR spectrum in the ν_{CO} (A) and ν_{RhH} (B) regions of the surface species formed after the treatment of the Rh(CO)(C_2H_4)/HY30 sample with H_2 at room temperature for 30 min (solid line) and corresponding deconvolution results (dashed line).

In contrast, the spectral region shown in Fig. 1B includes weak bands, the position of which remains unchanged during CO/^{13}CO experiments. To assign this region, H_2/D_2 substitution experiments were performed. When the Rh(CO)(C_2H_4)/HY30 sample was exposed to H_2 for 30 min, purged with He, and then exposed to a pulse of D_2, weak bands located in the 2180-2120 cm^{-1} region immediately disappeared, while new bands appeared in the 1580-1480 cm^{-1} region (Fig. 1.2).

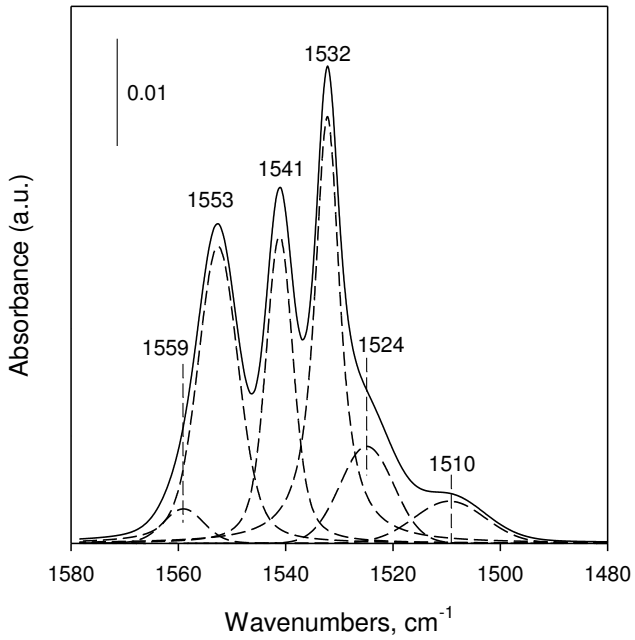

Fig. 1.2 FTIR spectrum in the ν_{RhD} region of the surface species formed after exposure of the Rh(CO)$(H)_x$/HY30 sample to D_2 (solid line) and corresponding deconvolution results (dashed line).

This result unambiguously confirms the assignment of bands in the 2180-2120 cm^{-1} region to the ν_{RhH} vibrations. Thus both CO/^{13}CO and H_2/D_2 experiments are consistent with the formation of Rh(CO)$(H)_x$ surface species upon exposure of Rh(CO)(C_2H_4)/HY30 to H_2 at room temperature.

When the structure of the $Rh(CO)(H)_x$ surface species thus formed was further probed by EXAFS, the existence of one carbonyl ligand coordinated to each Rh atom was confirmed by the presence of Rh–C and Rh–O* contributions with average coordination numbers of 0.9 and 1.0 at average distances of 1.84 and 2.96 Å, respectively. These species retain a mononuclear character (as no Rh–Rh contributions were observed) and continue to be bound to approximately two oxygen atoms of the zeolite framework, as evidenced by the presence of Rh–O contributions with an average coordination number of 2.5 at an average distance of 2.21 Å [34].

Therefore, the results described above provide solid evidence that the reactivity of zeolite-supported $Rh(CO)_2$ complexes toward H_2 can be altered by changing the ligand environment of the Rh sites, as the replacement of one CO ligand in the $Rh(CO)_2$ species by C_2H_4 opens up a direct pathway for the formation of $Rh(CO)(H)_x$ complexes. In contrast to zeolite-supported $Rh(CO)_2$ and $Rh(CO)(C_2H_4)$ complexes with relatively simple FTIR signatures, infrared spectra shown in Fig. 1.1 for the $Rh(CO)(H)_x$ species have a complex band structure. For example, deconvolution results shown in Figs. 1A and 1B (dashed lines) indicate that the ν_{CO} region of the spectrum includes three bands with maxima located at 2096, 2091, and 2086 cm^{-1}, while four bands centered at 2163, 2155, 2143, and 2129 cm^{-1} are present in the ν_{RhH} region. Furthermore, when the deconvolution procedure was also applied to the spectrum obtained during H_2/D_2 substitution experiments (Fig. 2), six bands located at 1559, 1553, 1541, 1532, 1524, and 1510 cm^{-1} were identified. The first four bands (i.e., 1559, 1553, 1541, and 1532 cm^{-1}) appear in this spectrum due to the isotopic shift of the 2163, 2155, 2143, and 2129 cm^{-1}

bands upon replacement of H by D in the $Rh(CO)(H)_x$ species, which is expected to be of approximately 600 cm^{-1} [46].

The two ν_{RhD} bands centered at 1524 and 1510 cm^{-1} are evidently new. Corresponding assignments for these bands, as well as the ν_{CO} bands, are discussed in the following sections.

1.3.2 Formation of $Rh(CO)(H)_x$ on HY Zeolites with Higher Al Content

To determine if the synthetic pathway described above is similar for HY zeolites with a higher Al content, $Rh(CO)_2$/HY15 and $Rh(CO)_2$/HY2.6 samples were prepared from the $Rh(CO)_2$(acac) precursor and thoroughly examined by FTIR, XPS, and EXAFS. Similar to the case of $Rh(CO)_2$/HY30, the results we reported elsewhere [33] indicate the formation of two types of $Rh(CO)_2$ species in these materials with characteristic ν_{CO} bands at 2117/2053 and 2110/2043 cm^{-1}, both of which are attached to the zeolite framework and have similar structural properties. However, the fraction of each species formed strongly depends on the Si/Al ratio, with more species of the latter type formed on zeolites with lower Si/Al ratios. The carbonyl ligands in both types of these zeolite-bound $Rh(CO)_2$ complexes react with gas phase C_2H_4 to form $Rh(CO)(C_2H_4)$ species. While the reaction rate was found to be significantly higher for the $Rh(CO)_2$ complex with the ν_{CO} bands at 2117/2053 cm^{-1}, exposure of these samples to C_2H_4 for approximately 30 min results in complete conversion of both types of the $Rh(CO)_2$ surface complexes into $Rh(CO)(C_2H_4)$ species. Furthermore, the $Rh(CO)(C_2H_4)$ complexes thus formed on HY15 and HY2.6 supports were found to be stable for an extended period of time under He flow, and their characteristic infrared bands were indistinguishable from those of the HY30 zeolite-supported $Rh(CO)(C_2H_4)$ species.

When the $Rh(CO)(C_2H_4)$/HY15 and $Rh(CO)(C_2H_4)$/HY2.6 samples were further exposed to H_2 at 25°C for 30 min, the infrared bands characteristic of the $Rh(CO)(C_2H_4)$ complexes disappeared, and new ν_{CO} and ν_{RhH} bands appeared in the 2110-2070 cm^{-1} and 2170-2120 cm^{-1} regions of the spectrum, respectively. The final spectra and deconvolution results characterizing H_2-treated $Rh(CO)(C_2H_4)$/HY15 and $Rh(CO)(C_2H_4)$/HY2.6 samples are shown in Figs. 1.3 and 1.4, respectively.

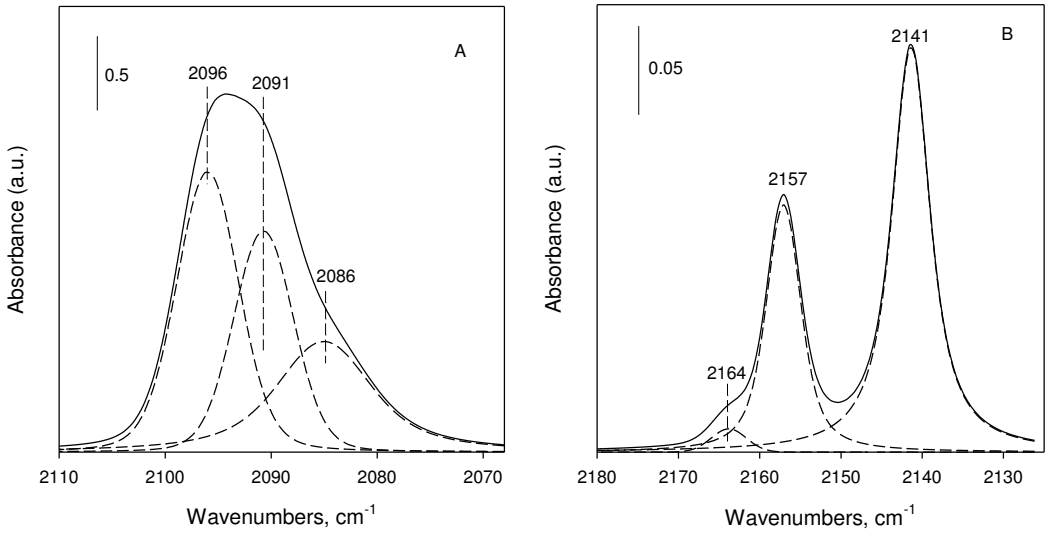

Fig. 1.3 FTIR spectrum in the ν_{CO} (A) and ν_{RhH} (B) regions of the surface species formed after the treatment of the $Rh(CO)(C_2H_4)$/HY15 sample with H_2 at room temperature for 30 min (solid line) and corresponding deconvolution results

This is quite an interesting result because it can be seen in the spectra that in all three cases (Figs. 1.1, 1.3 and 1.4) very similar combinations of the bands in the CO and Rh-H regions appear yet the relative fractions of each of those peaks on HY30, 15 and 2.6 supports are different as evidenced by the highly variable shape of those bands.

.

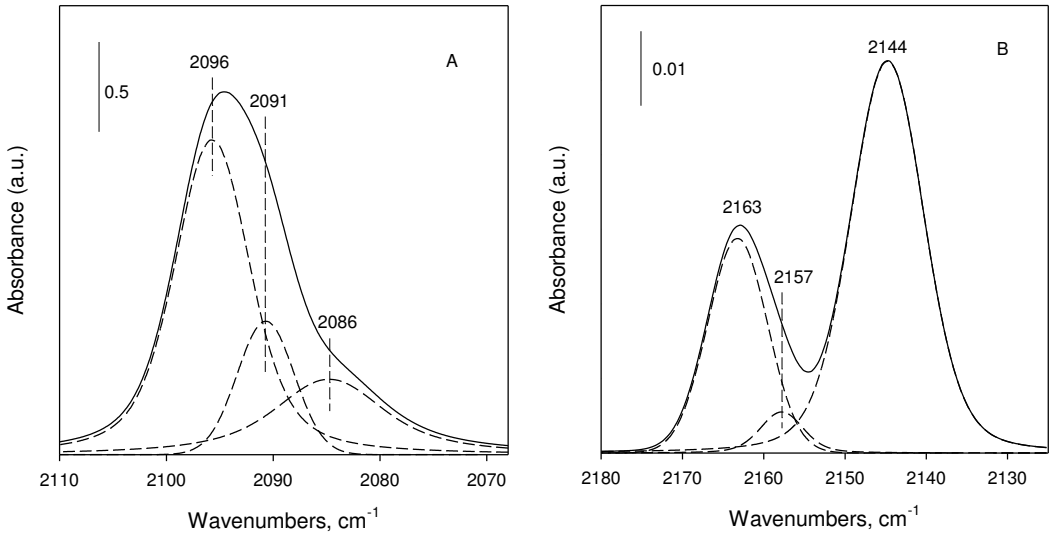

Fig. 1.4 FTIR spectrum in the ν_{CO} (A) and ν_{RhH} (B) regions of the surface species formed after the treatment of the $Rh(CO)(C_2H_4)$/HY2.6 sample with H_2 at room temperature for 30 min (solid line) and corresponding deconvolution results.

A comparison of spectra shown in Figs. 1.1, 1.3, and 1.4 indicates that the two-step synthesis of $Rh(CO)(H)_x$ surface species from zeolite-supported $Rh(CO)_2$ complexes can be achieved regardless of the Si/Al ratio of the HY zeolite, as indicated by the identical positions of the ν_{CO} and ν_{RhH} bands obtained. However, it also becomes evident that the relative intensities of these bands are affected by the Si/Al ratio of the zeolites used. For example, the FTIR results summarized in Table 1 show that the fraction of the ν_{CO} band at 2086 cm^{-1} does not change significantly as a function of the Si/Al ratio. In contrast, the contribution of the ν_{CO} band at 2096 cm^{-1} increases, while that of the ν_{CO} band at 2091 cm^{-1} decreases with an increase of the Al content of the zeolite, and the nature of these two bands clearly depends on the Si/Al ratio

.

Table 1.1 Vibrational frequencies characterizing HY zeolite-supported $Rh(CO)(H)_x$ complexes formed from different starting materials.

Starting material	Treatment	ν_{CO} bands, cm^{-1}	Relative fraction, %	ν_{RhH} bands, cm^{-1}	Relative fraction, %
$Rh(CO)_2(acac)$/HY30	C_2H_4 at 25°C followed by H_2 at 25°C	2096 2091 2086	25 47 28	2163 2155 2143 2129	7 28 34 31
$Rh(CO)_2(acac)$/HY15	C_2H_4 at 25°C followed by H_2 at 25°C	2096 2091 2086	41 31 28	2164 2157 2141	3 33 64
$Rh(CO)_2(acac)$/HY2.6	C_2H_4 at 25°C followed by H_2 at 25°C	2096 2091 2086	61 17 22	2163 2157 2144	28 4 68
$Rh(CO)_2(acac)$/HY30	NO at 25°C, followed by CO at 25°C, C_2H_4 at 25°C, and H_2 at 25°C	2096 2091 2084	37 40 23	2164 2157 2146 2141	1 34 2 63
$Rh(C_2H_4)_2(acac)$/HY30	CO at 25°C, followed by C_2H_4 at 25°C, and H_2 at 25°C	2091 2085 2079	34 56 10	2164 2159 2144 2127	13 17 66 3

When the same data are presented graphically (Fig. 1.5), it becomes evident that there is a linear correlation between the fractions of the ν_{CO} bands at 2096 and 2091 cm^{-1} and the Si/Al ratio of the zeolites used as supports. These trends further suggest that the ν_{CO} bands at 2096, 2091, and 2086 cm^{-1} belong to different surface species, however, the nature of the differences is not apparent at this point, and this issue will be addressed later in this chapter.

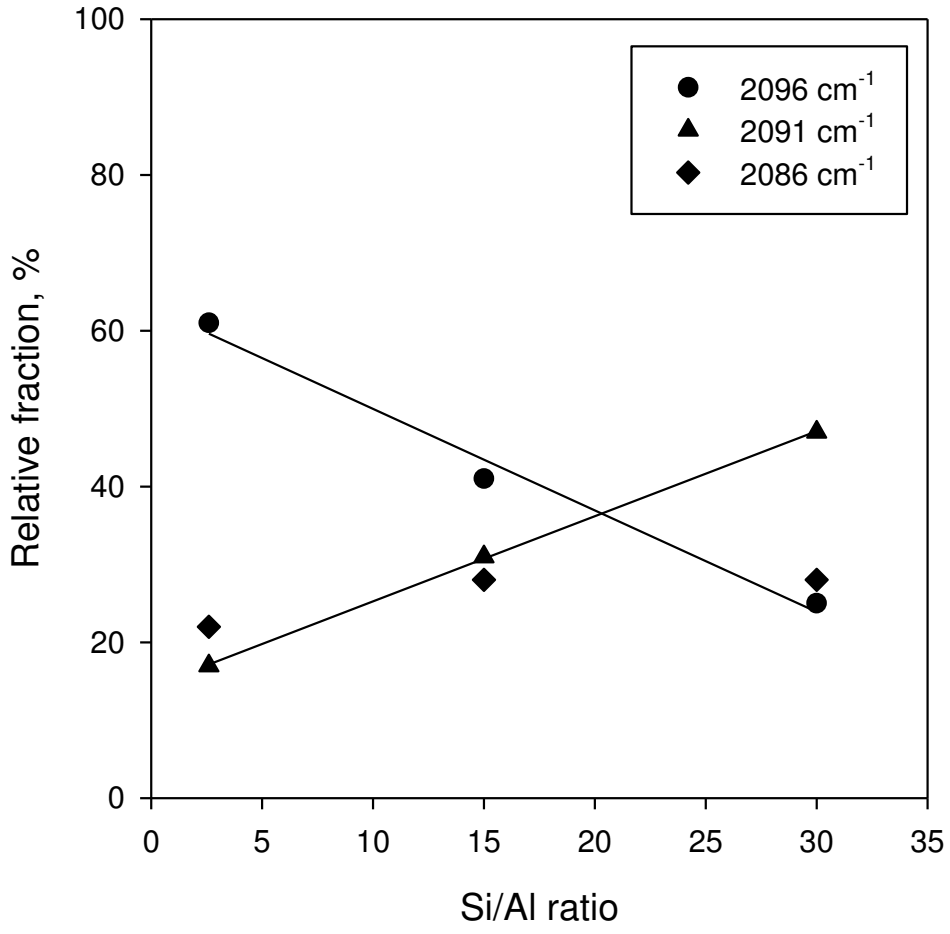

Fig. 1.5 Relative fractions of the ν_{CO} bands characterizing $Rh(CO)(H)_x$ complexes as a function of the Si/Al ratio (▲- 2091 cm^{-1}; ●- 2117 cm^{-1}, and ♦- 2086 cm^{-1}).

The results show in Table 1.1 for the ν_{RhH} region are more complex, as no obvious correlations between fractions of individual bands and Si/Al ratios can be drawn. However, apparent differences in spectra were observed depending on the zeolite nature. For example, the 2155, 2143, and 2129 cm^{-1} bands are all strong in the spectrum of the $Rh(CO)(H)_x$/HY30 sample (Fig. 1.1B), with each of them contributing approximately

30% to the overall spectrum, while the band at 2163 cm^{-1} appears as a weak shoulder and its contribution is small (approximately 7%).

The band at 2129 cm^{-1} is no longer present in the spectra of the $Rh(CO)(H)_x$/HY15 and $Rh(CO)(H)_x$/HY2.6 samples, indicating that this band is somewhat unique for the $Rh(CO)(H)_x$/HY30 material. In the case of $Rh(CO)(H)_x$/HY15 (Fig. 1.3 B), the 2157 and 2141 cm^{-1} bands are strong and their relative fractions are 33 and 64%, respectively, while the band at 2164 cm^{-1} is present only as a weak shoulder with a 3% contribution to the ν_{RhH} region. The spectrum of $Rh(CO)(H)_x$/HY2.6 also includes the ν_{RhH} bands at 2163, 2157, and 2144 cm^{-1} (Fig. 1.4 B), among which the latter band is the strongest, contributing approximately 68% to the overall spectrum. In this case, however, the band at 2157 cm^{-1} is weak with a relative fraction of approximately 4% and can be detected only by deconvolution. In contrast, the band at 2163 cm^{-1} appears to be relatively strong and its contribution to the overall spectrum is approximately 28%.

Overall, the FTIR results described above confirm the formation of $Rh(CO)(H)_x$ surface complexes on HY zeolites with different Si/Al ratios. The complex band structure of the ν_{CO} and ν_{RhH} regions observed in each case most likely indicates that a mixture of different $Rh(CO)(H)_x$ species exists on the surface of these zeolites, and that the fraction of each species formed depends to a certain degree on the Si/Al ratio. However, the nature of the differences is not immediately apparent but will be addressed later in the text.

1.3.3 Formation of $Rh(CO)(H)_x$/HY30 from $Rh(C_2H_4)_2(acac)$ Precursor

In contrast to $Rh(CO)_2$ surface complexes, HY30 zeolite-supported $Rh(C_2H_4)_2$ species formed from the $Rh(C_2H_4)_2(acac)$ precursor readily activate H_2 at room

temperature. In this case, however, quick hydrogenation of the C_2H_4 ligands accompanied by aggregation of Rh into small clusters takes place [10]. It has also been shown that the treatment of $Rh(C_2H_4)_2$/HY30 with pulses of CO yields $Rh(CO)_2$/HY30 [47]. Since the transformation of the $Rh(C_2H_4)_2$ into $Rh(CO)_2$ complexes is known to be complete and irreversible, the opportunity emerges to determine whether the $Rh(CO)(H)_x$ complexes finally formed from the $Rh(C_2H_4)_2$(acac) precursor have the same band structure in the ν_{CO} and ν_{RhH} regions as those formed from $Rh(CO)_2$(acac).

The $Rh(C_2H_4)_2$/HY30 sample prepared from the $Rh(C_2H_4)_2$(acac) precursor was exposed to CO pulses to form $Rh(CO)_2$/HY30, and then was treated with C_2H_4 to produce $Rh(CO)(C_2H_4)$/HY30. The identity of the surface species formed at each preparation step was characterized by FTIR, and since the spectra obtained were identical to those reported elsewhere[34,47], we excluded these spectra for the sake of brevity. As expected, when the $Rh(CO)(C_2H_4)$/HY30 sample thus prepared was further exposed to H_2 at 25°C for 30 min, the ν_{CO} and ν_{RhH} characteristic vibrations of the $Rh(CO)(H)_x$ complexes appeared in the 2110-2070 cm^{-1} and 2170-2120 cm^{-1} regions of the spectrum, respectively (Fig. 1.6). However, a comparison of this spectrum with that shown in Fig. 1.1 for $Rh(CO)(H)_x$/HY30 prepared from the $Rh(CO)_2$(acac) precursor reveals substantial differences between the surface species formed in each case. For example, the ν_{CO} region of the spectrum shown in Fig. 1.6A includes bands at 2091, 2085, and 2079 cm^{-1} with relative fractions of approximately 34, 56, and 10%, respectively (Table 1.1). Only two of these bands (i.e., at 2091 and 2085 cm^{-1}) are present in the spectrum of the sample prepared from the $Rh(CO)_2$(acac) precursor (Fig. 1.1A). This result is not entirely unexpected in the light of previous findings.

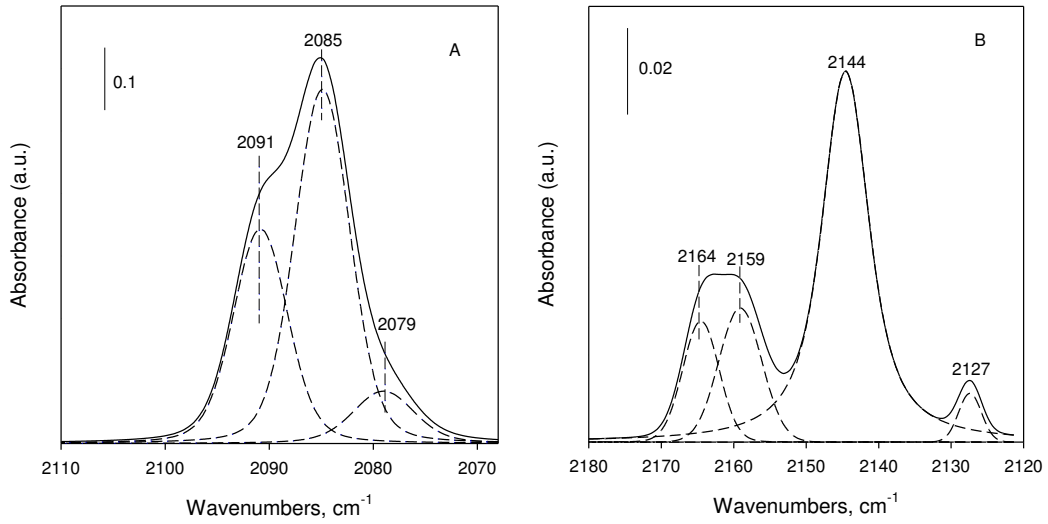

Fig. 1.6 FTIR spectrum in the ν_{CO} (A) and ν_{RhH} (B) regions of $Rh(CO)(H)_x$/HY30 formed from the $Rh(C_2H_4)_2(acac)$ precursor (solid line) and corresponding deconvolution results (dashed line).

Thus, the spectrum of $Rh(CO)(H)_x$ complexes prepared from $Rh(C_2H_4)_2(acac)$ does not include the ν_{CO} band at 2096 cm^{-1}, but it includes a new ν_{CO} band at 2079 cm^{-1}. In contrast, the ν_{RhH} region of this spectrum (Fig. 1.6B) includes four bands at positions very similar to those of the ν_{RhH} bands shown in Fig. 1.1B. In this case, however, it is obvious that the band at 2144 cm^{-1} dominates in the spectrum (66%), while the overall contribution of the remaining bands (i.e., 2164, 2159, and 2127 cm^{-1}) is approximately 34% (Table 1.1).

Therefore, the changes observed in the ν_{CO} region of $Rh(CO)(H)_x$ complexes prepared from the $Rh(C_2H_4)_2(acac)$ precursor did not affect the number of ν_{RhH} bands. However, the relative intensities of these bands are substantially different (Table 1.1). Interestingly enough, the sum of the relative fractions of the ν_{CO} bands at 2085 and 2079 cm^{-1} (approximately 66%) is exactly the same as the relative fraction of the 2144 cm^{-1} band in

the ν_{RhH} region. Likewise, the relative fraction of the ν_{CO} band at 2091 cm^{-1} (34%) corresponds to the sum of the relative fractions of the ν_{RhH} bands at 2164, 2159, and 2127 cm^{-1} (Table 1.1). While this could be coincidental, it may also indicate the formation of several types of $Rh(CO)(H)_x$ species with overlapping characteristic ν_{CO} and ν_{RhH} bands, and explain the complex band structure of these regions. The examples described so far further suggest that the contribution of each type of $Rh(CO)(H)_x$ species to the overall spectrum depends on the preparation route and the Si/Al ratio of the zeolite used.

1.3.4 Synthesis of Supported $Rh(CO)(H)_x$ from $Rh(NO)_2$ Species

Recently, we have examined the reactivity of HY30 zeolite-supported $Rh(CO)(H)_x$ species with CO, N_2, and C_2H_4 molecules [34]. To further expand the reactivity pattern for these species, the interactions of $Rh(CO)(H)_x$/HY30 with NO were monitored by FTIR, and results are shown in Figs. 1.7 and 1.8. Upon exposure of $Rh(CO)H_x$/HY30 prepared from the $Rh(CO)_2(acac)$ precursor to pulses of a 1% NO/He mixture, significant changes were observed in the infrared spectra. Difference spectra shown in Fig. 1.7 indicate that the majority of the ν_{CO} and ν_{RhH} bands originating from the $Rh(CO)(H)_x$ species disappeared after a 1 min pulse of NO at room temperature. Simultaneously, two strong ν_{CO} bands corresponding to $Rh(CO)_2$ complexes appeared at 2117 and 2052 cm^{-1} together with a weak band at 2021 cm^{-1}. Most likely, the latter band originates from coordinatively unsaturated Rh(CO) species [48], the fraction of which is evidently small. In addition, two strong ν_{NO} bands assigned to $Rh(NO)_2$ species appeared immediately at 1855 and 1779 cm^{-1} These bands are similar to the ν_{NO} bands of $Rh(NO)_2$ complexes (i.e., at 1862 and 1785 cm^{-1}) in ZSM-5 zeolites [49,50]. The ν_{CO} bands originating from $Rh(CO)_2$ and Rh(CO) surface species decreased in intensity during subsequent NO pulse.

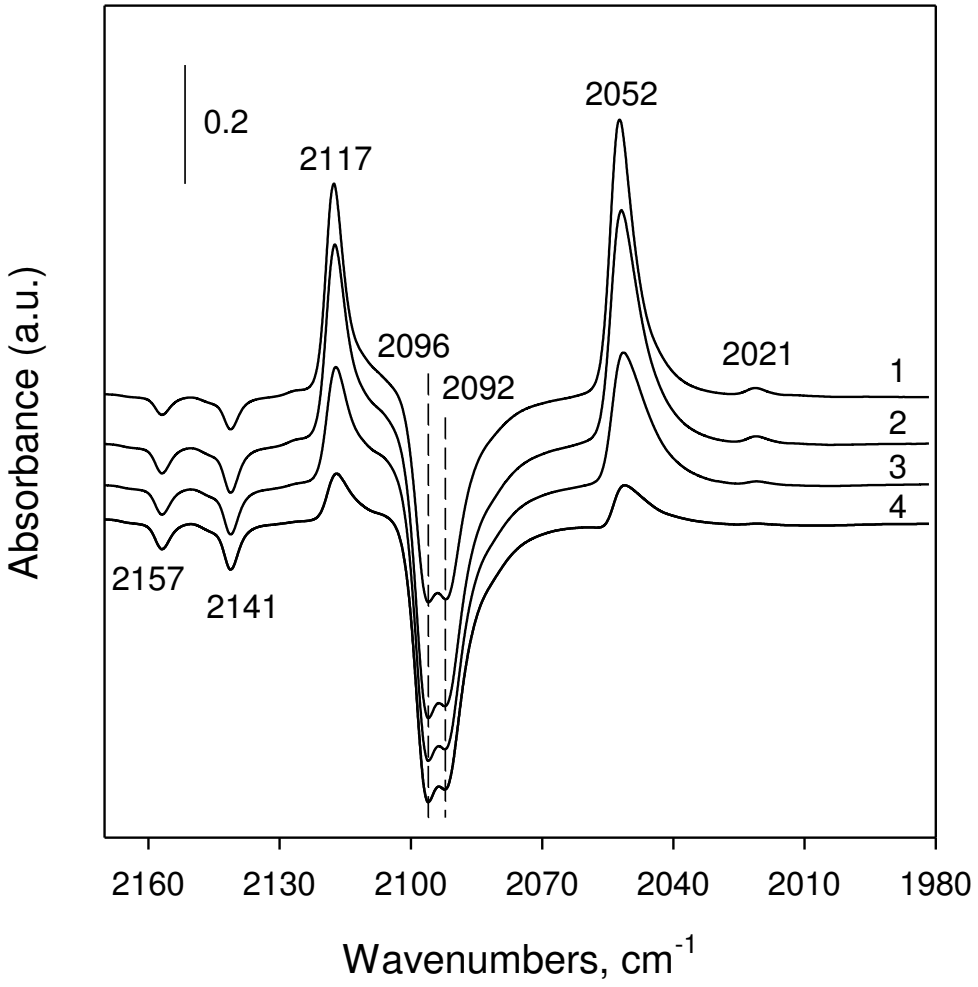

Fig. 1.7 Difference FTIR spectra illustrating changes in the ν_{RhH} and ν_{CO} regions after exposure of the $Rh(CO)(H)_x$/HY30 sample to a 1% NO/He pulse for: (1) 1 min, (2) 3 min, (3) 5 min, and (4) 11 min.

They disappeared from the spectra after approximately 11 min of NO exposure, while the development of the ν_{NO} bands assigned to the $Rh(NO)_2$ complexes was completed at that point. Unfortunately, these results do not allow us to determine whether hydride ligands in the surface species reacted with NO or were simply displaced by NO

molecules, as no new bands associated with possible reaction products were observed in other regions of the spectra (Fig. 1.8)

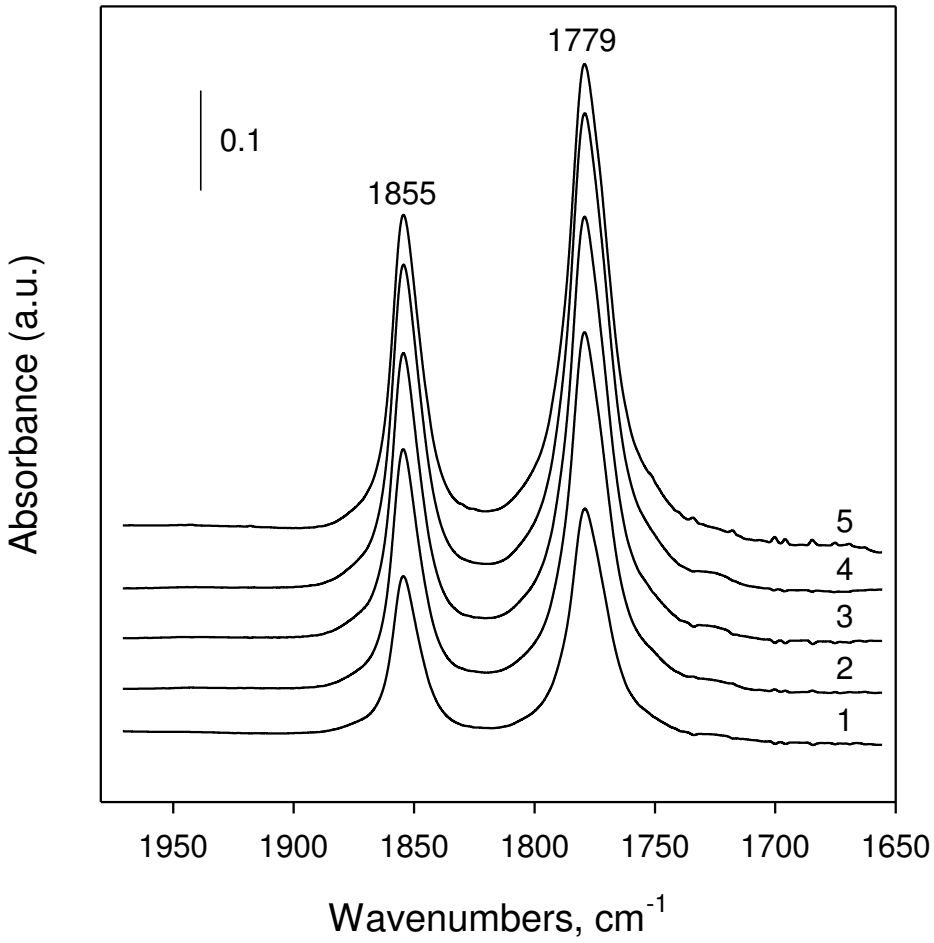

Fig. 1.8 Difference FTIR spectra of the $Rh(CO)(H)_x$/HY30 sample following exposure to a 1% NO/He pulse for: (1) 1 min, (2) 3 min, (3) 5 min, (4) 11 min, and (5) He flow 12 h.

However, they indicate that $Rh(CO)_2$ species play an intermediate role in the conversion of $Rh(CO)(H)_x$ complexes into square planar $Rh(NO)_2$ species.

The treatment of the $Rh(NO)_2$/HY30 sample thus formed with H_2 at room temperature does not change the infrared spectra obtained. Similar to the case of

$Rh(CO)_2$/HY30, this result shows that zeolite-supported $Rh(NO)_2$ complexes are not capable of activating H_2 at room temperature. While this result is predictable based on the similarities of structural and electronic properties of CO and NO as ligands, the behavior of $Rh(NO)_2$ toward C_2H_4 is completely different, since in this case treatment with C_2H_4 at room temperature does not lead to the displacement of a NO ligand. Therefore, even the subtle electronic differences of the CO and NO ligands appear to have a significant effect on the reactivity of $Rh(CO)_2$ and $Rh(NO)_2$ complexes with C_2H_4.

However, when the $Rh(NO)_2$ species were exposed to a pulse of CO, NO appeared in the gas phase, and $Rh(CO)_2$ species with characteristic ν_{CO} bands at 2117 and 2053 cm^{-1} were formed on the surface. This transformation is completely reversible, as the $Rh(NO)_2$ species are formed again after a pulse of NO is introduced. Furthermore, the $Rh(NO)_2$-$Rh(CO)_2$ transformation cycle can be repeated several times without any loss of infrared band intensities in the ν_{CO} and ν_{NO} regions, suggesting that facile substitution of CO/NO ligands indeed takes place and this process goes to completion.

Since the FTIR experiments described above indicate that the coordination environment of Rh sites in the $Rh(CO)_2$/HY30 sample can be reversibly changed, an opportunity has emerged to determine if this process affects the chemical properties of the Rh sites. Consequently, the $Rh(CO)_2$/HY30 sample prepared from the $Rh(CO)_2$(acac) precursor was exposed to several pulses of NO to yield $Rh(NO)_2$/HY30 that was further treated with several pulses of CO to reform the original $Rh(CO)_2$/HY30. The sample thus formed was exposed to C_2H_4 with the goal of determining if any changes in the reactivity of carbonyl ligands can be detected and how this affects the formation of $Rh(CO)(C_2H_4)$ surface complexes and their conversion to $Rh(CO)(H)_x$ species.

The results obtained show that the sequential CO-NO-CO replacement of ligands in HY30 zeolite-supported $Rh(CO)_2$ complexes does not substantially change the reactivity of carbonyl ligands toward C_2H_4, as the $Rh(CO)(C_2H_4)$ species are once again quickly formed upon exposure of the ligand exchanged $Rh(CO)_2$/HY30 sample to C_2H_4. Characteristic infrared bands of these species were found to be identical to those reported elsewhere [33,34] for similar complexes formed in the case of the original $Rh(CO)_2$/HY30 sample. Since our previous report shows that the $Rh(CO)(C_2H_4)$ complexes quickly react with pure H_2, the $Rh(CO)(C_2H_4)$/HY30 sample thus formed was further exposed to a 10%H_2/He mixture to generate $Rh(CO)(H)_x$ surface species at a lower rate. The FTIR spectra (Fig. 1.9 A and B) demonstrate the development of characteristic ν_{CO} and ν_{RhH} bands, respectively, of the $Rh(CO)(H)_x$ complexes as a function of time on stream. From these spectra, it is evident that the ν_{CO} band at 2096 cm^{-1} and the ν_{RhH} bands at 2157 and 2141 cm^{-1} appear first in the spectrum, and the intensity of these bands continues to increase in a similar fashion with time on stream. After approximately 30 min of exposure, new ν_{CO} bands at 2091 and 2084 cm^{-1} and ν_{RhH} bands at 2164 and 2146 cm^{-1} appear in the spectrum as shoulders, all of which become more prominent with time of exposure. After approximately 70 min on stream, no more changes were observed in the spectra, which were deconvoluted at that point to estimate the relative contribution of each band. Deconvolution results are shown in Figs. 1.10A and 1.10B for the ν_{CO} and ν_{RhH} regions, respectively, and are summarized in Table 1.1. A comparison of these results with those shown in Fig. 1.1 and Table 1.1 for the original $Rh(CO)_2$/HY30 sample indicates that the sequential CO-NO-CO replacement of ligands does not inhibit the

formation of $Rh(CO)(H)_x$ complexes, but the infrared signature of the complexes formed in this case is different.

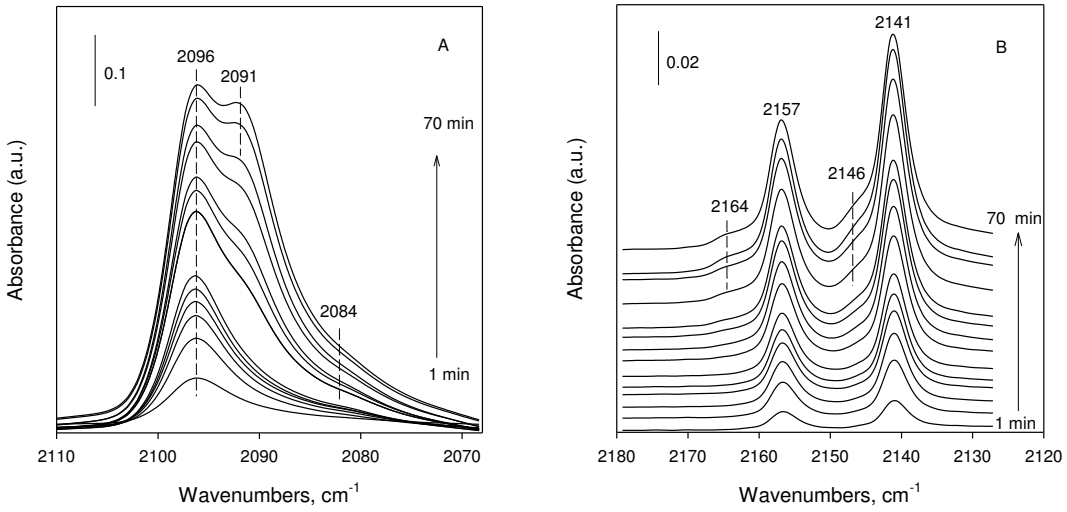

Fig. 1.9 Difference FTIR spectra illustrating the development of ν_{CO} (A) and ν_{RhH} (B) bands of $Rh(CO)(H)_x$ complexes formed on the surface of the $Rh(CO)_2$/HY30 sample that was previously subjected to a series of CO/NO/CO substitution reactions.

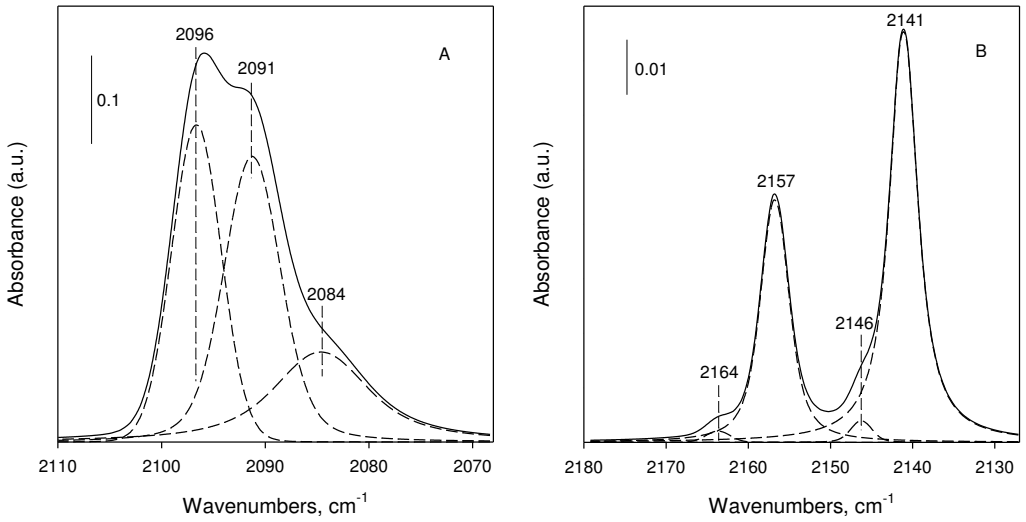

Fig. 1.10 Final FTIR spectrum (solid line) in the ν_{CO} (A) and ν_{RhH} (B) regions of the $Rh(CO)(H)_x$ species formed on the surface of the $Rh(CO)_2$/HY30 sample that was subjected to a series of CO/NO/CO substitution reactions (solid line) and corresponding deconvolution results (dashed line).

For example, the ν_{CO} region includes virtually the same set of bands, but the contribution of the ν_{CO} band at 2096 cm^{-1} to the overall spectrum is higher at the expense of the other two bands. More significant differences were observed in the ν_{RhH} region. This region continues to include the ν_{RhH} bands at 2164, 2157, and 2141 cm^{-1} with the last two contributing 97% to the overall spectrum. However, the ν_{RhH} band at 2129 cm^{-1} is no longer present in the spectrum, while a new very weak ν_{RhH} band appears as a shoulder at 2146 cm^{-1}.

3.5. Molecular Modeling of Zeolite-Supported Rh Complexes.

The results described so far show that $Rh(CO)(H)_x$ surface complexes can be formed from HY zeolite-supported $Rh(CO)_2$ species regardless of the Si/Al ratio of the zeolites used. As described above, they also can be formed on the surface of HY30 zeolite from either a $Rh(C_2H_4)_2$ precursor or a $Rh(CO)_2$ complex subjected to a sequence of CO-NO-CO substitution reactions. However, the infrared spectra of the $Rh(CO)(H)_x$ species formed in each case exhibit a complex band structure in the ν_{CO} and ν_{RhH} regions with the relative fraction of the bands present varying significantly from sample to sample. These results suggest that different types of $Rh(CO)(H)_x$ complexes may be formed with the relative concentration of each type varying from case to case. To further examine the differences between these $Rh(CO)(H)_x$ complexes and to provide better assignments for the infrared bands observed, periodic DFT calculations were performed. Such modeling takes into account the whole zeolite framework and provides information on the local structure and stability of the species formed in zeolite cavities [51,52].

As we have reported elsewhere [33], the $Rh^+(CO)_2$ complex located in the cavity of the highly dealuminated faujasite structure can be potentially attached to three different pairs

of oxygen atoms located at the AlO_4^- tetrahedron, all of which are accessible from the supercage. To distinguish between these three oxygen pairs involved in the anchoring of the Rh species, the supported $Rh(CO)_2$ complexes are denoted as $Rh(CO)_2$_a, $Rh(CO)_2$_b, and $Rh(CO)_2$_c. In the case of $Rh(CO)_2$_a complexes, the oxygen atoms are from two different but coupled four-membered rings, while in the case of $Rh(CO)_2$_b and $Rh(CO)_2$_c complexes, both oxygen atoms belong to the same four- and six-membered ring, respectively. Based on binding energies of the ligands calculated for these complexes, it was possible to conclude that the stability of supported Rh dicarbonyl species declines in the $Rh(CO)_2$_a > $Rh(CO)_2$_c > $Rh(CO)_2$_b order. The DFT calculations further predict that it is not possible to separate the $Rh(CO)_2$_a and $Rh(CO)_2$_c complexes in experimental FTIR spectra due to the overlap of their fingerprints in the ν_{CO} region. These predictions are consistent with the detection of two pairs of ν_{CO} bands in the FTIR spectra of $Rh(CO)_2$/HY samples at 2117/2053 and 2110/2043 cm^{-1}, allowing us to conclude that the $Rh(CO)_2$ complexes are attached to the zeolite framework in the $Rh(CO)_2$/HY samples in several configurations.

DFT results summarized in Table 1.2 further show that the binding energy of CO in faujasite-supported monocarbonyl $Rh^+(CO)$_a,b,c species varies between -255 and -221 kJ/mol, suggesting that the stability of these species also follows the Rh(CO)_a > Rh(CO)_c > Rh(CO)_b pattern. In this case, however, binding energy values are only slightly lower than the average binding energy per one CO molecule in the corresponding dicarbonyl complexes (i.e., from -257 to -237 kJ/mol), but are in agreement with earlier results for Rh^+ complexes in mordenite [53]. This finding is not surprising since the $Rh^+(CO)_2$ complex belongs to the special type of the supported bi-ligand species,

assigned by Hadjiivanov et al. [49,54,55] to the complex-specific dicarbonyls, as their formation is determined by the electronic properties of the metal cation but not by its coordination unsaturation on the specific support.

Table 1.2 Calculated binding energies and vibrational frequencies of faujasite-supported rhodium complexes.

Complex	BE	ν(C-O)^{calc} (cm^{-1})	ν(N-N)^{calc} (cm^{-1})	ν(C-O)^{exp} (cm^{-1})	ν(N-N)^{exp} (cm^{-1})	Δ^{e}_{CO}	Δ^{e}_{NN}	ν(Rh-H)^{calc} (cm^{-1})	Int.^{calc}, km/mol	ν(Rh-H)^{exp} (cm^{-1})	$\Delta^{e,f}$	ν(Rh-D)^{calc} (cm^{-1})	ν(Rh-D)^{exp} (cm^{-1})	Δ^{e}
Rh(CO)_a	-255	2028		2021		7								
Rh(CO)_b	-221	2031		2021		10								
Rh(CO)_c	-231	2031		2021		10								
Rh(CO)(H_2)_a[a]	-405	2071		2079 (or 2086)		8 -15		2157[b]	30	2157	0	1554	1553	1
Rh(CO)(H_2)_b[a]	-358	2074						2242[b]	7					
Rh(CO)(H_2)_c[a]	-370	2083		2086		-3		2168[b]	27	2164	4	1562	1564	-2
Rh(CO)$(H)_2$_a[c]	-402	2105		2096		9		2143	39	2143	0	1544	1541	3
Rh(CO)$(H)_2$_b[c]	-380	2097		2091		6		2166	38	2164	2	1560	1559	1
Rh(CO)$(H)_2$_c[c]	-382	2097		2091		6		2132	42	2129	4	1536	1532	4
Rh(CO)(H)_a	-321[d]	2088		2086		2		2097	90			1510	1510	0
Rh(CO)(H)_b	-302[d]	2087		2086		1		2107	84			1518	1524	-6
Rh(CO)(H)_c	-309[d]	2090		2086		4		2096	82			1510	1510	0
Rh(CO)(N_2)_a	-395	2070	2208	2062	2251	8	-43							
Rh(CO)(C_2H_4)_a	-466	2051		2053		-2								

Consistent with the previous reports [48], the calculated ν_{CO} frequencies in the modeled $Rh^+(CO)$_a,b,c monocarbonyl complexes fall in the 2031-2028 cm^{-1} range, and thus, should appear in experimental spectra at substantially lower frequencies than both ν_{CO} stretching modes of the $Rh(CO)_2$ complexes. Based on this prediction, the ν_{CO} band at 2021 cm^{-1} observed in the spectra of Fig. 1.7 most likely originates from $Rh^+(CO)$ species, as its position reasonably agrees with the range of calculated values.

The addition of hydrogen ligands to faujasite-supported $Rh^+(CO)$ species signifies the formation of Rh carbonyl hydride complexes. Therefore, we modelled six such complexes among which the $Rh(CO)(H)_2$_a, $Rh(CO)(H)_2$_b, and $Rh(CO)(H)_2$_c surface

species incorporate dissociated H_2 as a ligand, while the Rh(CO)(H_2)_a, Rh(CO)(H_2)_b, and Rh(CO)(H_2)_c surface species include molecular H_2 with elongated but not broken H−H bond as a ligand. Optimized structures of all these species are shown in Fig. 1.11, and selected structural parameters of all complexes are summarized in Table 1.3.

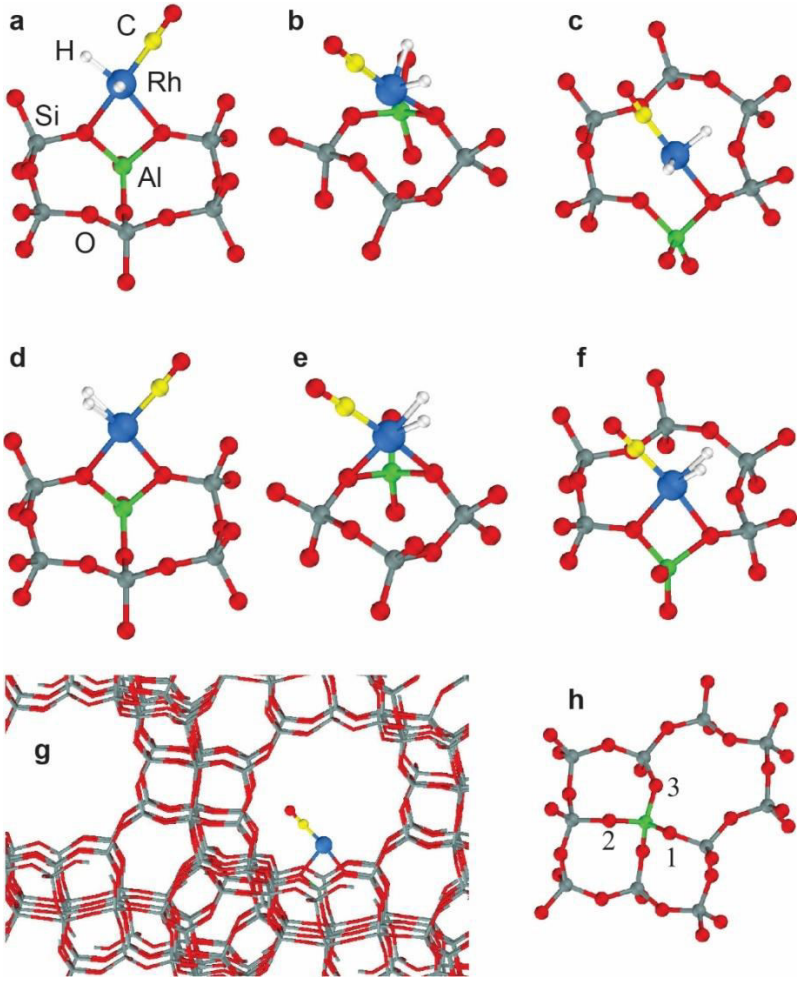

Fig. 1.11. Optimized local structures of faujasite-supported (a) Rh(CO)$(H)_2$_a, (b) Rh(CO)$(H)_2$_b, (c) Rh(CO)$(H)_2$_c, (d) Rh(CO)(H_2)_a, (e) Rh(CO)(H_2)_b, and (f) Rh(CO)(H_2)_c complexes; (g) Location of the complexes in the cavity of the faujasite structure represented by Rh^+(CO) for simplicity; (h) Notation of different O atoms around the Al center. In the complexes "a", "b" and "c", the Rh^+ cation is coordinated to zeolite O atoms denoted as shown in the panel h: "a" - 1 and 2; "b" - 2 and 3; "a", "c" - and 3. Color coding: Si – gray, O – red, Al – green, Rh – light blue, C – yellow.

Table 1.3 Selected structural data for faujasite-supported Rh complexes.

Complex	O-O[a] (pm)	Rh-C (pm)	Rh-H (pm)	Rh-O (pm)	C-O (pm)	H-H (pm)	OAlO degrees	ORhO degrees	CRhC degrees
Rh(CO)_a	262	181		211, 217	116.4		93.7	75.4	
Rh(CO)_b	265	181		216, 219	116.4		95.4	74.8	
Rh(CO)_c	260	181		215, 216	116.4		93.5	74.3	
$Rh(CO)(H_2)$_a	258	183	159, 159	212, 215	116.0	108	91.8	74.5	
$Rh(CO)(H_2)$_b	259	182	162, 162	215, 220	115.9	99	92.3	73.2	
$Rh(CO)(H_2)$_c	259	182	159, 160	214, 218	115.8	105	92.7	73.6	
$Rh(CO)(H)_2$_a	261	181	152, 154	211[b], 224[c]	115.7	191	93.6	73.8	86.1[d]
$Rh(CO)(H)_2$_b	266	182	153, 154	213[b], 243[c]	115.6	191	96.7	71.1	81.3[d]
$Rh(CO)(H)_2$_c	261	182	152, 155	214[b], 228[c]	115.7	197	94.6	72.3	84.3[d]
Rh(CO)(H)_a	261	184	155	212[b], 225[c]	115.6		93.6	73.3	85.2[d]
Rh(CO)(H)_b	266	184	155	212[b], 241[c]	115.6		96.7	71.6	80.2[d]
Rh(CO)(H)_c	262	184	155	214[b], 229[c]	115.7		94.8	72.3	83.3[d]
$Rh(CO)(N_2)$_a	260	183, 190[e]		209[f], 214[b]	115.8; 112.5[g]		92.3	75.7	88.1[d]
$Rh(CO)(C_2H_4)$_a	263	180, 213[h]		217, 218	116.3		94.6	74.6	

A comparison of binding energies reported in Table 2 for these two sets of complexes once again shows that the type "a" species in each set are the most stable ones. Interestingly, the $Rh(CO)(H_2)$_a and $Rh(CO)(H)_2$_a complexes are nearly isoenergetic with binding energy values of -405 and -402 kJ/mol, respectively. When the type "b" and "c" species are compared in these two sets, it becomes evident that the complexes incorporating dissociated H_2 as a ligand are more stable (i.e., by 22 and 12 kJ/mol, respectively) than the corresponding complexes with undissociated H_2.

Computational results further show that the $Rh(CO)(H)_2$_a, $Rh(CO)(H)_2$_b, and $Rh(CO)(H)_2$_c complexes with dissociated H_2 have one C−O vibrational frequency at 2105, 2097, and 2097 cm^{-1}, respectively (Table 1.2). Since these calculated frequencies are only 6-9 cm^{-1} higher than the ν_{CO} bands experimentally observed in our spectra at 2096 and 2091 cm^{-1}, we can assign the latter two ν_{CO} bands with confidence to the $Rh(CO)(H)_2$ species. In addition, the $Rh(CO)(H)_2$_a,b,c complexes also have asymmetric and symmetric Rh−H vibrations in the 2132-2166 cm^{-1} and 2200-2228 cm^{-1} regions, respectively. Since the intensity of the symmetric ν_{RhH} vibration is close to zero in all complexes examined, these bands cannot be observed experimentally and are therefore omitted from Table 2 for brevity.

In contrast, asymmetric ν_{RhH} vibrations predicted for $Rh(CO)(H)_2$_a, $Rh(CO)(H)_2$_b, and $Rh(CO)(H)_2$_c complexes at 2143, 2166, and 2132 cm^{-1}, respectively, are notably more intense (~40 km/mol) and should be visible in the experimental spectra. Based on these computational results, we can further conclude that the ν_{RhH} bands experimentally observed in FTIR spectra of $Rh(CO)(H)_x$/HY samples at 2164, 2143, and 2129 cm^{-1} clearly originate from $Rh(CO)(H)_2$ surface species differently attached to the zeolite

framework, as the difference in positions of experimental and calculated bands does not exceed 4 cm^{-1} in this case. Comparison of infrared bands calculated for $Rh(CO)(D)_2$_a, $Rh(CO)(D)_2$_b, and $Rh(CO)(D)_2$_c complexes (i.e., 1544, 1560, and 1536 cm^{-1}, respectively) with those experimentally observed in Fig. 2 at 1541, 1559, and 1532 cm^{-1} provides additional evidence for the formation of $Rh(CO)(H)_2$ surface species, strongly reinforcing our previous conclusion. Furthermore, the calculated intensities of the ν_{CO} bands assigned to $Rh(CO)(H)_2$ complexes were found to be more than one order of magnitude higher (i.e., 516-713 km/mol) than those of ν_{RhH} vibrations, which is also in agreement with the difference in intensity of the ν_{CO} and ν_{RhH} bands observed in experimental spectra.

The $Rh(CO)(H_2)$_a, $Rh(CO)(H_2)$_b, and $Rh(CO)(H_2)$_c complexes with undissociated H_2 are expected to have three vibrational frequencies (i.e., C−O, H−H, and Rh−(H_2)) related to the ligands. Since the stability of the $Rh(CO)(H_2)$_b complex is significantly lower (i.e., by 47 kJ/mol) than that of the most stable $Rh(CO)(H_2)$_a structure, the former species are omitted from the following discussion. Calculation results summarized in Table 2 suggest that $Rh(CO)(H_2)$_a and $Rh(CO)(H_2)$_c complexes have the ν_{CO} vibrational bands at 2071 and 2083 cm^{-1}, respectively. In fact, the ν_{CO} band experimentally observed at 2086 cm^{-1} in the FTIR spectra of all samples examined provides a close match for the calculated ν_{CO} frequency of $Rh(CO)(H_2)$_c species, suggesting that such complexes are likely formed on the surface of all dealuminated zeolites. While the calculated ν_{CO} vibration of the most stable $Rh(CO)(H_2)$_a complex (i.e., 2071 cm^{-1}) is 15 cm^{-1} lower than the lowest ν_{CO} band position (i.e., 2086 cm^{-1}) observed in the experimental spectra shown in Figs. 1.1A, 1.3A, and 1.4A, there is a

possibility that it may be contributing to the latter band. The calculated frequency of such species is closer to the experimental spectrum of the $Rh(CO)(H)_x$/HY30 sample prepared from the $Rh(C_2H_4)_2(acac)$ precursor, as evidenced by the ν_{CO} band at 2079 cm^{-1} (Fig. 6A) that provides a close match (within 8 cm^{-1}) to the calculated ν_{CO} frequency of the $Rh(CO)(H_2)$_a species.

The Rh−(H_2) vibration of $Rh(CO)(H_2)$ is expected to appear in the 2093-1995 cm^{-1} region with essentially zero intensity, and therefore cannot be observed in experimental FTIR spectra. In contrast, the ν_{HH} vibrations of $Rh(CO)(H_2)$_a and $Rh(CO)(H_2)$_c complexes are expected to appear at 2157 and 2168 cm^{-1}, respectively (Table 1.2), and this prediction corroborates well (within 4 cm^{-1}) with two of the experimentally observed Rh−H (H−H) vibrational frequencies at approximately 2164 and 2156 cm^{-1}. Since fingerprints of both $Rh(CO)(H_2)$_a and $Rh(CO)(H_2)$_c complexes are clearly evident in this region for all samples examined (Table 1), we can further suggest that the ν_{CO} band experimentally observed at 2086 cm^{-1} could also be assigned to the $Rh(CO)(H_2)$_a species, although the difference between experimental and calculated frequencies is relatively large (i.e., 15 cm^{-1}).

In addition, the data of Table 2 also show that Rh(CO)(H)_a, Rh(CO)(H)_b, and Rh(CO)(H)_c surface complexes with one H atom as a ligand and the optimized structures shown in Fig. 1.12 have binding energies of the ligands varying from -321 to -302 kJ/mol with respect to CO and $1/2H_2$ in the gas phase. Once again, Rh(CO)(H)_a complexes appeared to be the most stable in this set. Calculated ν_{CO} frequencies for these three complexes are 2088, 2087, and 2090 cm^{-1}, respectively. Since the split between

these three bands is small (i.e., 1-3 cm^{-1}), they are expected to overlap in experimental spectra, complicating the identification of the specific species formed.

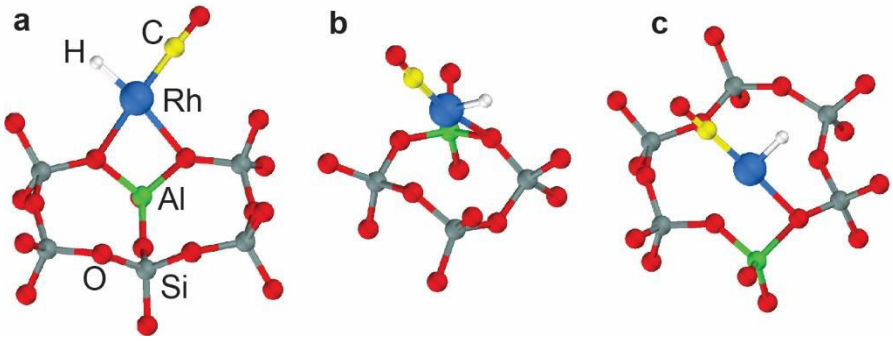

Fig. 1.12 Optimized local structures of faujasite-supported (a) Rh(CO)(H)_a, (b) Rh(CO)(H)_b, and (c) Rh(CO)(H)_c complexes. Color coding: Si – yellow, O – red, Al – dark blue, Rh – silver, C – brown.

However, all these calculated frequencies corroborate well (within 4 cm^{-1}) with the experimentally observed ν_{CO} band at 2086 cm^{-1}, suggesting that the latter band is in fact a composition band that most likely originates from both Rh(CO)(H) and Rh(CO)(H_2) complexes. Corresponding ν_{RhH} vibrations for Rh(CO)(H) complexes are expected to appear at 2097, 2107, and 2096 cm^{-1} (Table 1.2) but cannot be visualized in experimental spectra due to the overlap with significantly more intense ν_{CO} bands originating from Rh(CO)(H), Rh(CO)$(H)_2$, and Rh(CO)(H_2) complexes that appear in the 2105-2071 cm^{-1} region. However, if we consider Rh(CO)(D) instead of Rh(CO)(H) complexes, the former species have characteristic ν_{RhD} vibrations in the 1518-1510 cm^{-1} region, which is free of any ν_{CO} bands (Table 1.2). Consistent with this prediction, the spectrum of Rh(CO)$(H)_x$/HY30 exposed to D_2 pulses includes two ν_{RhD} bands at 1524 and 1510 cm^{-1}

(Fig. 1.2) both of which corroborate reasonably well with calculated ν_{RhD} frequencies, indicating that various Rh(CO)(H) species are also formed on the surface of this material.

Finally, as the hydride ligands in $Rh(CO)(H)_x$ surface complexes can be replaced by N_2 to form $Rh(CO)(N_2)$ species with an end-on N_2 coordination[34] and since $Rh(CO)(C_2H_4)$ surface complexes are precursors for rhodium carbonyl hydride species, the most stable $Rh(CO)(N_2)$_a and $Rh(CO)(C_2H_4)$_a species were also modeled to make the series of surface species more complete.

The $Rh(CO)(N_2)$_a complex is iso-structural to the most stable $Rh(CO)_2$_a complex. The binding energy of the two ligands is -395 kJ/mol, which is 119 kJ/mol lower than the binding energy of the two CO ligands in $Rh(CO)_2$_a due to significantly weaker adsorption of N_2 on the Rh^+ site (Table 1.2). Using the monocarbonyl complex Rh(CO)_a as a reference, one can calculate that the binding energy of N_2 in the mixed $Rh(CO)(N_2)$_a complex is only -140 kJ/mol. Calculated ν_{CO} and ν_{NN} frequencies of $Rh(CO)(N_2)$_a are 2070 and 2208 cm^{-1}, respectively. While the former band corroborates quite reasonably (within 8 cm^{-1}) with the ν_{CO} vibration experimentally observed at 2062 cm^{-1} for such complexes, the position of the latter band is by 43 cm^{-1} lower as compared to the ν_{NN} vibration (i.e., 2251 cm^{-1}) observed experimentally. Most likely, additional corrections should be applied to the reference ν_{NN} frequency to minimize the discrepancy in calculated and experimental values observed for this band [56].

The results obtained for the $Rh(CO)(C_2H_4)$_a complex indicate that the binding energy of the CO and ethylene ligands is -466 kJ/mol (Table 1.2). Once again, using the monocarbonyl complex Rh(CO)_a as a reference, one can estimate that the binding energy of C_2H_4 in the mixed $Rh(CO)(C_2H_4)$_a complex is -211 kJ/mol, which is higher

than the binding energy of N_2 by 71 kJ/mol, but lower than the binding energy of CO by 44 kJ/mol. Similar to the majority of other complexes described above, the calculated ν_{CO} vibrational frequency of $Rh(CO)(C_2H_4)$_a is 2051 cm^{-1}, which is in good agreement with the experimental value of 2053 cm^{-1} reported elsewhere [34].

1.3.6 Combination of Experimental and Modeling Results

The combination of experimental and DFT calculation results described above provides strong evidence for the formation of $Rh(CO)(H_2)$, $Rh(CO)(H)_2$, and Rh(CO)(H) complexes on the surface of dealuminated HY zeolites. Since three different pairs of oxygen atoms in the zeolite framework are capable of accommodating each of these species, nine individual complexes attached differently to the zeolite framework and characterized by a specific set of infrared bands in the ν_{CO} and ν_{RhH} regions coexist on the surface. The overlap of the infrared bands of these complexes further explains the complex band structure observed in the ν_{CO} and ν_{RhH} regions of experimental spectra. Unfortunately, it is not possible to identify all nine specific complexes in the ν_{CO} region of experimental spectra either because the difference in calculated ν_{CO} frequencies (even for the same type of species) is at or below the spectral resolution, or because the ν_{CO} bands originating from different type complexes have positions which are too close to be resolved. Three bands experimentally observed in the ν_{CO} region are evidently combination bands that represent all nine carbonyl hydride complexes formed, and only tentative assignments for them can be suggested. The $Rh(CO)(H)_2$ complexes with dissociated hydrogen are primarily responsible for the ν_{CO} band at 2096 cm^{-1} and may contribute to the 2091 cm^{-1} band, while the $Rh(CO)(H_2)$ species with undissociated hydrogen are mainly responsible for the ν_{CO} band at 2086 cm^{-1}. The Rh(CO)(H)

complexes with one H atom as a ligand partially contribute to both the ν_{CO} bands at 2091 and 2086 cm^{-1}.

Similar analysis can be applied to the ν_{RhH} (ν_{HH}) region. In this case, however, differences in the position of bands characterizing various types of surface species are larger and, therefore, more bands are typically observed in this region. DFT calculations further show that Rh(CO)(H) species do not have characteristic vibrations in the 2180-2120 cm^{-1} region, indicating that the experimental spectra shown in Figs. 1.1B, 1.3B, 1.4B, 1.6B, and 1.11B only include bands from Rh(CO)(H_2) and Rh(CO)$(H)_2$ type complexes. While the majority of ν_{RhH} and ν_{HH} vibrations in these two types of complexes are well resolved, the ν_{RhH} and ν_{HH} bands characterizing Rh(CO)$(H)_2$_b and Rh(CO)(H_2)_c complexes, respectively, are located too close to each other, suggesting that the band experimentally observed at 2164 cm^{-1} is the combination band that represents both of these species. The band at approximately 2155 cm^{-1} can be assigned to Rh(CO)(H_2) complexes, while those in the 2145-2129 cm^{-1} region to Rh(CO)$(H)_2$ complexes with dissociated hydrogen. The formation of Rh(CO)(H_2) and Rh(CO)$(H)_2$ type complexes is further confirmed by H_2/D_2 exchange experiments, as a good agreement between calculated and experimental ν_{RhD} and ν_{DD} frequencies of Rh(CO)$(D)_2$ and Rh(CO)(D_2) complexes, respectively, was observed.

The formation of Rh(CO)(H) complexes with one atomic H ligand under the experimental conditions used cannot be confidently confirmed from the spectra shown in Figs. 1.1A, 1.3A, 1.4A, 1.6A, and 1.11A because relatively weak ν_{RhH} bands of these complexes are screened by the far more intensive ν_{CO} vibrations and, therefore, cannot be observed experimentally. However, the corresponding ν_{RhD} vibrational bands of such

complexes should appear in the 1518-1510 cm^{-1} region, and could be observed in the experiments with deuterium. In fact, the ν_{RhD} bands experimentally observed at 1524 and 1510 cm^{-1} in spectra of $Rh(CO)(H)_x$/HY30 exposed to D_2 match well the calculated ν_{RhD} frequencies, and their presence provides unambiguous evidence for the formation of Rh(CO)(H) complexes.

1.4 Conclusions

$Rh(CO)_2$ complexes were used as precursors for the surface mediated synthesis of $Rh(CO)(H)_x$ species. The carbonyl ligands of these complexes react with gas phase C_2H_4 to form $Rh(CO)(C_2H_4)$ species and subsequently well-defined $Rh(CO)(H)_x$ complexes when the former are exposed to H_2 at room temperature. The Si/Al ratio of the zeolite used has no effect on this two-step synthetic pathway. Zeolite-supported $Rh(C_2H_4)_2$ and $Rh(NO)_2$ can also be used as precursors, but both complexes must be converted into $Rh(CO)_2$ first to allow the formation of $Rh(CO)(H)_x$ species. The $Rh(CO)(H)_x$ species thus formed are characterized by a set of well-defined ν_{CO} and ν_{RhH} bands in their FTIR spectra. However, the relative intensities of these bands are affected by the Si/Al ratio of zeolites and the nature of the precursor used. DFT calculation results provide strong evidence for the formation a family of $Rh(CO)(H_2)$, $Rh(CO)(H)_2$, and Rh(CO)(H) complexes on the surface of dealuminated HY zeolites. Since three different pairs of oxygen atoms in the zeolite framework are capable of accommodating each of these species, nine individual complexes attached differently to the zeolite framework and characterized by a specific set of infrared bands in the ν_{CO} and ν_{RhH} (ν_{HH}) regions coexist on the surface. It is not possible to identify all nine specific complexes in the experimental spectra either because the difference in calculated frequencies is at or below

the spectral resolution, or because the ν_{CO} and ν_{RhH} (ν_{HH}) bands originating from different type complexes have positions which are too close to be resolved. Therefore, the overlap of the infrared bands of these complexes explains the complex band structure observed in the ν_{CO} and ν_{RhH} (ν_{HH}) regions of experimental spectra. Finally, it appears that the fraction of each individual complex formed varies substantially with the Si/Al ratio of zeolites and the nature of the precursor used, and therefore, has an effect on the number of infrared bands experimentally observed and the overall shape of infrared spectra

CHAPTER 2. CATALYTIC ETHYLENE HYDROGENATION AND DIMERIZATION BY HY ZEOLITE SUPPORTED RHODIUM DICARBONYL, RHODIUM CARBONYL ETHYLENE AND RHODIUM CARBONYL HYDRIDE SINGLE-SITE COMPLEXES

2.1 Introduction

Supported transition-metal complexes have been attracting a lot of attention lately due to their potential of having possibly comparable catalytic activity and selectivity as their homogeneous analogues.[1-3] Since the single-site nature of these complexes renders them molecular in nature, it is sometimes possible to observe similar reactivity towards specific substrates as their precursors in solution. Due to the absence of intrinsic difficulties associated with formation of particles of multiple sizes/different reactive sites, it becomes possible to have a certain degree of control over a specific reaction on a truly molecular level.[4-6] Such control is widely implemented in homogeneous catalysis where steric and electronic effects induced by ligands of an organometallic complex have marked influence on activity.[7-10]

It has been shown for certain anchored complexes that not only their molecular nature remains preserved but their reactivity towards certain molecules drastically changes.[11-13] In this case, the influence of support could be a crucial factor determining the activity.[5,14] Under very specific conditions, the support could also

provide additional active sites – Bronsted or Lewis acid sites.[15,16] For such reactions, the way to improve the performance of a molecular heterogeneous catalyst would be to determine particular pathways of interaction between the support and the catalyst during catalysis.

Olefin hydrogenation by transition-metal molecular complexes is one of the most widely studied reactions. Wilkinson started a revolution in organometallic chemistry when he showed that $RhCl(PPh_3)_3$ could be used as a catalyst for olefin hydrogenation in liquid phase.[17] Afterwards, when the viability of the organometallic route has been largely established, numerous attempts have been undertaken to create single-site hydrogenation catalysts by immobilizing Rh complexes on silica,[18,19] alumina, zeolites,[19] and polymers.[20]

Gates et all demonstrated that HY zeolite supported $Rh(C_2H_4)_2$ complexes exhibit activity in ethylene hydrogenation to ethane and dimerization to n-butenes.[29,30] It was speculated that the selectivity for ethane hydrogenation compared to dimerization could be markedly increased by converting Rh complexes into small Rh clusters prior to reaction or, alternatively, by supporting $Rh(C_2H_4)_2$ species on a surface with enhanced electron donating properties such as MgO.[22] It was proposed that the mechanism of butenes formation involves ethylene interaction with both the rhodium centre and the acidic Si-OH-Al sites.

We have demonstrated before that HY zeolite-supported $Rh(CO)_2$ species are also active in ethylene hydrogenation probably due to the formation of rhodium carbonyl hydride $Rh(CO)(H)_x$ complexes under sequential ethylene/hydrogen treatment[23,24]. Herein, we further explore the catalytic activity of HY-supported $Rh(CO)_2$ species for

both ethylene hydrogenation and dimerization reactions and show the exact cooperative/non-innocent role of the zeolite support in these catalytic processes.

2.2 Experimental Methods

2.2.1 Reagents and Materials

Dicarbonylacetylacetonato rhodium (I) $Rh(CO)_2(acac)$ (acac = $C_5H_7O_2$) (Strem, 98% purity) was used as supplied. n-Pentane (Aldrich, 99% purity) and Tetrahydrofuran (Aldrich, >99.9 %) were refluxed under N_2 in the presence of Na/benzophenone ketyl to remove traces of moisture and deoxygenated by sparging of dry N_2 prior to use. All glassware used in preparation steps was previously dried at 120°C. He, H_2 and C_2H_4 (Airgas, all UHP grade) were additionally purified to their use by passage through oxygen/moisture traps (Agilent) capable of removing traces of O_2 and water to 15 and 25 ppb, respectively. CBV760, CBV720, and CBV600 dealuminated HY zeolites (Zeolyst International) with Si/Al atomic ratios of 30, 15, and 2.6, respectively, were calcined in flowing O_2 at 300°C for 3 h and then evacuated at 10^{-3} Torr and 300°C for 16 h. For simplicity, these zeolite supports are further denoted as HY30, HY15, and HY2.6, respectively. All treated supports were stored and handled in a glovebox (MBraun) filled with dry N_2. The residual water and O_2 concentrations in the glovebox were kept below 0.1 ppm. Potassium dicyanoaurate (Strem, 99 % purity), Chlorotrimethylsilane (Aldrich, > 99.9 % purity) were used as supplied (Strem). Ethanol anhydrous (Aldrich, > 99.5 % purity) was also used as received.

2.2.2 Preparation of Supported Samples

The syntheses and sample transfers were performed with exclusion of air and moisture on a double-manifold Schlenk line and in a N_2-filled MBraun glove box. Supported samples were prepared by slurrying the $Rh(CO)_2(acac)$ precursor with a corresponding powder support in n-pentane under N_2 for 24 h at room temperature, followed by overnight evacuation at 25°C to remove the solvent. In each case, the $Rh(CO)_2(acac)$ precursor was added in the amount needed to yield samples containing 1 wt% Rh. The Rh weight loading was verified by inductively coupled plasma-mass spectrometry (ICP-MS) analysis (Galbraith Laboratories Inc.).

Reaction between $Si(CH)_3Cl$ in pentane solution and HY30 complexes was performed in Schlenk flask with exclusion of air and moisture prior to anchoring $Rh(CO)_2Acac$. The solid was dried under the vacuum and transferred into a glovebox. All prepared samples were stored and handled in a glovebox filled with N_2 to prevent possible contamination and decomposition of supported species.

2.2.3 FTIR Spectroscopy

A Nicolet Nexus 470 spectrometer equipped with a MCT-B detector cooled by liquid nitrogen was used to collect spectra with a resolution of 2 cm^{-1}, averaging 64 scans per spectrum. Each powder sample was pressed into a self-supported wafer with a density of approximately 20 mg/cm^2 and mounted in a home-made cell connected to a gas

distribution manifold. The cell design allowed for the treatment of samples at different temperatures, while various gases flowed through the cell.

2.2.4 X-Ray Photoelectron Spectroscopy Measurements

XPS measurements were conducted using a Kratos AXIS Ultra DLD XPS system equipped with a monochromatic Al Ka source. The binding energy is calibrated using an Ag foil with $Ag3d_{5/2}$ set at 368.21 ± 0.025 eV for the monochromatic Al X-ray source. The monochromatic Al Ka source was operated at 15 keV and 120 W. The pass energy was fixed at 40 eV for the detailed scans. A charge neutralizer (CN) was used to compensate for the surface charge. The powder samples (approximately 5 mg) were loaded into the air-tight cell in the N_2-filled glovebox. The sample was then transferred without air exposure into the UHV chamber for the XPS analysis. The C1s signal with a binding energy of 285.0 eV was used as an internal reference for calibration of the Rh $3d_{5/2}$ and Rh $3d_{3/2}$ binding energy values. All binding energies reported in this work were measured with a precision of ±0.1 Ev. XPS data were analyzed by nonlinear curve fitting using the XPSPEAK software version 4.1. In all cases, a linear-type background was subtracted from the spectra and a curve fit was performed using the minimum number of G/L-type peaks that provides a good fit. In each case the fitting routine was completed when the coefficient of determination (R^2) value was 0.98 or higher.

2.3 Results and Discussion

2.3.1 Activity of HY Zeolites in Ethylene Hydrogenation

In order to investigate the activity of site-isolated rhodium complexes supported on HY zeolites, it is important to gain insight into catalytic properties of the support (HY 30, 15, 2.6) in ethylene hydrogenation/dimerization that would serve as a base-line for the supported rhodium complexes.

It was previously demonstrated that La, Y, Cr, Nd, Gd-containing Y-type zeolites show some activity in ethylene hydrogenation[25,26] In these studies, several adsorbed forms of C_2H_4 and H_2 were detected on zeolites and oxides, and the catalytic activity went through a maximum with the increase of the M content in zeolite.

Van BokHoven[27] et al explored adsorption of ethylene on HY2.6 at different temperatures using in situ Al K edge EXAFS analysis. Obtained EXAFS data are consistent with the presence of a few intermediates on the surface: at lower temperature weakly adsorbed form of ethylene exists on Bronsted acid H-sites associated with oxygen bridges between Al and Si which are proposed to be catalytically relevant sites for various reactions; at room and higher temperature alkoxy intermediates start to form; further increase in temperature leads to oligomerization and coke formation.

We performed ethylene hydrogenation at RT on HY 30, 15 and 2.6. In all cases, formation of ethane was observed. Only trace amounts of butenes were formed, and their exact amounts could not be measured due to limitations of GC. Obviously, HY 30, 15 and 2.6 all catalyze ethane formation at room temperature, although TOF are quite small.

The ethane TOF strongly depends on Si/Al ration in the zeolite. Plotting TOF against Si/Al ratio reveals a linear dependence on dealumination (Fig. 2.1)

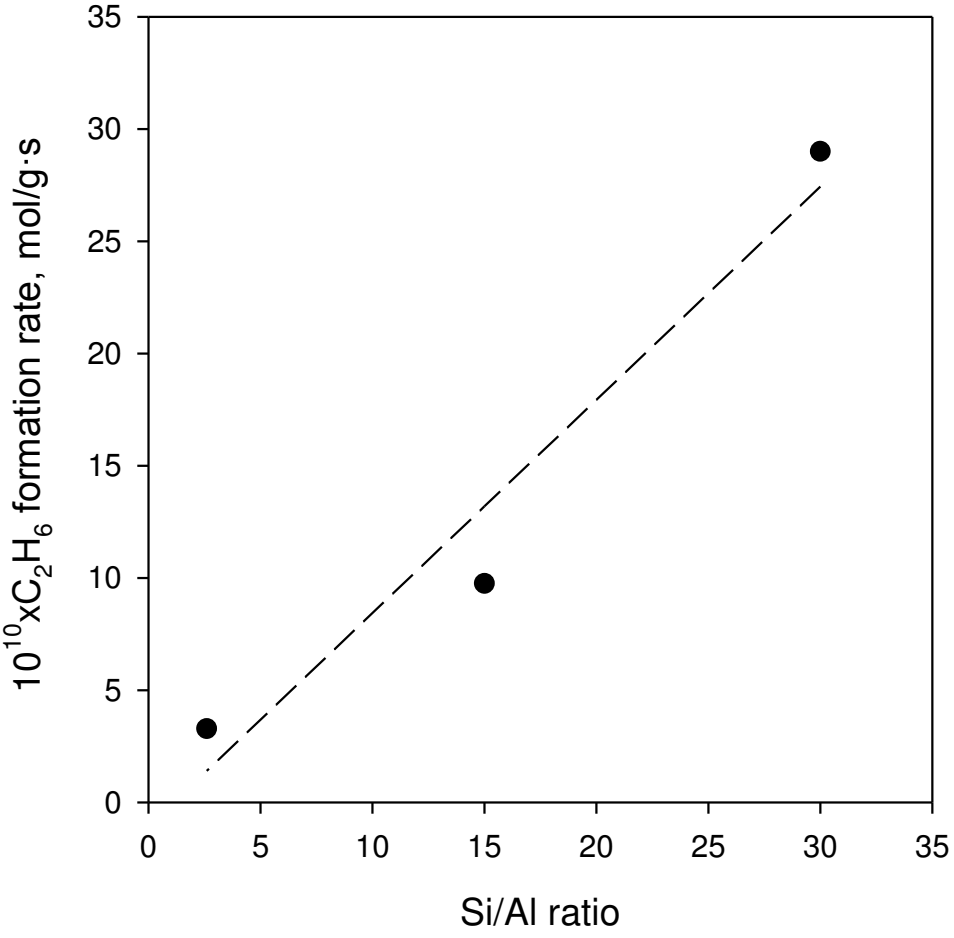

Fig. 2.1 Hydrogenation activity of dealuminated HY zeolites as a function of Si/Al ratio. (Reaction conditions: 25°C; GHSV= 12000 ml/g·h; feed composition: 76 Torr C_2H_4/608 Torr H_2/He balance).

The total amount of surface silanol groups in all zeolites is the same. The amount of stronger Bronsted acid sites is the highest in HY 2.6 but it has the lowest activity of all. The dealumination degree correlates with the strength of a Bronsted acid site[28], which leads to stronger adsorption of ethylene Thus, catalytic activity of HY zeolites increases with the increase in the strength of Bronsted acid sites.

2.3.2 Hydrogenation of Ethylene Ligands in HY Supported $Rh(C_2H_4)_2$ and $Rh(CO)(C_2H_4)$ Complexes

Synthesis of $Rh(C_2H_4)_2$/HY30 complexes was previously described[29]. Its interaction with ethylene at room temperature leads to hydrogenation of ethylene ligands and formation ethane in the gas phase (confirmed by mass-spectroscopy) as well as agglomeration of rhodium into small clusters, according to the EXAFS data reported elsewhere[29,30,].Experiments to monitor the amount of ethane formed during interaction woth H_2 were carried out in order to quantify the total amount of pi-bonded ethylene. The molar ratio of ethane formed to the total ratio of rhodium present in the sample was 2.4 which is very close to initial ratio of ethylene and rhodium in the single-site $Rh(C_2H_4)_2$/HY30 complex (Fig. 2.2).

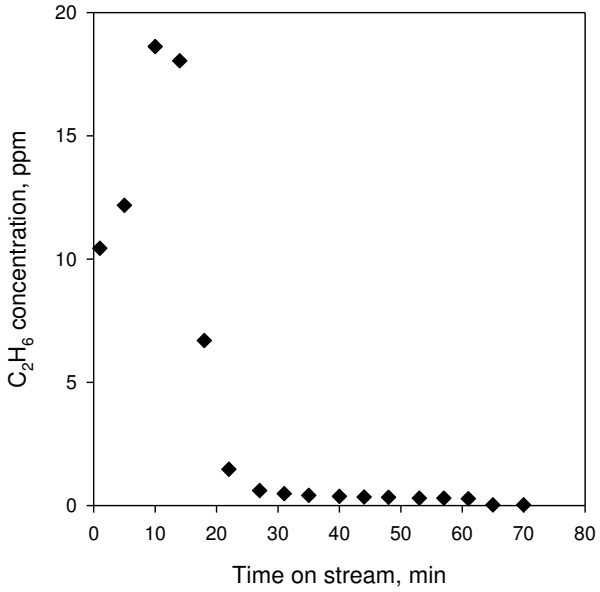

Fig. 2.2 Formation of C_2H_6 as a function of time during treatment of $Rh(C_2H_4)_2$/HY30 with H_2 at 25°C.

This means that reaction is irreversible and proceeds with 100% yield. Also, it corroborates the expected stoichiometry and structure of the synthesized $Rh(C_2H_4)_2$ supported on HY30.

Our group and Gates et al[24,30] demonstrated that the reaction of $Rh(CO)_2$/HY complexes with ethylene leads to the formation of site isolated $Rh(CO)(C_2H_4)$/HY complexes. Since $Rh(C_2H_4)_2$ and $Rh(CO)(C_2H_4)$ are structurally similar and both contain pi-bonded ethylene ligands that react with hydrogen to form ethane in the gas phase[24], and zeolite-supported mixed rhodium carbonyl hydride, it was important to establish the same correlations for such complexes.

The reaction was performed in-situ: $Rh(CO)_2$/HY30 was loaded into the reactor, reacted with C_2H_4, purged with N_2 for an hour, then reacted with hydrogen. During all these treatments, products were continuously analyzed with online GC. Formation of 1,3-butadiene and n-butenes was evident during C_2H_4 reaction with $Rh(CO)_2$. The initial TOF for butadiene at ca 0.3 s^{-1} drops to 0.08 s^{-1} during 1 hour whereas the TOF for butenes steadily increases (Figs. 2.3 and 2.4). Note that for HY zeolites, treatment with ethylene or C_2H_4/H_2 does not lead to any measurable C_4 products formation. Therefore, this catalytic effect can be attributed to the presence of site-isolated rhodium complexes in HY zeolites. Moreover, these complexes are capable of catalyzing formation of butadiene and isomeric n-butenes. It is known that the only product of reaction between $Rh(CO)_2$ and ethylene is $Rh(CO)(C_2H_4)$ (Fig. 2.5). Hydrogenation of $Rh(CO)(C_2H_4)$ leads to the selective formation of rhodium carbonyl-hydride complexes and evolution of ethane in the gas phase.

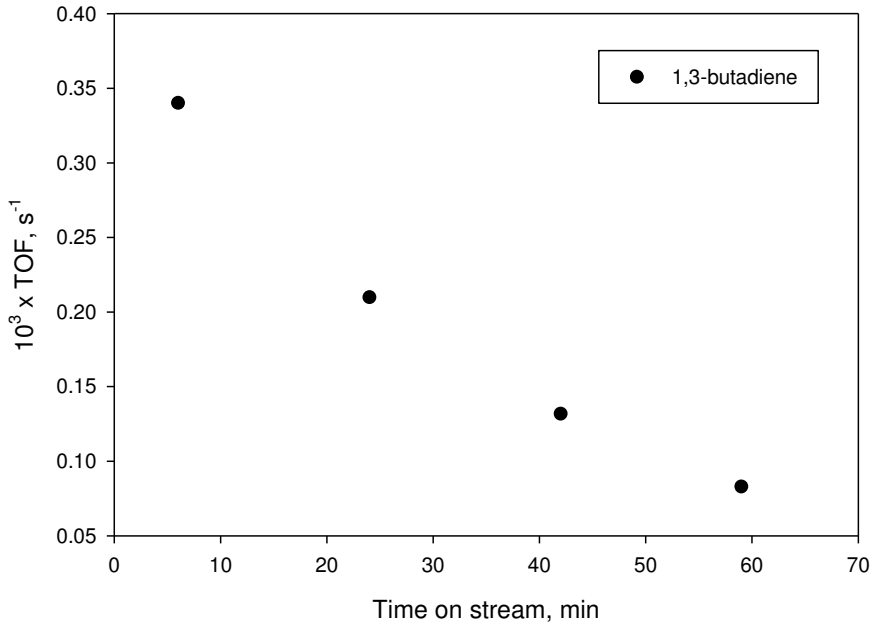

Fig. 2.3 Formation of 1,3-butadiene as a function of time during treatment of $Rh(CO)_2$/HY30 with C_2H_4 at 25°C.

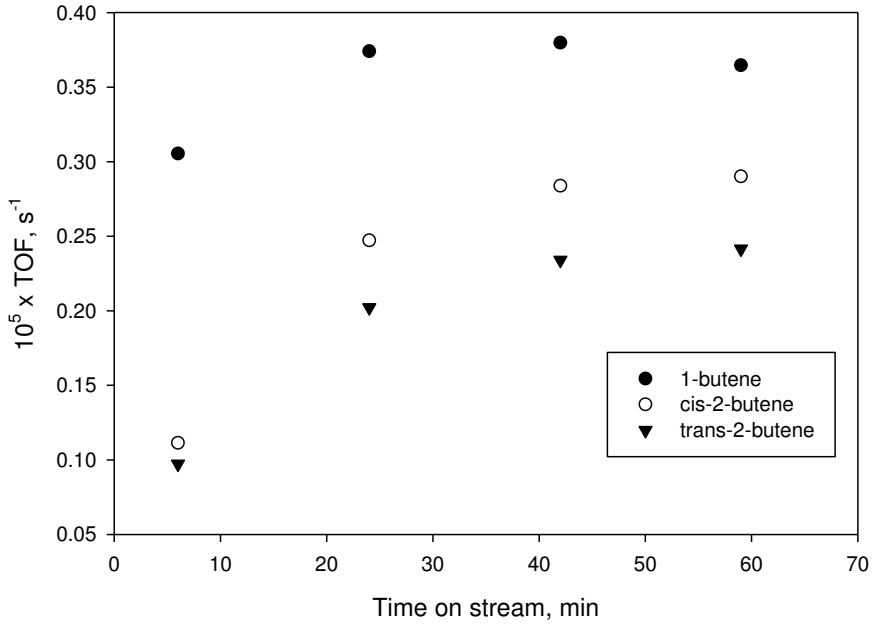

Fig. 2.4 TOF for isomeric n-butenes formation during ethylene treatment of $Rh(CO)_2$/HY30.

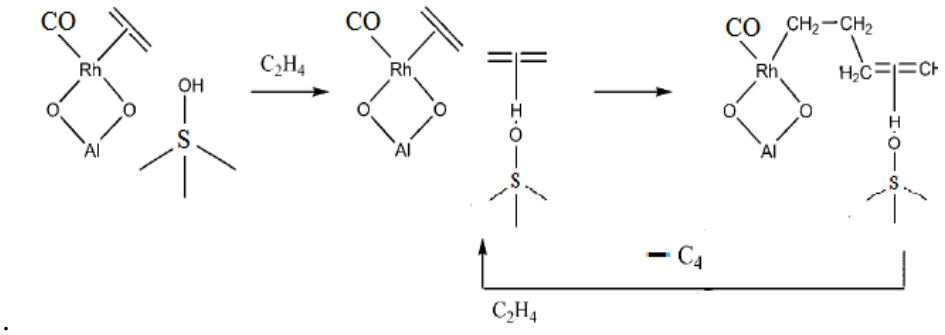

Fig. 2.5 Schematic representation of catalytic butene formation during ethylene treatment of $Rh(CO)_2$/HY30.

Ethane formation is fast and irreversible. After 10 min there is virtually no ethane formed which is similar to the beahvior of the supported $Rh(C_2H_4)_2$/HY30 complex (Fig.2.6).

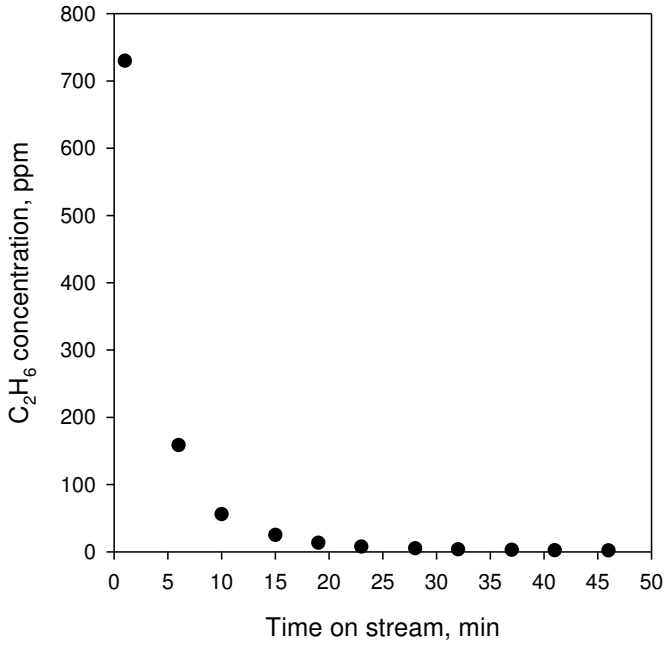

Fig. 2.6. Formation of C_2H_6 as a function of time during treatment of $Rh(CO)(C_2H_4)$/HY30 with H_2 at 25°C.

Ethane to rhodium ratio in the samples is summarized in Table 2.1:

Table 2.1 Ethane/Rh ratio during H_2 treatment of in-situ prepared $Rh(CO)(C_2H_4)$ on various zeolites.

Sample	Pre-treatment used	Surface species formed	C_2H_6/Rh molar ratio
$Rh(C_2H_4)_2$/HY30	none	$Rh(C_2H_4)_2$	2.4
$Rh(CO)_2$/HY30	C_2H_4 at 25 °C for 1 h followed by He for 1 h	$Rh(CO)(C_2H_4)$	49.0
$Rh(CO)_2$/HY15	C_2H_4 at 25 °C for 1 h followed by He for 1 h	$Rh(CO)(C_2H_4)$	81.0
$Rh(CO)_2$/HY2.6	C_2H_4 at 25 °C for 1 h followed by He for 1 h	$Rh(CO)(C_2H_4)$	132.0

Unlike for the supported $Rh(C_2H_4)_2$/HY complex, the numbers are not stoichiometric. The ratio in all cases is significantly higher than allowed by stoichiometry of the formed $Rh(CO)(C_2H_4)$/HY complexes. This leads us to the conclusion that the process is catalytic in its essence. So where does additional ethylene come from when we flow only H_2? At this point, it becomes apparent that the surface during ethylene treatment retains ethylene. This adsorption of ethylene is not surprising and has been investigated[32,33]. Furthermore, this adsorbed ethylene gets hydrogenated during $Rh(CO)H_x$ and $h(CO)(C_2H_4)$ interaction with gas-phase H_2 which implies either the high mobility of the adsorbed ethylene (in this case ethylene moves across the surface until it encounters activated hydrogen and gets hydrogenated) or the hydrogen spills over onto the surface via Rh assisted pathways and it is mobile on the surface and capable of hydrogenating the adsorbed ethylene species. Mobility of the alkylcarbenium cations formed via interaction

of an olefin with a Bronsted acid site of zeolites is implied in zeolite-assisted isomerization and polymerization of olefins[34]. On the other hand, Gates et al implied reverse hydrogen spill over from Rh onto the surface[35]. At this stage, it remains unclear what the exact hydrogenation pathway is, although one might argue that the surface mobility of spilled over hydrogen should be greater than carbenium ions due to simple size comparison and ability to "hop"[36].

C_2H_6/Rh ratio plotted against dealumination degree reveals almost a perfect linear fit

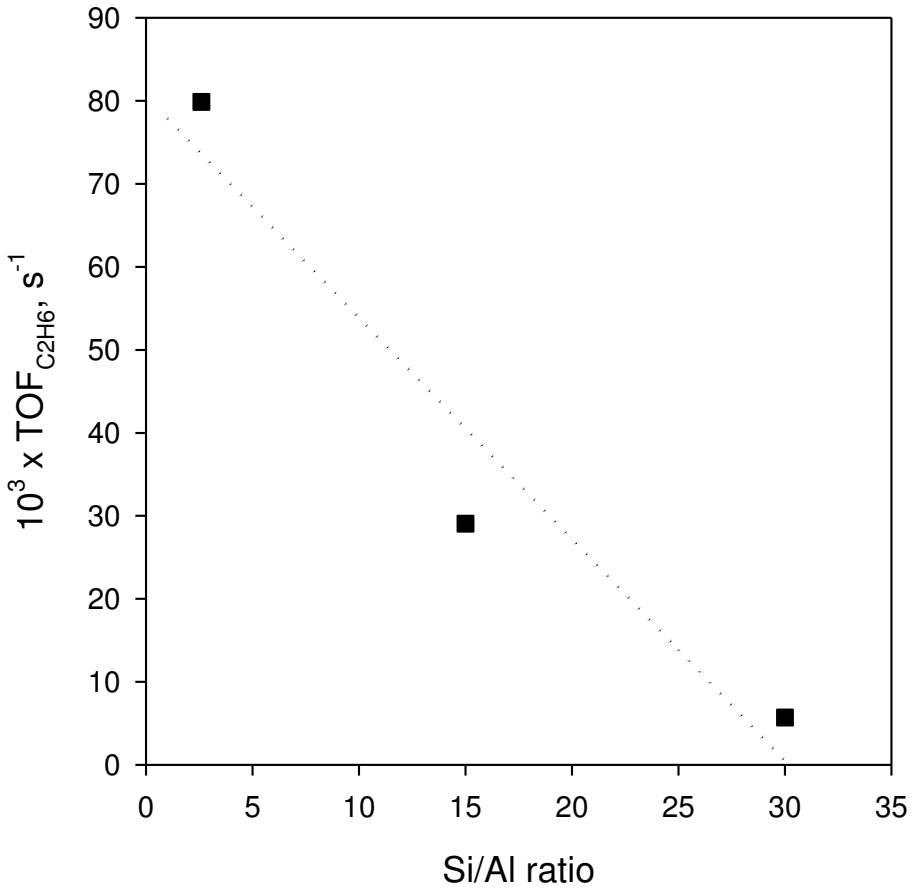

Fig. 2.7 Ethane/Rhodium ratio depending on Si/Al ratio (zeolite) used.

In this case, however, it is different than hydrogenation activity for HY zeolites with no Rh: hydrogenation activity decreases with dealumination degree, i.e. the number of Bronsted acid sites.

This confirms that the cause of this discrepancy is most likely the different hydrogenation mechanisms on HY and Rh/HY catalysts. For HY zeolites the strength of the Bronsted acid site is the crucial factor for hydrogenation.

For Rh-assisted hydrogenation of pre-adsorbed C_2H_4, the number of Bronsted acid sites capable of keeping ethylene on the surface is important. It does not allow us to distinguish between the likelihood of these two possible mechanistic pathways: the one in which adsorbed ethylene comes to the rhodium site to be hydrogenated, or the hydrogen spills over onto the surface. Although we noted that from a simplistic "steric size" point of view, mobility of H should be greater on the surface, we speculate that the H that is a hydride ligand on rhodium and forms a Rh-H bond with an approximate energy of 60 kcal/mole[37] – the breaking of this bond with the following coordination of the hydride ligand to the surface which requires the energy to break the Rh-H bond and then create a kind of H-relay on zeolite capable of operating only by successive bond breaking-bond formation events, is less likely.

2.3.3 $Rh(CO)_2$ Supported on HY30, 15 and 2.6 Zeolites in Ethylene Hydrogenation and Dimerization

Site-isolated rhodium dicarbonyl complexes supported on HY zeolites are active in ethylene hydrogenation, with a typical TOF/Time on stream plot presented in Fig. 2.8.

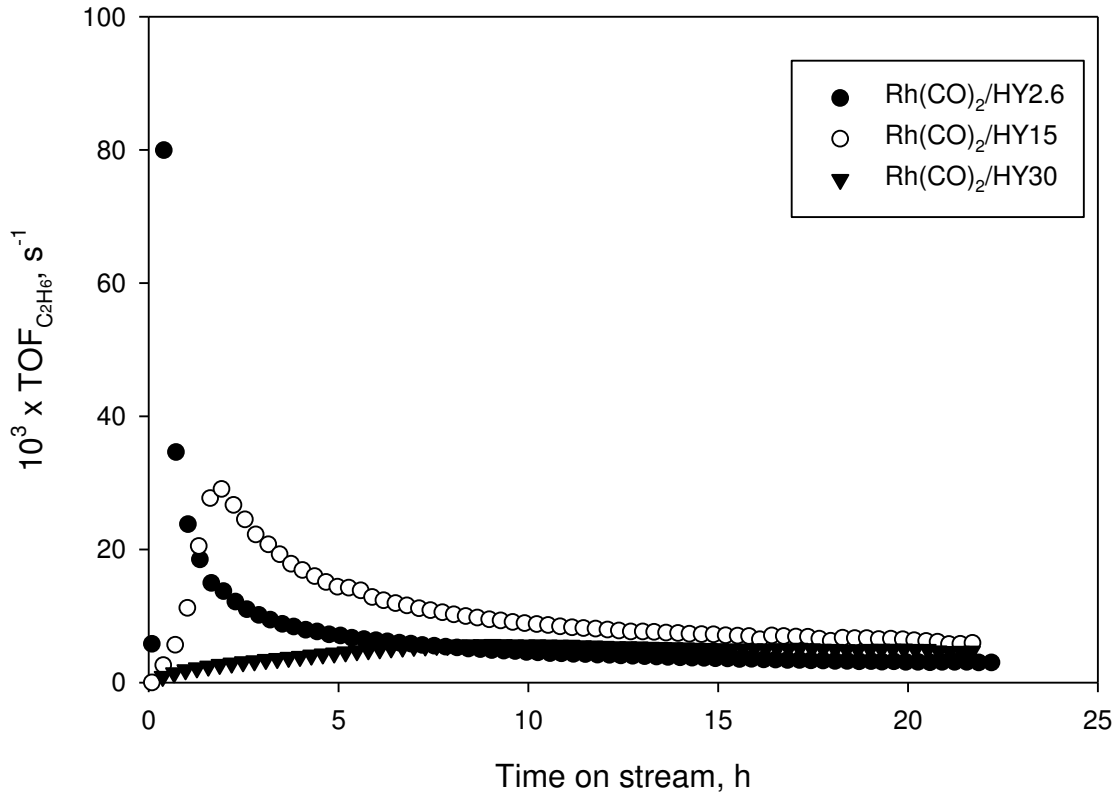

Fig. 2.8 Comparison C_2H_4 hydrogenation activity of $Rh(CO)_2$ complexes on different HY zeolites as a function of time on stream. (Reaction conditions: 25°C; GHSV= 60000 ml/g·h; feed composition: 76 Torr C_2H_4/608 Torr H_2/He balance; total C_2H_4 conversion below 5%).

Based on these data, it is clear that all $Rh(CO)_2$/HY complexes are active catalysts for ethane formation. The initial activities follow the range HY2.6>HY15>HY30. After approximately 10 hours, all three catalysts reach steady state with significant TOF drops for $Rh(CO)_2$ on HY15 and 2.6 while for $Rh(CO)_2$/HY30 there is no drop, and even after 20 h on stream it remains stable and has higher activity than $Rh(CO)_2$ on HY15 and 2.6 samples. Such a rapid drop in hydrogenation activity could be indicative of poisoning of active sites: it is well-known that the higher the amount of Bronsted acid sites, the higher

the rate of formation of carbonaceous and condensed aromatics in the zeolite pore[that act as a catalytic poison by blocking catalytically active sites.

Ethane is not the only product formed. Isomeric n-butenes are also produced in a gas phase revealing unique activity of rhodium carbonyl complexes for ethylene dimerization. Results of the typical experiment performed at 608 Torr of H_2 and 76 Torr of C_2H_4 under ambient conditions show rates of ethane, butene-1, cis-2-butene and trans-2-butene formation with time on stream (TOS) (Figs. 2.9, 2.10 and 2.11).

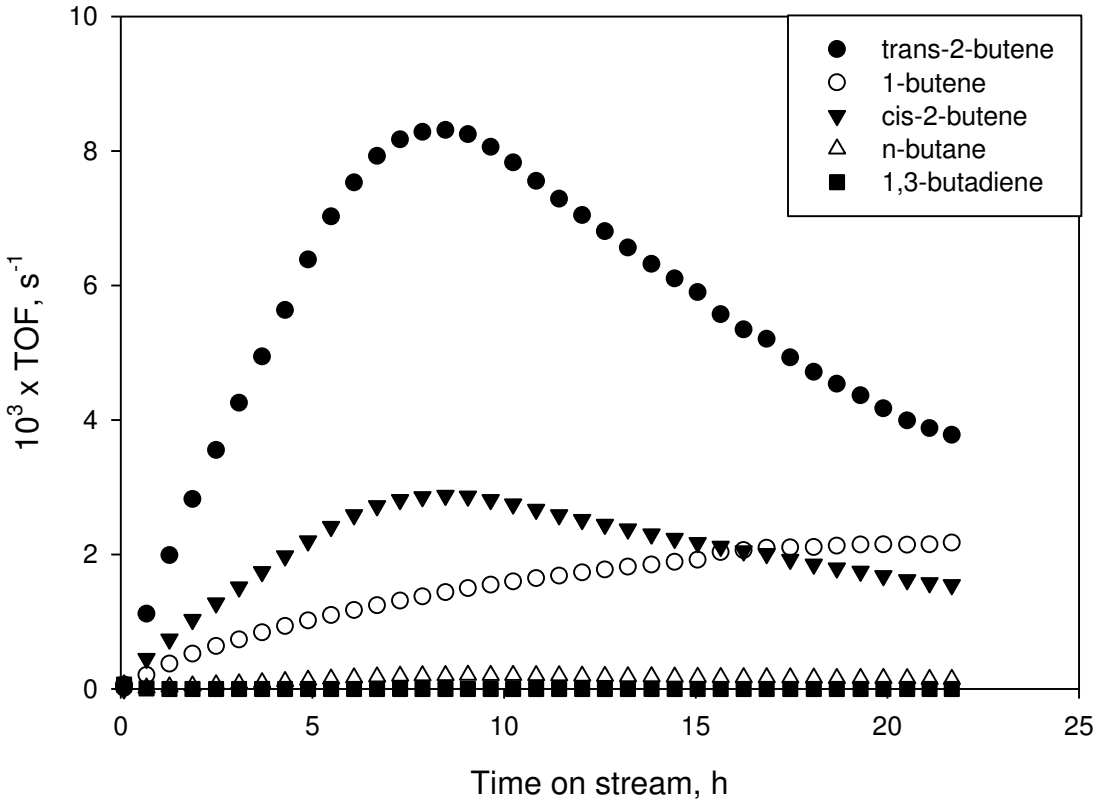

Fig. 2.9 Dimerization activity of $Rh(CO)_2$/HY30 as a function of time on stream. (Reaction conditions: 25°C; GHSV= 60000 ml/g·h; feed composition: 76 Torr C_2H_4/608 Torr H_2/He balance; total C_2H_4 conversion below 5%).

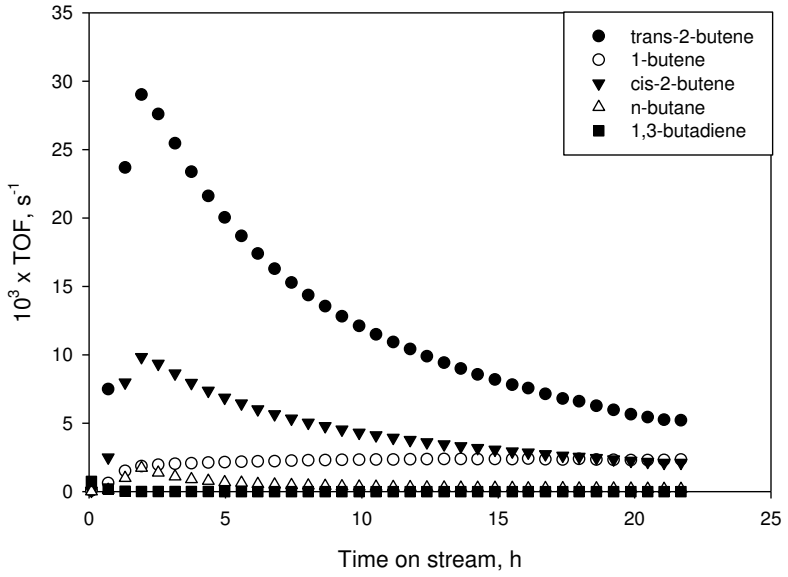

Fig. 2.10 Dimerization activity of $Rh(CO)_2$/HY15 as a function of time on stream. (Reaction conditions: 25°C; GHSV= 60000 ml/g·h; feed composition: 76 Torr C_2H_4/608 Torr H_2/He balance; total C_2H_4 conversion below 5%).

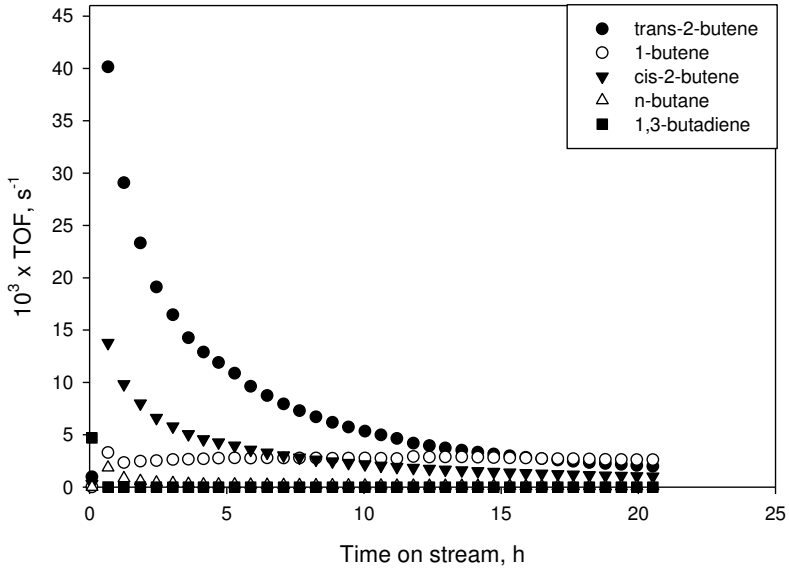

Fig. 2.11 Dimerization activity of $Rh(CO)_2$/HY2.6 as a function of time on stream. (Reaction conditions: 25°C; GHSV= 60000 ml/g·h; feed composition: 76 Torr C_2H_4/608 Torr H_2/He balance; total C_2H_4 conversion below 5%).

Although ability of HY zeolite-supported $Rh(C_2H_4)_2$ complexes to promote ethylene hydrogenation and ethylene dimerization was described in literature [21,22], the fact that $Rh(CO)_2$ species are capable of facilitating similar transformation is somewhat unexpected. More specifically, it was reported that poisoning of Rh sites with CO results in complete catalyst deactivation. [22]

Ethylene dimerization activity is unusual. Only molecular Rh-complexes promoted with HHalogen were active in ethylene dimerization in solution as was described by Cramer[38]. In his study, the catalytic cycle involving the catalytically active highly-reactive $C_2H_5Rh(III)Cl_2(C_2H_4)$ anionic intermediate was deduced.

Based on a series of precise kinetic and NMR measurements, the lability of Hal ligand as well as presence of protons in the solution were the absolute requirement for this reaction. Moreover, the first-order coordination between the rate of butane-1 formation and concentrations of $[H^+]$ was discovered.

Based on these data, the following tentative mechanism for ethylene dimerization on HY supported carbonyl complexes could be deduced: one of the CO ligands in $Rh(CO)_2$ complex is substituted with ethylene yielding $Rh^I(CO)(C_2H_4)$ species. The following transformation implies oxidative addition of hydrogen and formation of formally 18-electron $Rh^{III}(CO)(C_2H_4)(H)_2$ complexes which rapidly undergo hydride ligand migration giving $Rh^{III}(CO)(C_2H_5)(H)$ structures. The subsequent reductive elimination of ethane from such surface species yields coordinatively unsaturated and highly reactive 14-electron $Rh^I(CO)$ complexes which immediately coordinate ethylene from a gas phase closing up the catalytic cycle. In contrast to hydrogenation, the mechanistic aspects of ethylene dimerization involving rhodium dicarbonyls are not obvious and have not been

discussed. The closest analogue to such species reported in literature with substantial activity in butenes formation are HY zeolite-supported $Rh(C_2H_4)_2$ complexes which are proposed to operate via bifunctional mechanism which involve Rh sites and Brønsted acid sites of the zeolite support. [21]

Comparison of activities and selectivies for C_2H_4 hydrogenation/dimerization for various zeolites is summarized in Table 2.2.

Table 2.2 Catalytic properties of HY zeolite-supported $Rh(CO)_2$ complexes in conversion of C_2H_4 at maximum activity.

Sample	TOF (s^{-1})[a]		Product selectivity (mol %)[a]	
	C_2H_6	C_4	C_2H_6	C_4
$Rh(CO)_2$/HY30	5.69×10^{-3}	12.82×10^{-3}	31	69
$Rh(CO)_2$/HY15	29.04×10^{-3}	42.44×10^{-3}	40	60
$Rh(CO)_2$/HY2.6	79.88×10^{-3}	73.98×10^{-3}	55	45

2.3.4 Comparison of Catalytic Activities of HY and Alumina-Supported Rh complexes

The possibility of the support to play a role of the macroligand affecting properties and reactivity of supported complexes has been discussed.[39-44] It is of merit to mention that support effect are magnified when atomically dispersed metals or small metal clusters are anchored on the support.[42,45]

It was shown, for instance, that temperature of CO ligand hydrogenation when using immobilized $Rh(CO)_2$ species as catalysts depends on the support and it decreases in the

following order NaX < Al_2O_3 < NaY < TiO_2 which is consistent with decreasing electron accepting properties of supports.[42] It is remarkable, that when highly dispersed Rh clusters were used, CO hydrogenation activity varied over 200-fold dependent upon the support (SiO_2, $A1_2O_3$, MgO, CeO_2 and TiO_2 were used).[41] In another work it was demonstrated that activity of low nuclearity supported Rh clusters (2-4 atoms in size) in 1,3-butadiene hydrogenation is biased to electronic properties of the support and exceptional selectivity to 1-butene was obtained on MgO which possesses of significantly higher electron-donating properties than zeolite Y.[37]

In order to understand if the support has some effect on catalytic properties of supported $Rh(CO)_2$ complexes, the catalytic performance of Al_2O_3 and HY30 supported $Rh(CO)_2$ complexes was compared. It is implied that the key intermediates responsible for catalytic activity of HY zeolite-supported $Rh(CO)_2$ species in ethylene hydrogenation could potentially be $Rh(CO)(H)_x$ complexes which can be synthesized selectively on zeolite surface via sequence of C_2H_4-H_2 reactions.[24] Interestingly, similar transformations performed with Al_2O_3-supported $Rh(CO)_2$ complexes does not result in the formation of $Rh(CO)(H)_x$ species.

FTIR spectra in CO stretching region of the initial $Rh(CO)_2/Al_2O_3$ sample exhibits two bands at 2090 cm^{-1} and 2014 cm^{-1} characterizing symmetric and asymmetric vibrations of CO ligands, respectively, with an average FWHM of approximately 24 cm^{-1}. The infrared peaks of HY30-supported $Rh(CO)_2$ species are extremely narrow with FWHM of about 6 cm^{-1} suggesting their high structural uniformity with ν(CO) bands located at 2117 cm^{-1} and 2051 cm^{-1}. We note that EXAFS measurements confirmed the presence of site-isolated $Rh(CO)_2$ species on both supports[46]. Such a significant

difference in positions of v(CO) peaks is a first indication of quite different properties of Al_2O_3 and HY zeoltie as ligands and, more specifically, it reveals stronger electron-accepting properties of zeolite oxygen atoms (Fig. 2.12).

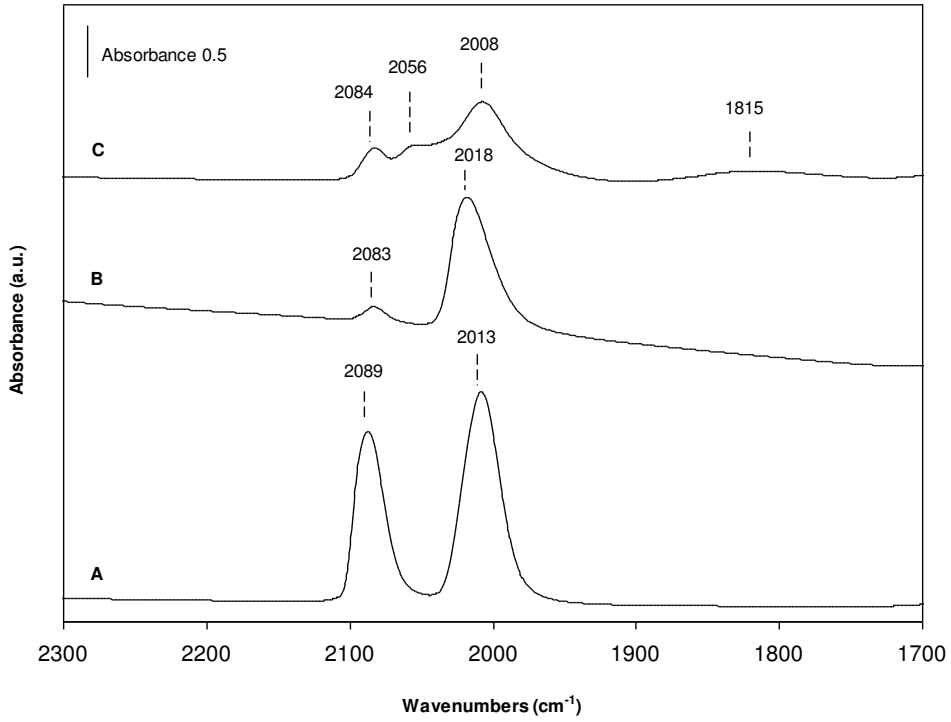

Fig. 2.12 FTIR spectra in the CO region of $Rh(CO)_2/Al_2O_3$ (A) in He (B) after exposure to C_2H_4 for 10 h (C) after exposure to H_2 for 30 min.

When $Rh(CO)_2/Al_2O_3$ sample was exposed to stream of ethylene for 10 hours (followed by helium purge), the band at 2090 cm^{-1} lost about 90 % of its initial intensity and shifted to 2083 cm^{-1} while the band at 2014 cm^{-1} broadened and slightly blue-shifted to 2018 cm^{-1}. Simultaneously, weak features appeared at 3075, 3057, 3010, and 2978 cm^{-1} characterizing v(CH) vibrations of ethylene π bonded to Rh center. In contrast, in case if $Rh(CO)_2$/HY30 sample ethylene pulse of only 3 minutes was sufficient to remove 97 % of 2117 cm^{-1} band intensity and no shift of the $\nu_{as}(CO)$ peak at 2052 cm^{-1} was detected.

Consistent with the presence of ethylene ligand on Rh, the bands in ν(C–H) region were also identified although at slightly different positions: 3094, 3070, 3021, and 2986 cm^{-1}. These data suggest that ethylene exposure to $Rh(CO)_2$ species results in its coordination on Rh site yielding $Rh(CO)(C_2H_4)$ complexes. We note that for both supports C_2H_4/CO substitution was reversible, i.e. pulse of CO led to immediate reappearance of bands characterizing initial $Rh(CO)_2$ complexes indicating that CO affinity to Rh is very high regardless of the support.

It is known that $Rh(CO)(C_2H_4)$ complexes can be converted into stable $Rh(CO)(H)_x$ species in hydrogen flow.[24] More specifically, this transformation is accompanied by evolution of a strong band at 2091 cm^{-1} and weak features at 2170-2120 cm^{-1} region in FTIR spectrum characterizing v(CO) and v(Rh-H) vibrations in the rhodium carbonyl hydride complexes, respectively. In contrast, exposure of Al_2O_3-supported $Rh(CO)_2(C_2H_4)$ species to hydrogen for 60 minutes led to the appearance of bands at 2056 cm^{-1} and 1815 cm^{-1} with no peaks evolving in 2100-2200 cm^{-1} region. Simultaneously, weak features in v(CH) region disappeared from the spectrum and ethane was detected in a gas phase with mass-spectrometry suggesting that observed changes are associated with hydrogenation of ethylene ligands into ethane. This result clearly indicates that unlike in case of zeolite-supported sample, rhodium hydrides species are not formed. The bands at 2050-2070 cm^{-1} and 1800-1900 cm^{-1} region were previously reported in literature and are normally assigned to carbonyl groups linearly and bridged bound to metallic rhodium species, respectively.[47-49] We also note that similar bands evolved in the spectrum when Al_2O_3-supported $Rh(CO)_2$ complexes were heated in H_2 to 100 ºC (2053 cm^{-1}, 1830 cm^{-1}) . We propose that at this temperature

rhodium dicarbonyls become mobile and aggregate into rhodium particles (but temperature is not high enough for carbonyls to fully react).

We exclude formation of $Rh_4(CO)_{12}$ and $Rh_6(CO)_{16}$ clusters under given conditions (after C_2H_4-H_2 sequence) for several reasons. First, FTIR signatures of these species supported on alumina have four bands with at least one band located in 2080 cm^{-1} region: 2083s, 2060ms, 2004s, and 1802w ($Rh_6(CO)_{16}/Al_2O_3$) and 2383s, 2058ms, 2032s, and 2002w cm^{-1} ($Rh_4(CO)_{12}/Al_2O_3$).[50] Secondly, Rh/CO ratios in $Rh_6(CO)_{16}$ and $Rh_4(CO)_{12}$ complexes are 0.375 and 0.333, respectively, which is lower than in $Rh(CO)_2/Al_2O_3$ sample indicating that there are not enough CO molecules on the surface to form Rh_4 or Rh_6 carbonyl clusters. Finally, formation of small metallic rhodium aggregates (not Rh4 or Rh6 clusters) from alumina supported $Rh(CO)_2$ species was reported by Wovchko et al when they investigated transformations of these complexes in hydrogen atmosphere under the UV light.[51] Therefore, we infer that, unlike in case of HY zeolite, alumina facilitates aggregation of Rh species upon consecutive exposure of $Rh(CO)_2$ complexes to C_2H_4 and H_2. However, it can be suggested that transient formation of alumina-supported $Rh(CO)(H)_x$ species occur since ethylene hydrogenation into ethane could only proceed via intermediate formation of hydrides but the former complexes are not stabilized by the support and immediately recombine into Rh aggregates.

We propose that among key factors contributing to different surface chemistry of rhodium species on alumina and HY zeolite are metal oxidation state in supported complexes and structure of the support surface. FTIR data and XPS measurements show that Rh formally more electron positive when supported on HY zeolite than on alumina. As a result, we expect less backdonation (donation of electron density from filled d

orbitals of Rh to empty antibonding orbitals of CO) occurring in case of zeolite-supported $Rh(CO)_2$ species and, consequently, weaker Rh-C bond (more liable) if compared to Al_2O_3-anchored rhodium carbonyl complexes. Besides, we propose that remarkable stability of HY zeolite-supported $Rh(CO)(H)_x$ complexes could be related to Si/Al ratio in the framework. More specifically, it is known that excess negative charge around isolated Al sites of the zeolite framework is the primary reason for the coordination of $Rh(CO)_2$ fragment to such sites.[46] These sites do not exist on alumina where surface is relatively energetically homogeneous favoring Rh migration under the reducing conditions.

Such different surface chemistry of rhodium complexes on alumina and dealuminated zeolite has drastic impact on catalytic performance of these materials. Fig. 2.13 demonstrates activity of HY30 and Al_2O_3 supported samples in ethylene hydrogenation with time on stream (TOS). HY30-supported sample has an induction period of about 6 hours associated with C_2H_4/CO exchange with TOF reaching about 0.04 s^{-1} after that period. In contrast, Al_2O_3-supported sample exhibits virtually no activity with TOF being nearly 0.003 s^{-1} after 20 h on stream. This result confirms the key role of Y zeolite-supported $Rh(CO)(H)_x$ complexes in ethylene hydrogenation suggesting that these species are intermediates in this reaction.

Moreover, this result points at the unique nanoenvironment inside the pores of dealuminated Y zeolites. This environment not only stabilizes the isolated mononuclear rhodium dicarbonyl species through the direct chemical interaction with the framework oxygens associated with the aluminium atom, but it also serves as a very unusual ligand (macroligand) that renders them catalytically active.

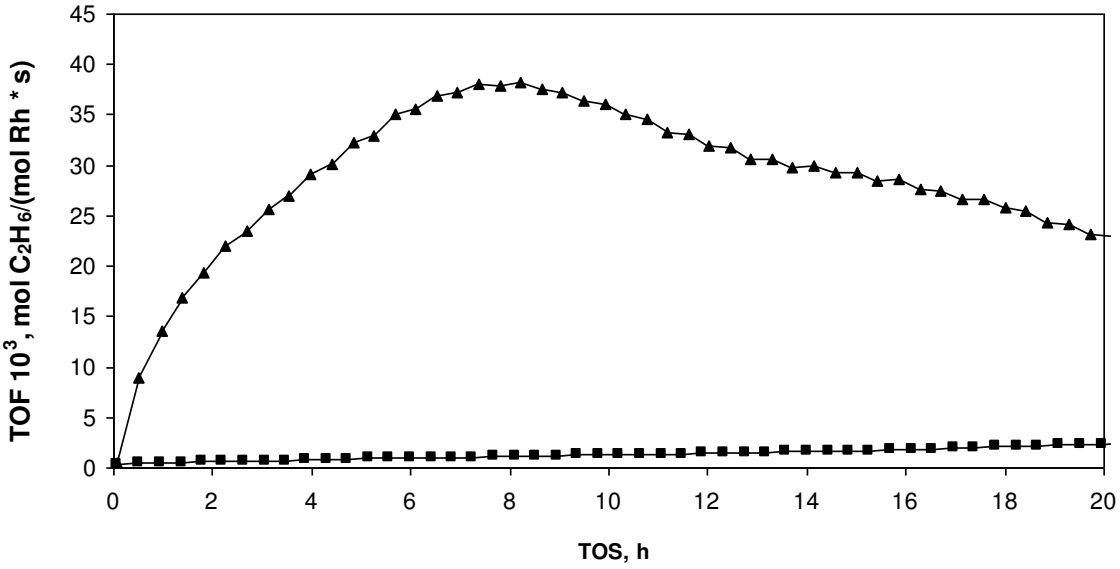

Fig. 2.13 Rates (Turn Over Frequencies) for Ethane formation with Time on Stream (TOS) for (▲) $Rh(CO)_2$/HY15 and (■)$Rh(CO)_2/Al_2O_3$ at 76 Torr of C_2H_4 608 Torr of H_2.

2.3.6 Kinetics and Ethylene Hydrogenation and Dimerization on HY30 Supported $Rh(CO)_2$ Complexes

It was demonstrated that HY30 zeolite-supported $Rh(C_2H_4)_2$ complexes active not only in ethylene hydrogenation but also have significant activity in ethylene dimerization into n-butenes.[35] It was also noted that poisoning of Rh sites with CO results in almost complete catalyst deactivation towards formation of butenes as well hydrogenation.[35] However, since we demonstrated that HY zeolite-supported $Rh(CO)_2$ species are active in ethylene hydrogenation, it is of particular interest to understand weather same complexes could promote ethylene dimerization. In order to explore activity of HY zeolite-supported $Rh(CO)_2$ in these reactions we performed the set of experiments with varying partial pressures of H_2 and C_2H_4. In the first series of experiments C_2H_4 partial pressure was kept

at 76 Torr while H_2 partial pressure was varied in the 76-608 Torr range. Results presented herein (Table 2.3) clearly demonstrate significant increase in a rate of ethane formation (TOF) with H_2 partial pressure.

Table 2.3 Kinetic Data for C_2 and C_4 products for the reaction on $Rh(CO)_2$/HY30.

Sample	Product	Order in H_2	Order in C_2H_4
$Rh(CO)_2$/HY30	Ethane	0.7	0.4
	n-butane	1.0	0.4
	Trans-2-butene	0.8	1.2
	Cis-2-butene	0.7	1.1
	1-butene	0.4	1.3

Linearization of these data with respect to steady-state TOF yields the 0.7 order dependence towards partial pressure of H_2. Many examples of kinetic data published on alkene hydrogenation catalyzed by homogeneous complexes of rhodium show the first order dependence on hydrogenation pressure.[52,53] In our case, however, the number is lower. The rate-dependence of ethane formation on ethylene partial pressure under given conditions is about 0.4. Coupled with dependence on hydrogen partial pressure, this result is the typical example of competitive adsorption of hydrogen and ethylene on one rhodium center. Indeed, our combined FTIR and catalytic results demonstrate the unique reaction network, characteristic of these particular complexes:

$Rh(CO)_2 + C_2H_4 \rightarrow Rh(CO)(C_2H_4)$

$Rh(CO)(C_2H_4) + H_2 \rightarrow Rh(CO)(H)_2 + C_2H_6$

$Rh(CO)(H_2) + C_2H_4 \rightarrow Rh(CO) + C_2H_6$

$Rh(CO) + H_2 \rightarrow Rh(CO)(H)_2$

$Rh(CO) + (C_2H_4) \rightarrow Rh(CO)(C_2H_4)$

Therefore, the kinetics of ethane formation are somewhat more complex than for typical homogeneous systems. The rates of butene (trans-2-butene, cis-2-butene, 1-butene) and butane formation are also dependent on H_2 and ethylene partial pressures (Table 2.3).

Rate dependence on ethylene partial pressure for all butenes is close to 1, which is higher than for ethane formation. This result is not surprising taking into account the fact that two ethylene molecules have to come in contact to form the C-C bond, and is consistent with the formidable rate dependence for dimerization reactions. For n-butane which is a minor product, the rate of formation and dependence on ethylene pressure is the same as for ethane (the major alkane formed in complete hydrogenation). This suggests similar pathway for complete hydrogenation of both ethylene and butenes. The dependence of butene formation on hydrogen partial pressure is an interesting result since no hydrogen is consumed in dimerization reaction according to chemical stoichiometry. Yet it clearly demonstrates that hydrogen are involved in this reaction as well, and it is not a simple metallocycle type mechanism observed for ethylene oligomerization on various complexes in liquid phase.[54] It is also a clear analogy for our heterogeneous system with Cramer's findings in the homogeneous system[38], for dependence of butene-1 rate formation on proton concentration – in which protons become hydrides during the

initial oxidative addition step, and then form butane-1 during beta-hydride elimination from the Rh-Butyl intermediate.

As it was previously mentioned, during catalysis a mixture of butenes is formed. For a typical mechanism, involving only the organometallic Rh-Butyl intermediate, butene-1 should always be the major kinetic product due to steric considerations. It is exactly what was observed by Cramer during the liquid phase dimerization of ethylene on Rh-C_2H_4 complexes. In our case, however, the acidic groups of zeolite might play an important role in this process. Zeolites are known to catalyze isomerization of butene-1. As Domen and coworkers showed[55], this process does not even necessarily involve the carbenium intermediates and might be a unique feature of the solid zeolite material with unique acidic properties and internal pore structure.

Interestingly, for liquid phase reactions catalyzed by protons the equilibrium ratio between cis and trans-butenes is about 1:3. That ratio is finely preserved in all catalytic results at steady-state. Therefore, we can tentatively conclude that butene-1 is formed on the Rh center, and then it undergoes isomerization on the acidic zeolite sites.

2.3.7 Kinetic Isotope Effect in Ethylene Hydrogenation

KIE in a useful tool in assessing feasibility of various mechanisms for various reactions, including alkene hydrogenation reactions[56]. Replacement of hydrogen with deuterium at steady state and measurement of the change in reaction rate often aids in elucidating the nature of intermediates involved in rate-determining step (or steps). The summary for all the performed measurements is presented below:

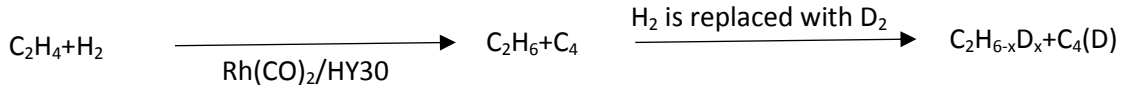

For C_2H_6 $K_{(H)}/K_{(D)}=0.75$

For C_4 $K_{(H)}/K_{(D)}=0.81$

Fig. 2.14 Illustration of Kinetic Isotope Effect (KIE) measurement for $Rh(CO)_2$/HY30 during ethylene hydrogenation and dimerization.

Normally, the kinetic isotope effect values are expected to be 1 or greater than 1. In our case, however, there is a clear inverse kinetic isotope effect.

For ethane formation, the kinetic isotope effect value is 0.75. For the formation of isomeric butenes the observed kinetic isotope effect value is 0.81.

It is known[57] that the majority of R–H *vs* R–D reductive elimination reactions are characterized by inverse KIEs, due to the increased thermodynamic stability of the Rh-D vs Rh-H agostic intermediates, thus effectively lowering the transition state energy and leading to higher reaction rates. Brookhart et al[58], for example, invoked the formation of complexes with alpha-agostic interactions in Co-assisted polymerization of ethylene in liquid phase.

The formation of such intermediates with Rh-H and Rh-D interactions in our case is the reason for the observed values that are below 1.

The observed KIE directly demonstrates involvement of reductive elimination steps with agnostic intermediates in the rate determining step for ethylene hydrogenation as well as dimerization.

2.3.8 Possible Mechanisms of Ethylene Hydrogenation and Dimerization by HY Supported Rhodium Complexes

Ethylene dimerization over zeolites has been described.[59,60] The mechanism is believed to involve Bronsted or Lewis acid sites and generally considered as sequence of the following elementary steps: coordination of olefin to the active site, protonation of olefin and formation of alkylcarbenium ion, addition of second olefin (chain propagation) to alkylcarbenium ion, and deprotonation.[59] Two types of mechanisms were proposed which consider formation of either carbenium ion of alkoxy structure.[59] However, our experiments as well as literature reports suggest that at ambient conditions HY zeolites have negligible activity in this reaction. Thus, observed activity should be ascribed either to rhodium complexes alone or a joint action of rhodium complexes and acidic active sites on zeolite surface. The oligomerization of olefins using metal complexes in solution also received significant attention.[61] The commercial process of ethylene dimerization into butene-1 currently utilizes a combination of triethylaluminum and titanium or zirconium alkoxides $Ti(OAr)_4/AlEt_3$ catalyst functioning trough the metallacyclic mechanism which does not require external source of protons.[62,63] Rhodium compounds are also known to promote this reaction with most focus of the research in this direction being on rhodium halide complexes.[38] It is suggested that bis(ethylene) complex of monovalent rhodium (i.e. $Rh_2Cl_2(C_2H_4)_2$ or $Rh(C_2H_4)_2(acac)$) is converted by reaction with HCl into an ethylrhodium(III) which further coordinates second ethylene molecule yielding a butyl fragment.[38]

It was proposed by Serna et al, while investigating mechanism of ethylene dimerization over HY-supported $Rh(C_2H_4)_2$ species, that only one of ethylene ligands on

Rh centre is engaged in reaction while another ligand is converted into ethyl group and present as spectator.[64] The second ethylene that participates in a reaction is proposed to coordinate to -OH group associated with Al atom (bridging –OH groups) in the vicinity of Rh site. It is important to note that this mechanism does not imply formation of carbenium ions (i.e. protonation of either of two participating ethylenes) and hydrogen is thought to spill on a surface to replenish protons in –OH groups of Al-OH-Si moieties removed upon complex immobilization which involved in a catalytic cycle as a binding sites for second ethylene molecule (one is activated on Rh center).[64] The role and type of these Al sites that give rise to acidic –OH groups involved in a reaction are not clear. Author suggested that Al-OH-Si moiety could be the same as one responsible for complex binding or originate from neighboring Al sites.

We note that our catalytic system is structurally very similar to one described by Serna et al with the only difference that CO ligand instead of ethyl group is present as a spectator. This inference is evidenced by very similar reaction rates found in this work and reported by Serna et al. However, such a strong dependence of dimerization kinetics on hydrogen partial pressure raises the question regarding the role of hydrogen in this process. More specifically, it is not clear weather its role is limited to interaction with surface hydroxyls (spillover) or it is needed to produce rhodium ethyl species which could further be converted into ethane (hydrogenation pathway) or interact with second ethylene molecule to yield C_4 chain (dimerization pathway). As we pointed out above, the closest analog to our supported catalyst are rhodium ethylene halide complexes which require proton source to operate.[38] In fact, the catalytically active species $[Rh(C_2H_4)_2(Cl)_2]^-$ are isoelectronic (i.e. also 16 electron species) to $Rh(C_2H_4)_2(acac)$ and

to supported $Rh(C_2H_4)$ complexes (since zeolite surface is considered as 3 electron donor in this case) indicating electronic and structural similarity between supported and unsupported complexes. Considering significant dependence of C4 olefins formation rate on partial pressure of hydrogen and the fact that dimerization according to beta-hydrogen transfer route (with participation of hydride ligand) is known for rhodium complexes in solution, [38] we could assume similar mechanism for supported complexes.

This alternative mechanism which we have to consider does not involve participation of ethylene molecule adsorbed on acid –OH group in dimerization catalysis but implies coordination of additional ethylene ligand to Rh center. In this case the complex has to retain 16 electrons configuration in order for dissociative addition of hydrogen to occur. We note that zeolite surface is regarded as 3 electron donor implying that metal interacts with one frame oxygen atom via covalent bond (contributing 1 electron to total electron count) and with –OH group via dative bond (contributing 2 electrons to total electron count). The dative bond is originating from the donation of lone electrons pair on oxygen of the –OH group to Rh and considered to be labile. According to the proposed pathway, additional ethylene molecule enters Rh coordination environment and essentially occupies coordination space which previously has been filled by the –OH group. At the next step dissociative addition of hydrogen occurs yielding $Rh^{III}(CO)(C_2H_4)_2(H)_2$ species and raising the total electron count up to 18 electrons. The following migration of hydride leads to the formation of ethyl group giving 16-electron $Rh^{III}(CO)(C_2H_5)(C_2H_4)(H)$ complex. Formation of C4 chain occurs via insertion of ethylene into $Rh\text{-}C_2H_5$ bond resulting in formation of $Rh^{III}(CO)(C_4H_7)(H)$ species. Since ethylene ligand is now converted vacating a coordination space on Rh and the formal electron count dropped to

14 electrons (which is nonstable electron configuration), we propose that at this stage –OH group recoordinates to metal raising the total electron count to 16 electrons. Finally, beta-elimination of hydrogen from butyl ligand yields butene-1 coordinated to Rh center in π mode which subsequently evolves in a gas phase leaving $Rh^{III}(CO)(H)_2$ complexes.

We note that this is a tentative mechanism which is alternative to one proposed by Serna et al and it does not involve surface –OH groups as active sites for dimerization catalysis. In order to clarify the reaction mechanism and, in particular, role of -OH groups we performed experiments when amount of acidic hydroxyls exposed to gas phase ethylene was varied. This can be done in two ways: either by using HY zeolites with different Si/Al ratios (which automatically implies different hydroxyls coverage) at constant Rh loading (1 wt %) or use same HY zeolite (HY30) and immobilize different amount of $Rh(CO)_2$ complexes (anchoring mechanism implies consumption of one acidic –OH group per one $Rh(CO)_2(acac)$ molecule reacted).

2.3.9 Ethylene Hydrogenation and Dimerization With HY15 and HY2.6 Supported Rhodium Complexes

Characterization of samples obtained after interaction of $Rh(CO)_2(acac)$ with zeolites having Si/Al ratio of 2.6 (HY2.6) and 15 (HY15) reported elsewhere[65] reveals that although supported $Rh(CO)_2$ complexes are structurally identical, two types of binding sites for $Rh(CO)_2$ species are present which were suggested to be due to different Al types/Al distribution in these zeolites. Catalytic tests were performed at 608 Torr of H_2 and 76 Torr of C_2H_4 under ambient conditions and demonstrated significant variation of catalytic activity with the HY family. Fig. 2.8 HY2.6 supported sample exhibited a sharp

spike in ethane and n-butenes formation rates with a maximum at approximately 30 minutes TOS followed by a rapid decline in activity. In case of HY15 supported sample the TOF maximum appeared at about 2.2 hours with a following moderate decline. We note that at maximum activity HY2.6 and HY15 supported rhodium species showed reaction rates 7.2 and 3.2 times higher than HY30 supported, respectively.

It is peculiar that the activity towards the formation of n-butenes follows the same trends as formation of ethane suggesting that both reactions could probably involve the same active site and both are likely affected by same factors. (Figures 2.9, 2.10 and 2.11) Consistent with our previous observations, butenes composition close to equilibrium achieved only at early stages of the reaction, namely, before maximum activity is reached and deactivation started to prevail. FTIR spectra in v(C-H) region collected on used samples show substantial difference in amount of accumulated hydrocarbons. (Fig. 2.15) More specifically, the integrated intensities of v(C-H) bands in case of HY2.6-based samples is significantly higher than on HY15, HY30-supported materials suggesting that Al rich zeolite promotes formation of oligomers which is consistent with observed deactivation pattern.

Such a significant difference in activities of HY zeolite-supported $Rh(CO)_2$ complexes exhibited in the initial period of the reaction is of particular interest. Since experimental conditions and metal loading were kept the same in these experiments, the observed difference in activity should be associated with different amount of –OH groups. The alternative explanation of this effect could be a change of active site structure (possible reduction of rhodium and formation of rhodium clusters or nanoparticles). However, rhodium clustering was not observed (vide infra).

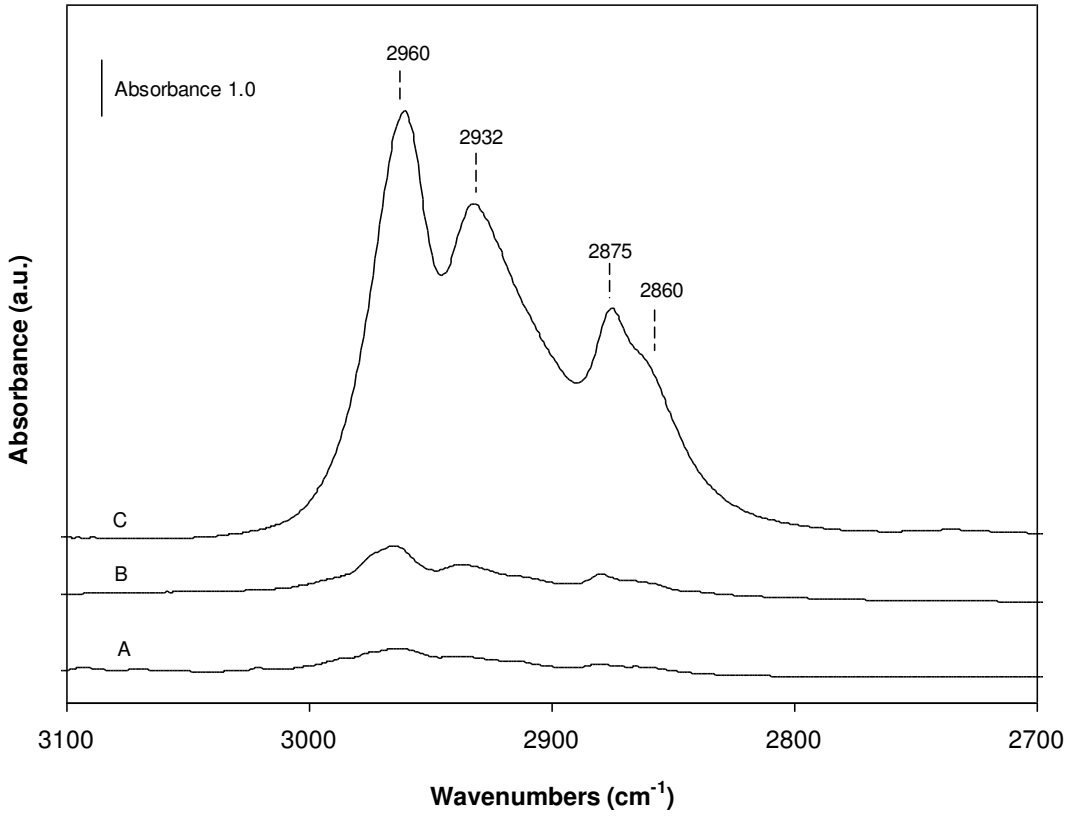

Fig. 2.15 FTIR spectra in the CH region of $Rh(CO)_2$/HY30(A), $Rh(CO)_2$/HY15(B), $Rh(CO)_2$/HY2.6 after reaction: 608 Torr of H_2 and 76 Torr of C_2H_4 for 20 h.

In order to understand whether rhodium aggregation is responsible for a boost in HY2.6 and HY15 based catalysts activity, XPS characterization of samples before and after reaction was performed. XPS results for fresh $Rh(CO)_2$ complexes supported on HY30, HY15, and HY2.6 indicated Rh 3d binding energy of 308.8 eV, 308.8 eV, and 308.5 eV, respectively, corresponding to rhodium in +1 oxidation state which is consistent with most literature reports.[66,67] XPS data on samples after reaction showed no evidence of Rh species with binding energy below 308.3 eV suggesting that rhodium

clustering is unlikely. Although we admit that formation of Rh_6 or Rh_4 clusters on HY supports could be a possibility (especially in case of Al reach supports such HY2.6), literature data suggest that the drop in the Rh 3d binding energy a of approximately 0.7 eV should be expected for $Rh(CO)_2$ to Rh_4/Rh_6 transformation.[68] Additionally, exposure of a used samples to a pulse of CO results in immediate reappearance of v(CO) bands with same integrated intensity as initial $Rh(CO)_2$ complexes regardless of a support indicating that structurally Rh sites remained unaltered. Although we do recognize that oxidative disruption of small Rh clusters with CO could occur, experiments with CO adsorption on Y zeolite-supported Rh clusters characterized by $N_{Rh-Rh} = 4.6$ revealed no evidence of this process taking place to a measurable extend.

Table 2.4 XPS data characterizing $Rh(CO)_2$ species supported on HY30, HY15, and HY2.6 zeolties after reaction in 608 Torr H_2, 76 Torr C_2H_4 for 20 h.

Sample	Rh $3d_{5/2}$, eV	FWHM, eV	Rh $3d_{3/2}$, eV	FWHM, eV
$Rh(CO)_2$/HY30	308.4	2.1	313.1	2.1
$Rh(CO)_2$/HY15	308.5	1.8	313.2	1.8
$Rh(CO)_2$/HY2.6	308.7	2.2	313.4	2.2

Thus, increase activity of HY15 and HY2.6 based materials should be attributed to the influence of the support. We note the striking similarities between plots showing rates of ethane formation (as well as trans- and cis-2-butene) in experiments with HY30 supported rhodium complexes performed at 607 Torr of H_2 and different C_2H_4 partial pressures (38 -152 Torr) and experiments carried out at 607 Torr of H_2/76 C_2H_4 with HY15 and HY2.6 supported samples. One of the possible explanations for these data

could be a purely kinetic factor of surface concentration of ethylene. Interaction of ethylene with Bronsted acid sites of zeolites is known and often reported as first step in ethylene dimerization mechanism over zeolties. Thus, one can assume that concentration of ethylene on the surface could be varied by either changing partial pressure of ethylene in a gas phase or by changing number of surface binding sites – hydroxyl groups.

If ethylene coverage at giving experimental conditions is not full (and we assume that at low partial pressure of ethylene this holds true) than the reaction rate (dimerization) should be defined by proximity of acid sites to Rh centers (-OH groups density) and partial pressure of ethylene in a gas phase. In case of HY30 zeolite, there is only about 1 Al atom and, therefore, only 1 –OH group per supercage.[69] The Rh loading of 1 wt% allows only for 1 Rh per 8 supercages making the probability of close location of Rh to a –OH group in case of HY30 small. In case of HY15 and HY2.6 materials, there are approximately 2 and 6 Al atoms per supercage[69], respectively, making the likehood of close proximity of Rh and Brønsted acid site higher.

Finally, we have to acknowledge the possible effect of extraframework Al species (EFAL). It is proposed that up to 50 % of Al atoms in HY2.6 zeolite are nonframework and exist as EFAL species [69] which could serve as binding sites for supported $Rh(CO)_2$ complexes. Although the exact role of EFAL species in catalytic performance of supported Rh complexes in hydrogenation and/or dimerization reaction is not clear, it is reported that Y zeolites with high EFAL content greatly enhance hydrogen transfer reactions (H/D exchange etc) at elevated temperatures.[70,71] One of the proposed explanations attributes this effect to so called “superacidity” of bridging Al-OH-Si hydroxyls due to close proximity of these sites to the the extraframework AlOH species

(Lewis acid sites).[72] However, since all our experiments were conducted under ambient conditions, we consider such effects negligible.

One of the possible ways to elucidate whether Brønsted –OH groups are responsible for enhanced activity of HY2.6 supported sample would be to make them inaccessible for ethylene molecules, i.e. to block them with another more strongly binding molecule. This can be done by using water as it was reported that water and ethylene compete for Bronsted acid sites and physisorbed water prevents the adsorption of the olefin.[73] The ultimate condition that has to be met in this case is that water must not interact with Rh sites and we showed previously that, unless water is present in a gas phase, it does not coordinate to Rh species.[65] In order to prepare samples with different water content, the HY2.6 zeolite was subject to pretreatments at deferent calcination temperatures before $Rh(CO)_2$ complexes were immobilized on its surface (100, 200, 300 and 400 ºC). FTIR spectrum characterizing sample treated at 100°C revealed the presence substantial amounts of water as evidenced by infrared bands at approximately 3500 and 1630 cm^{-1} assigned to stretching and bending vibrations, respectively, of H_2O molecules hydrogen-bonded to zeolite –OH groups. (Fig. 2.16 and 2.17) The sample treated at 200°C showed significant decline in intensity of bands characterizing H_2O while new features emerged at 3630 and 3565 cm^{-1} designating acidic hydroxyls. Finally, samples after thermal treatments in the 300-400°C temperature range revealed no evidence of surface-bound H_2O. Catalytic performance of those materials measured. These data indicate that there is about 30 % drop in ethane formation rate at maximum activity for sample treated at 100 ºC if compared to samples calcined 200 ºC, 300 ºC, and 400 ºC and deactivation patterns for all four samples are very similar.

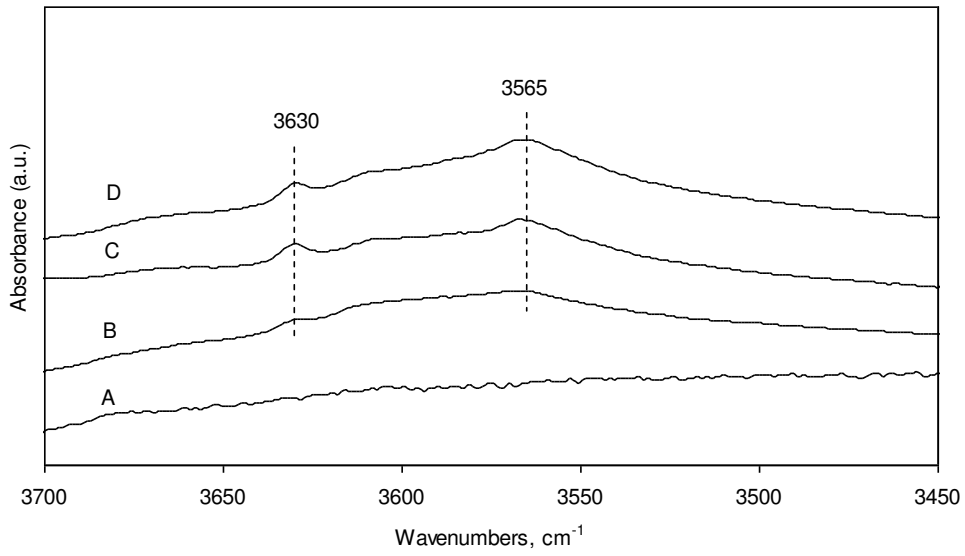

Fig. 2.16 FTIR spectra in the OH region of $Rh(CO)_2$/HY2.6 sample obtained by reaction of $Rh(CO)_2$(acac) with HY2.6 zeolite calcined at 400 ºC (A), 300 ºC (B), 200 ºC (C), and 100 ºC (D).

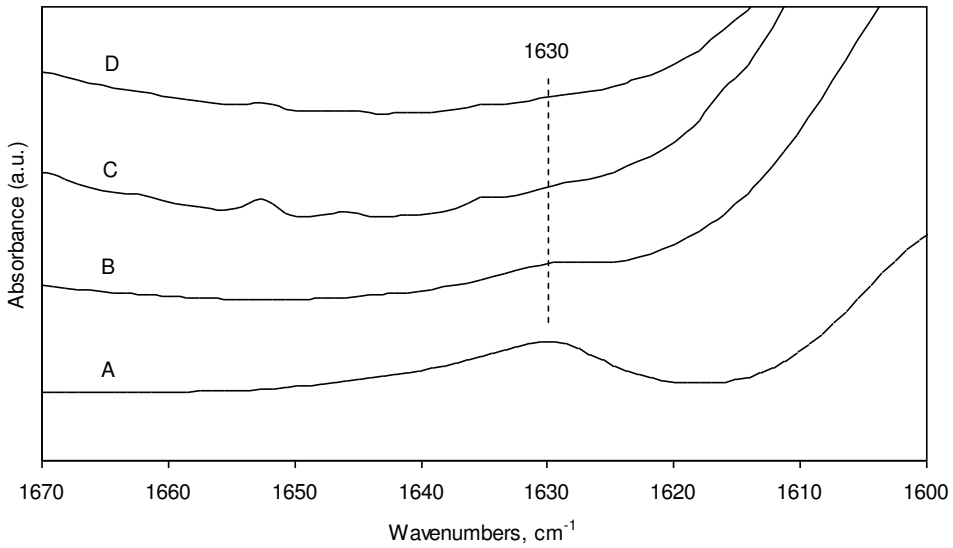

Fig. 2.17 FTIR spectra in the H_2O region of $Rh(CO)_2$/HY2.6 sample obtained by reaction of $Rh(CO)_2$(acac) with HY2.6 zeolite calcined at 100 ºC (A), 200 ºC (B), 300 ºC (C), and 400 ºC (D).

There is also a relatively small decrease in activity towards trans-2-butene and cis-2-butene formation (Catalytic results are presented in Figs .2.18, 2.19 and 2.20) and virtually no change in TOF of butene-1 formation for H_2O rich sample (100 ºC calcined). (Fig. 2.21) These catalytic results certainly suggest that blocking Bronsted acid sites with water does indeed influence the catalyst activity in both ethylene hydrogenation and dimerization reactions although the magnitude of the observed effect is not huge.

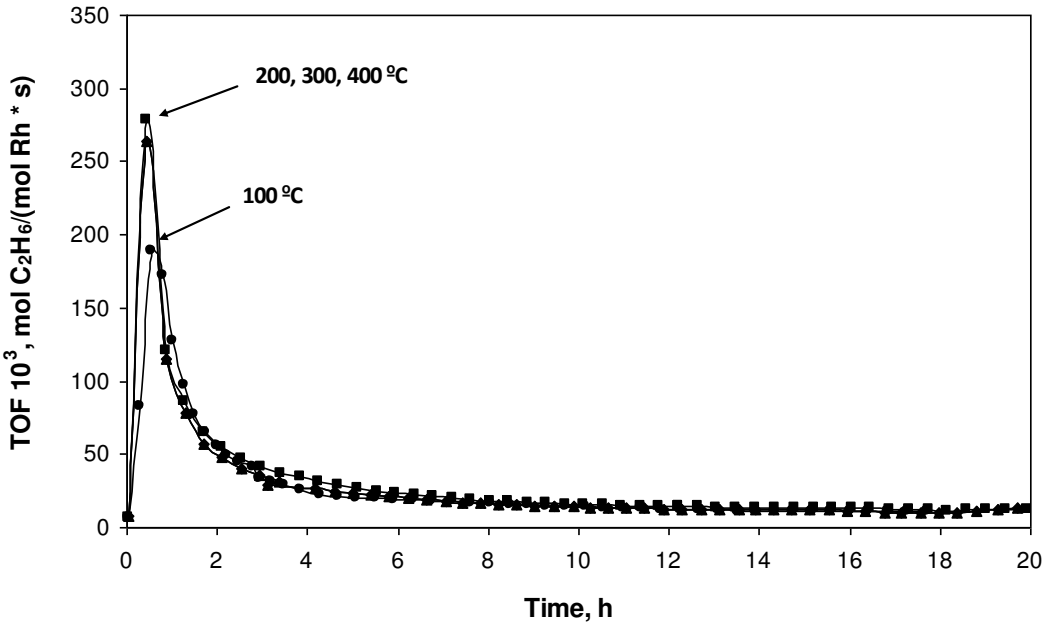

Fig. 2.18 Turn Over Frequencies (TOF) for ethane formation with Time on Stream (TOS) for $Rh(CO)_2$/HY2.6 sample with HY2.6 zeolite calcined at 100 ºC (●), 200 ºC (■), 300 ºC (▲), and 400 ºC (♦).

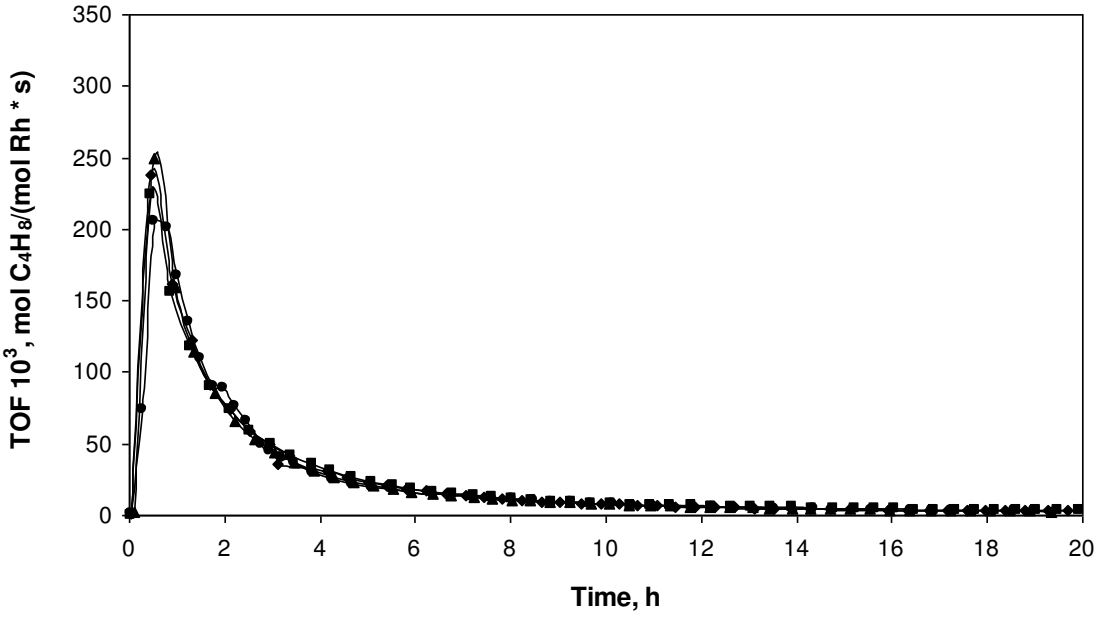

Fig. 2.19 Turn Over Frequencies (TOF) for Trans-2-butene formation with Time on Stream (TOS) for $Rh(CO)_2$/HY2.6 sample with HY2.6 zeolite calcined at 100 ºC (●), 200 ºC (■), 300 ºC (▲), and 400 ºC (♦).

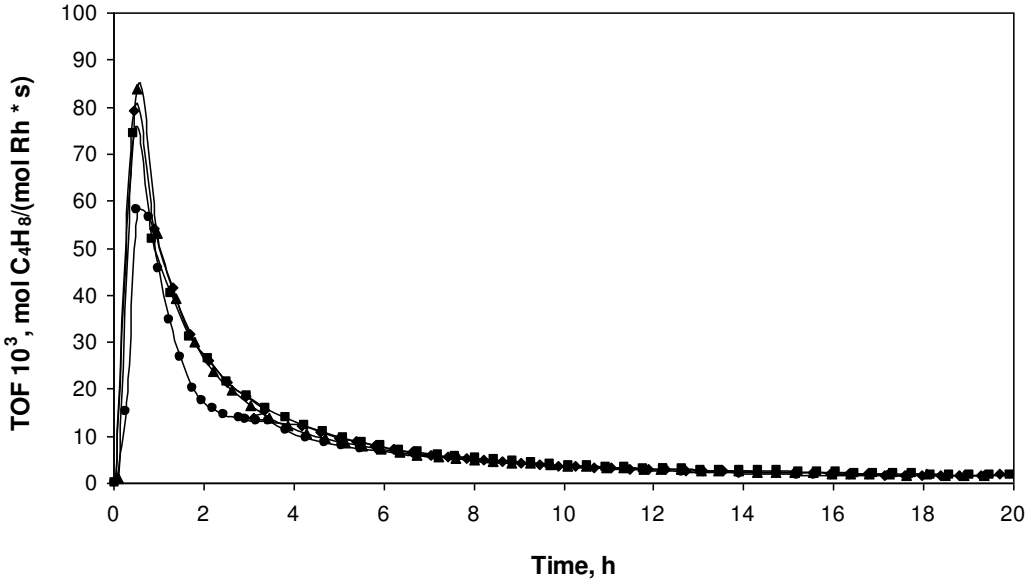

Fig. 2.20 Turn Over Frequencies for cis-2-butene formation with Time on Stream (TOS) for $Rh(CO)_2$/HY2.6 sample with HY2.6 zeolite calcined at 100 ºC (●), 200 ºC (■), 300 ºC (▲), and 400 ºC (♦).

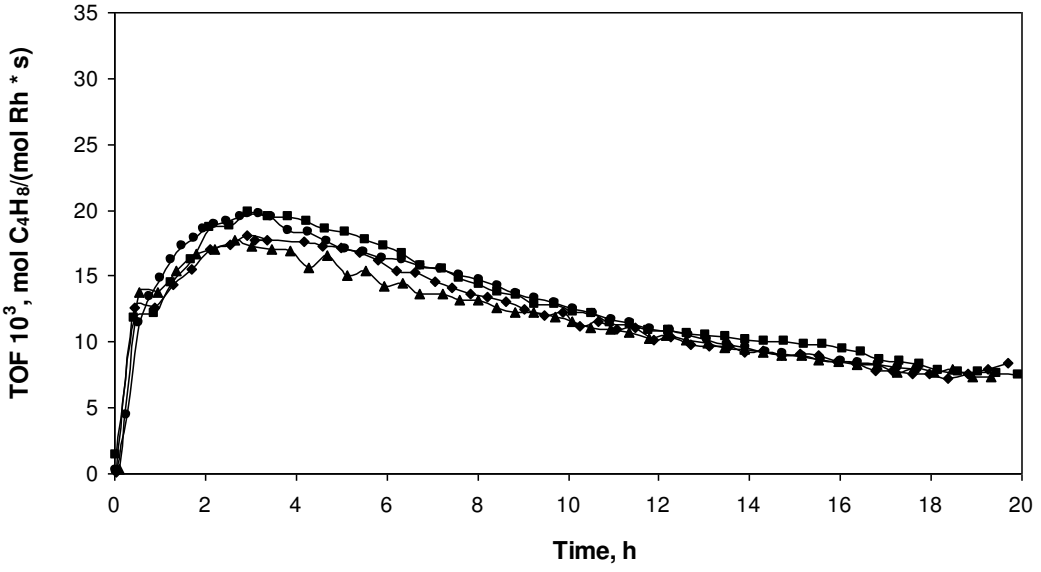

Fig.2.21 Turn Over Frequencies of Butene-1 formation with Time on Stream (TOS) for $Rh(CO)_2$/HY2.6 sample with HY2.6 zeolite calcined at 100 ºC (●), 200 ºC (■), 300 ºC (▲), and 400 ºC (♦).

2.3.10 Catalytic Ethylene Hydrogenation and Dimerization on HY30 Zeolite-Supported Rhodium Dicarbonyl Complexes with Variable Rhodium Loadings

The alternative way to vary amount of acidic hydroxyls that could serve as binding sites for ethylene molecules and participate in dimerization catalysis would be to immobilize different amount of $Rh(CO)_2(acac)$ complexes. We note that protonation of the acetylacetonate ligand by the bridging –OH group is the only expected and known pathway for complex immobilization. It means that each zeolite has only a certain number of sites capable of accommodating Rh complexes. In order to reveal the maximum Rh uptake when complexes are still chemically bound to the oxygens around aluminium atom, FTIR measurements of samples prepared by interaction of HY zeolite with different amount of $Rh(CO)_2(acac)$ were conducted. We used zeolite with the lowest Al content in a framework (HY30) where limiting chemisorption capacity is expected at reasonably low Rh loadings.

FTIR spectra in v(CO) region for samples with 1, 2, 3 and 4 % wt of Rh are presented in Fig 2.22. For samples with 1 and 2 % wt of Rh only bands at 2117 and 2053 cm^{-1} are observed suggesting the presence of anchored $Rh(CO)_2$ species. As Rh loading was increased to 3 and then to 4 % wt, two new band pairs appeared in spectra. More specifically, for the sample with 3 % wt of Rh the bands at 2107, 2039 cm^{-1} and 2093, 2025 cm^{-1} were detected indicating partially reacted and unreacted $Rh(CO)_2(acac)$ complexes. Similar features were observed for the sample with 4 % wt loading (2105, 2038 cm^{-1} and 2090, 2024 cm^{-1}), in this case however intensities of bands at 2090 and 2024 cm^{-1} characterizing physisorbed $Rh(CO)_2(acac)$ complexes are increased.

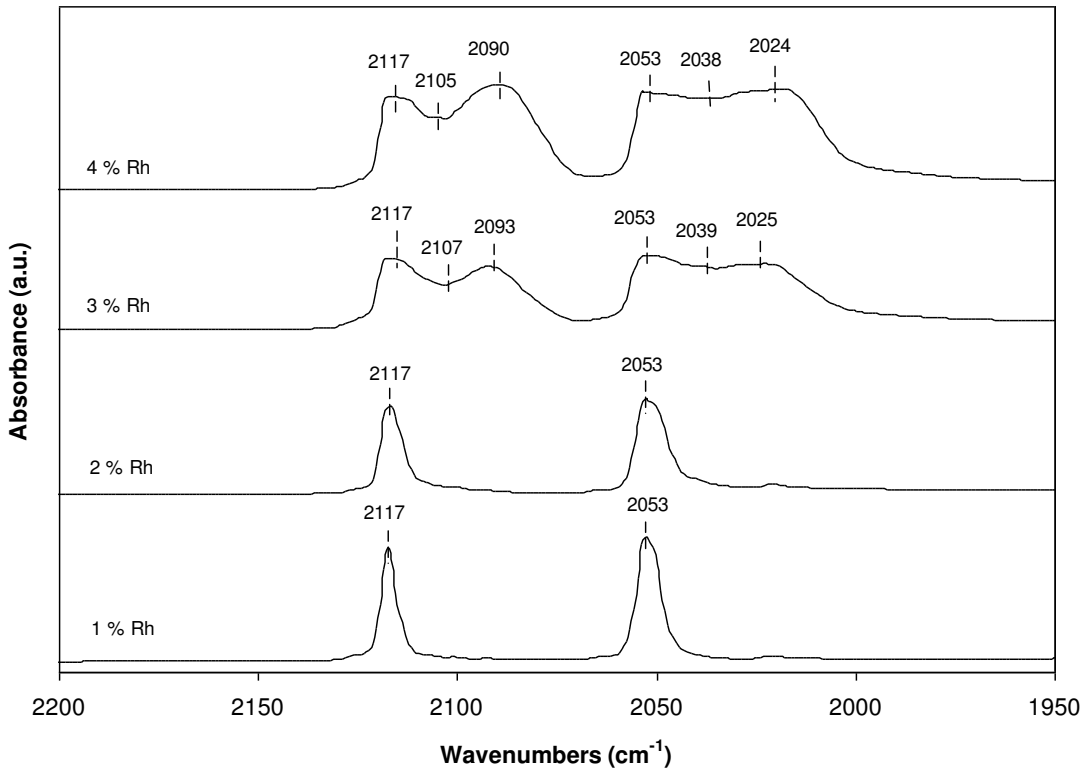

Fig.2.22 FTIR spectra of the CO region of $Rh(CO)_2$/HY30 at different Rh loading: 1, 2,3,and 4 %wt.

The above mentioned results suggest that the maximum capacity of HY30 zeolite towards chemisorption of precursor complexes is somewhere between 2 and 3 % wt and, therefore, the following catalytic testing was performed for the sample with 2 % wt Rh loading. Catalyst activity in both ethylene hydrogenation and ethylene dimerization was evaluated at 76 Torr of C_2H_4 and 608 Torr of H_2 under ambient conditions (as described before). Fig 2.23 compares activities of HY30 supported $Rh(CO)_2$ species at 1 % and 2 % wt Rh loadings and indicates that the rate of ethane formation experienced about 50 % drop as Rh loading increased from 1 to 2 % wt. Similar pattern was observed for the rate of n-butenes formation (butene-1, trans-2-butene and cis-2-butene),

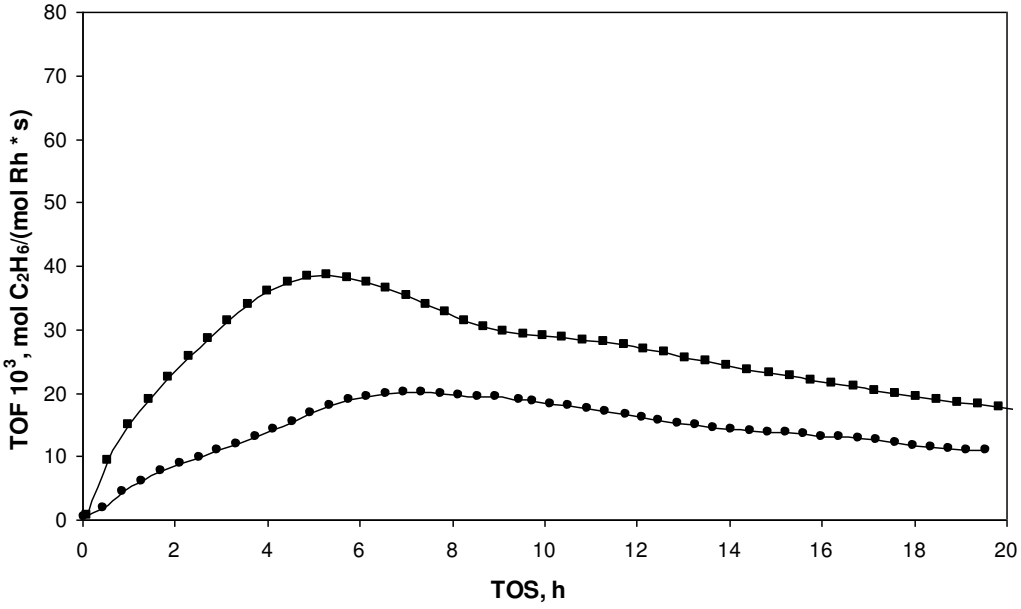

Fig.2.23 Rates (Turn Over Frequencies) of ethane formation with Time on Stream (TOS) for $Rh(CO)_2$/HY30 with 1 % wt Rh(●), 2% wt Rh(■).

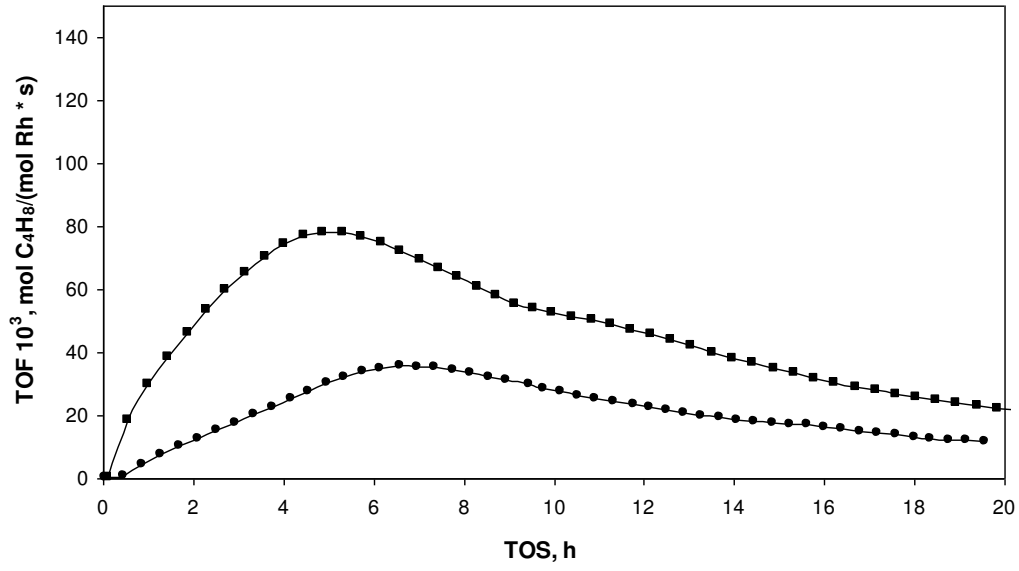

Fig.2.24 Rates (Turn Over Frequencies) of Butenes (Trans-2-butene, Cis-2-butene, Butene-1) formation with Time on Stream (TOS) for $Rh(CO)_2$/HY30 with 1 % wt Rh(●), 2% wt Rh(■).

These data imply that both processes follow the same trend, confirming our conclusion that they probably through very similar intermediates. We note that the observed behavior is consistent with activities detected for $Rh(CO)_2$ complexes supported on HY zeolites with different Si/Al ratios but, in fact, demonstrates the reverse trend - decrease in the rate of dimerization and hydrogenation with decrease of acidic hydroxyls coverage. Such a strong dependence of the dimerization rate on the amount of surface –OH groups points out to the key role of these sites in dimerization catalysis.

To explore this further, we plotted the hydrogenation and dimerization activity of $Rh(CO)_2$ supported on HY 30, 15 and 2.6 against the Si/Al ration (which is essentially inversely proportional to the total number of Bronsted acid sites in the zeolite). These results are summarized in Figs. 2.25 and 2.26.

These results fully confirm and strengthen our previous findings. They show almost perfect linear dependence of the dimerization activity on the amount of Bronsted acid groups which is in line with the results obtained by Cramer for ethylene dimerizarion on the rhodium complex in solution in the presence of acid. This is the direct analogy of the supported sample to the organometallic complex in solution. Also, there is clearly a straightforward dependence of the hydrogenation pathway on the amount of Bronsted acid sites.

In summary, we can conclude that ethylene dimerization and hydrogenation involves both Rh complexes and –OH groups of the zeolite as active sites.

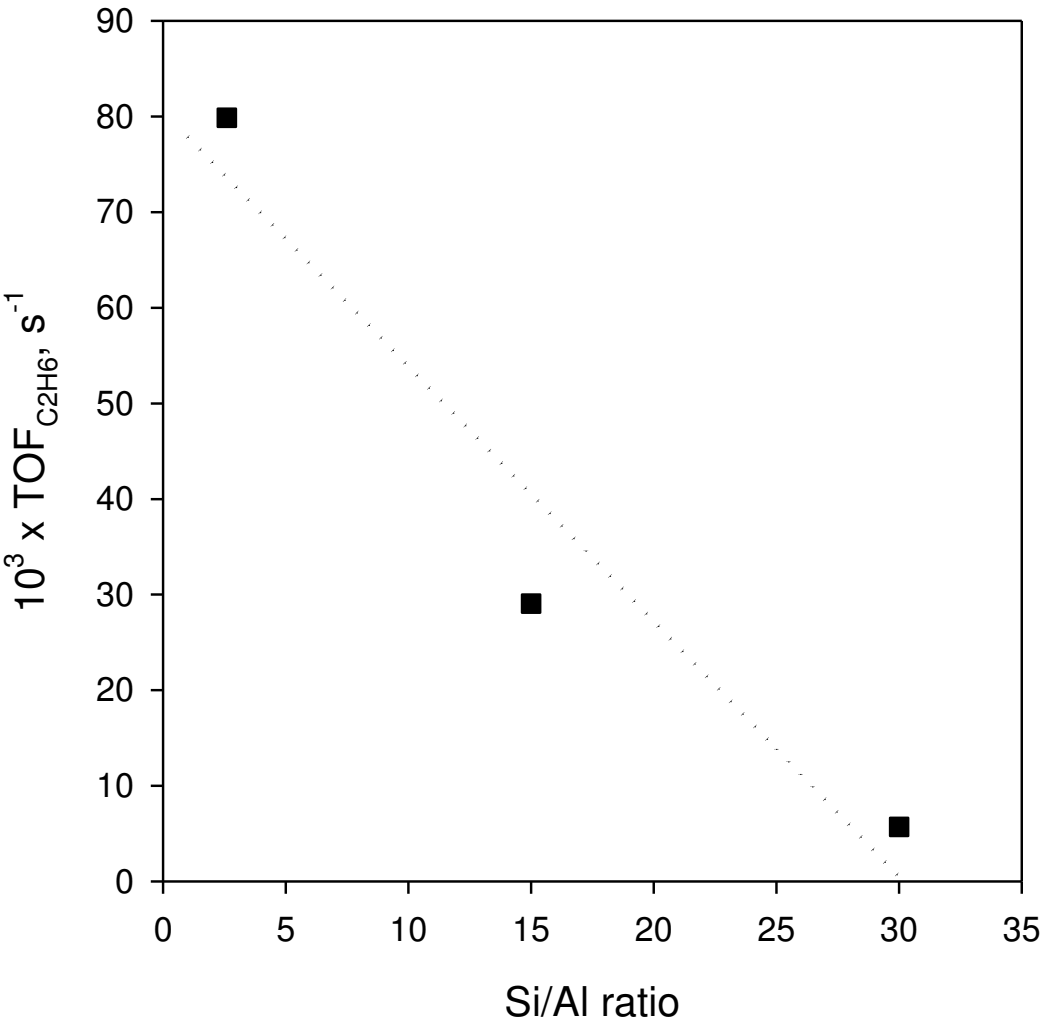

Fig. 2.25 Hydrogenation activity of HY zeolite-supported $Rh(CO)_2$ complexes as a function of Si/Al ratio. (Reaction conditions: 25°C; GHSV= 60000 ml/g·h; feed composition: 76 Torr C_2H_4/608 Torr H_2.

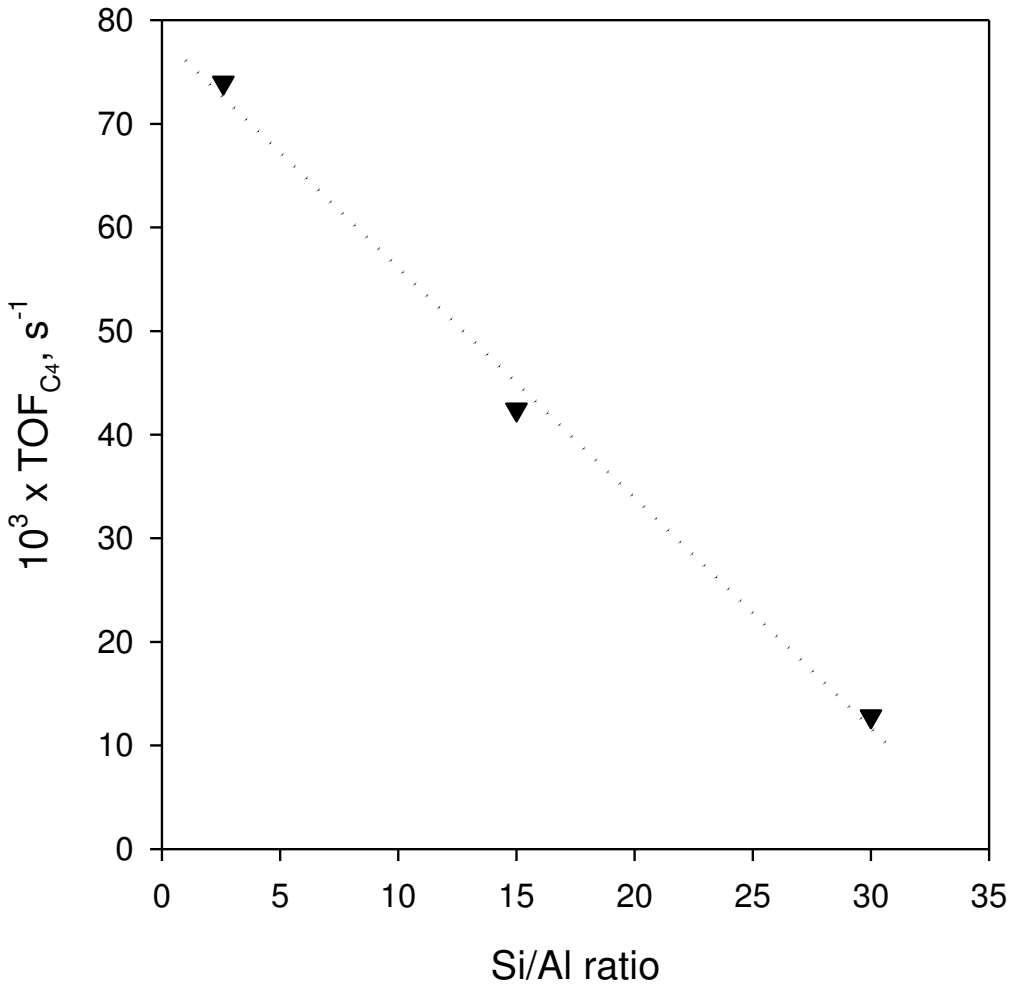

Fig. 2.26 Dimerization activity of HY zeolite-supported $Rh(CO)_2$ complexes as a function of Si/Al ratio. (Reaction conditions: 25°C; GHSV= 60000 ml/g·h; feed composition: 76 Torr C_2H_4/608 Torr H_2/He balance; total C_2H_4 conversion below 5%).

2.3.11 Tuning Selectivity of Ethylene Dimerization Pathway on $Rh(CO)_2$ HY30 Supported Complexes

Tuning the selectivity of a chemical reaction promoted by homogeneous catalyst is normally achieved by modifying electronic and/or steric properties of a metal complex.[74,75] This implies detailed understanding of a reaction mechanism and reactivity of modified catalyst. The mechanism of ethylene dimerization discussed above suggests cooperative action of Rh complex and neighboring –OH group implying that both sites have to be located in close proximity to each other.

One of the more selective approaches to modifying the selectivity to the dimerization pathway would be to "switch off" –OH groups. This can be done using trimethylchlorosilane which is known to selectively react with –OH groups of the surface to form $–Si(CH_3)_3$ groups on the surface with a quantitative yield:

$$S\text{-}OH + Si(CH_3)_3Cl \rightarrow S\text{-}O\text{-}Si(CH_3)_3 + HCl$$

Three samples were produced, in which the desired amount of –OH functionalities was switched off prior to the reaction (with respect to 1% Rh amount): 20, 80 and 100 percent respectively. The selectivity trends are summarized in Table 2.5.

The selectivity trend suggests that we have been able to progressively turn off the dimerization pathway by blocking the -OH Bronsted acid groups and achieved 100% selectivity to ethane when all –OH groups were blocked. It finally sets the record clear and proves the dimerization pathway proceeds only in the presence of –OH groups on the surface while ethane dimerization proceeds with and/or Bronsted acidic surface hydroxyls. Further clarification of the question pertaining to ethane formation in the presence or absence of OH groups is provided in the next chapter.

Table 2.5 Selectivity at steady-state for C_2 and C_4 products on $Rh(CO)_2$/HY30.

%-OH group switched off	Ethane, TOF*10^3 s^{-1}	C_4 products, TOF*10^3 s^{-1}	Ethane Selectivity, %	C4 Products Selectivity, %
0	5.6	12.8	31	69
20	6.8	1.7	80	20
80	5.0	1.4	80	20
100	6.8	0	100	trace

2.3.12 Revised Mechanism of Ethylene Hydrogenation and Dimerization by HY Zeolite-Supported $Rh(CO)_2$ Complexes

STEM imaging of Rh(CO)2/HY30 catalysts after catalysis shows lack of rhodium segregation/clustering after catalysis (Fig. 2.27). The mononuclear nature of the catalytic center is finely preserved during catalysis.

Also, the comparison of the ethylene hydrogenation catalytic activity for the HY30 Supported $Rh(CO)_2$, $Rh(CO)(C_2H_4)$ and $Rh(CO)H_x$ catalysts is presented in Fig. 2.28. These data reveal that despite the initially variable ligand environment around the metal center, at steady state the ethane related activity for all the catalysts is the same. It means that eventually the same intermediates are present on the surface, most likely Rh(CO) or $Rh(CO)(C_2H_4)$. The initial rapid hydrogenation of ethylene on $Rh(CO)H_x$ catalyst clarifies the ability of Rh hydrides to quickly hydrogenate gas phase ethylene and form ethane, this is probably how ethylene can be hydrogenated in the absence of acidic protons on the surface (when we switch off all protons).

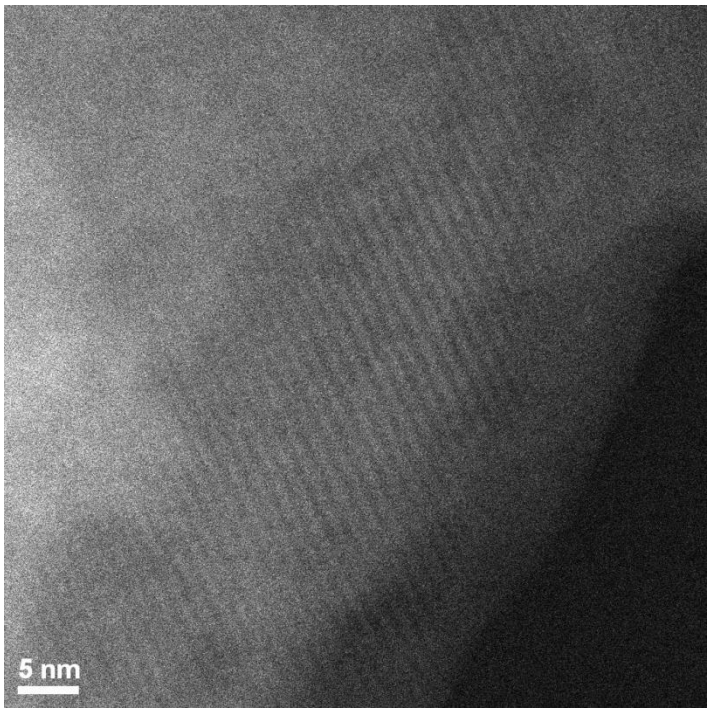

Fig. 2.27 High-angle annular dark-field (Z-contrast) STEM image of $Rh(CO)_2$/HY30 after 20 h catalysis. The image shows only individual Rh atoms and no Rh clusters.

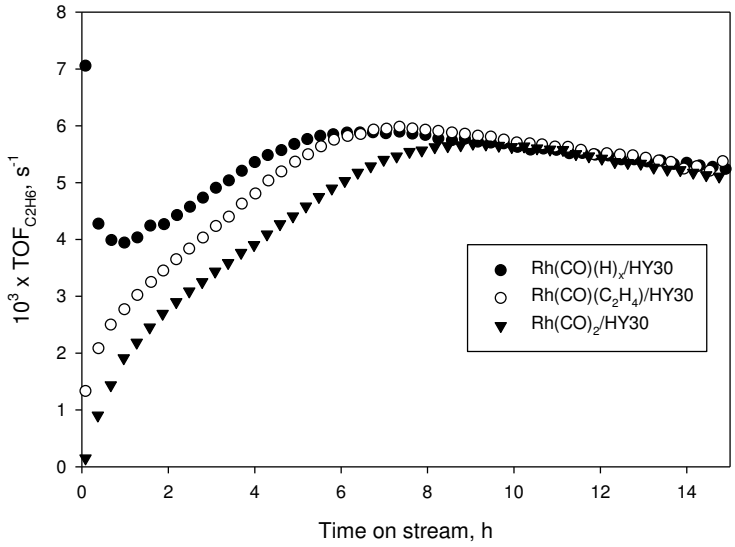

Fig. 2.28 Hydrogenation activity of different HY30 zeolite-supported Rh complexes as a function of time on stream. (Reaction conditions: 25°C; GHSV= 60000 ml/g·h; feed composition: 76 Torr C_2H_4/608 Torr H_2).

Knowing this and all the previous collected data, a revised mechanism displaying the network of reactions for ethylene hydrogenation/dimerization can be drawn (Fig. 2.29)

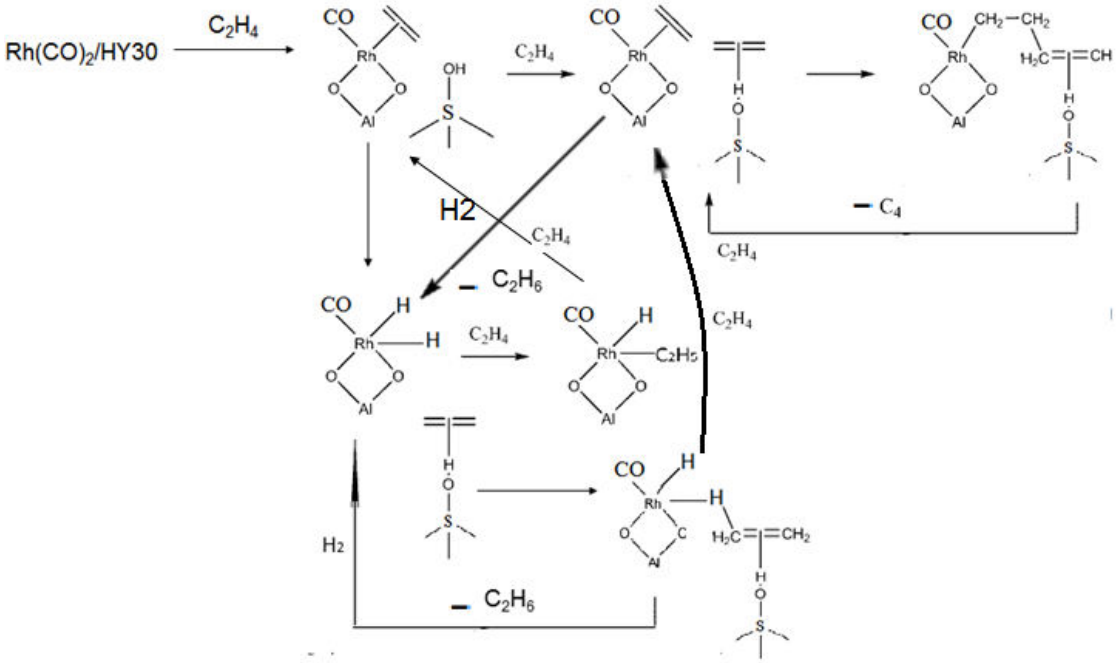

Fig. 2.29 The catalytic ethylene hydrogenation and dimerization network on $Rh(CO)_2$/HY complexes. C4 products form only via surface assisted pathway. Ethane forms on single Rh site (via reduction elimination route) as well as on the Rh/Surface cooperative site.

2.4 Conclusions

HY zeolite-grafted rhodium dicarbonyl, carbonyl ethylene and carbonyl hydride complexes are active in both ethylene hydrogenation and dimerization under ambient conditions. The Bronsted acidic groups of support are of crucial importance in defining catalytic functions of supported rhodium carbonyl complexes for the dimerization pathway, and partially, for the hydrogenation one. More specifically, HY zeolite and

Al_2O_3-supported rhodium species exhibit very different surface chemistry and, as a result, different catalytic properties which are proposed to be due substantially different electron withdrawing properties of these supports. Activity measurements revealed that Al_2O_3-anchored $Rh(CO)_2$ complexes are inactive in ethylene hydrogenation and dimerization. Kinetic data acquired on HY zeolite-supported catalyst indicate that ethane and C_4 formation rates depend on partial pressure both hydrogen and ethylene of suggesting that probably both reactions involve Rh-H species as active intermediates. Inverse Kinetic Isotope effect value for both C_2 and C_4 products confirms this conclusion. The role of the support in dimerization mechanism was investigated in experiments where amount of acidic –OH groups available for ethylene adsorption was varied. These results conclusively demonstrated that zeolite surface is involved in the C-C bond formation reaction and revealed the bifunctional nature of HY zeolite-supported rhodium species in ethylene dimerization. Finally, we demonstrated that catalytic activity of HY zeolite-supported $Rh(CO)_2$ complexes can be tuned by modifying the amount of acidic –OH groups and the dimerization pathway can be switched off completely.

CHAPTER 3. SYNTHESIS AND CHARACTERIZATION OF HY ZEOLITE SUPPORTED RHODIUM DINITROSYL COMPLEXES AND THEIR USE AS CATALYSTS FOR ETHYLENE HYDROGENATION AND DIMERIZATION

3.1 Preface

HY Zeolite-supported mononuclear $Rh(NO)_2$ complexes can be selectively formed upon exposure of $Rh(CO)_2$/HY to the gas phase NO/He. They are structurally similar to $Rh(CO)_2$/HY with Rh(I) retaining square planar geometry and nitrosyl ligands adopting a linear configuration. N-Rh-N angle on average is slightly larger than the C-Rh-C angle for analogous rhodium carbonyl complexes. Two types of species are formed on the support as evidenced by deconvolution of the FTIR ν_{NO} region.

The ratio between type I and type II species depends on Si/Al ratio, although not as drastically as for $Rh(CO)_2$/HY. $Rh(NO)_2$/HY30 is active in ethylene hydrogenation and ethylene dimerization under ambient conditions. This is the first unprecedented example of supported transition-metal nitrosyl complex capable of performing a catalytic reaction. Moreover, this is the first example of a site-isolated Rh complex with ligands other than ethylene or carbonyl, which can catalyze both ethylene hydrogenation and dimerization. Unlike its dicarbonyl counterpart, dinitrosyl rhodium complex has a uniquely different reactivity

towards ethylene and hydrogen, that is, it activates hydrogen without hydride formation (and ethylene weakly bonds to it).

At steady state, it shows higher activity (0.01 vs 0.0056 s^{-1}) and selectivity (60% vs 32%) towards ethane formation. The zeolite support appears to play an important role for both dicarbonyl and dinitrosyl Rh species. Activity measurements performed on HY zeolite-supported catalyst at 76-608 Torr of H_2 and 38-152 Torr of C_2H_4 uncover dependence of both hydrogenation and dimerization pathways on partial pressure of hydrogen while the dimerization pathway shows a greater dependence on the partial pressure of ethylene.

The mononuclear site-isolated nature of the Rh species is preserved even after 20 hours of continuous catalysis as evidenced by FTIR data and HAADF-STEM images of the used catalyst. .That is, for the first time, the precise variation of the ligand (and therefore electronic) environment around a single metal center anchored to the support (the concept ubiquitous in solution organometallic chemistry) has been achieved on a single site scale in heterogeneous catalysis and its effects on structure-catalytic property relationships have been unambiguously studied for $Rh(CO)_2$/HY30 and $Rh(NO)_2$/HY30 .

3.2 Introduction

The idea of having a mononuclear single-site catalyst that retains its integrity during catalysis is very attractive[1-4]. Indeed, multiple liquid phase catalytic processes with organometallic complexes are known, such as methanol carbonylation (the so-called Monsanto process)[5] on single-site $[Rh(CO)_2I_2]^-$ complexes and hydroformylation (which

remains the largest homogeneous catalytic process in the world with more than 15 billion tons of aldehydes and alcohols produced on yearly basis) on various single-site Co and Rh hydride complexes[6,7]. Such processes with 100% dispersion of essentially molecular metal species offer remarkable activity and selectivity but have a few drawbacks: catalysts often suffer fast deactivation, and the separation of reagents and products can be very tricky[8]. Heterogeneous catalysts, on the other hand, often demonstrate improved stability and ease of product/catalyst separation. Therefore, significant effort has been invested into preparation of heterogeneous analogues of molecular complexes: such species are considered molecular in nature often allowing for similar reactivity patterns as exhibited by their molecular precursors in solution[9-11]. Pioneered by Basset and Gates, this approach proved fruitful for some areas like alkane and olefin methathesis, olefin hydrogenation and polymerization. For instance, Gates and coworkers were the first to demonstrate that HY-zeolite supported $Rh(C_2H_4)_2$ and $Ir(C_2H_4)_2$ complexes exhibit activity not only in ethylene hydrogenation but also in ethylene dimerization to a mix n-butenes.[12,13] Activity of supported single-site Rh and Ir complexes in ethylene dimerization in absence of halides and presence of hydrogen is a truly unique feature, since the only known Rh complex to run this reaction is $Rh(C_2H_4)_2Cl$ dimer[14].

We showed earlier that the whole family of RhL_2/HY complexes ($Rh(CO)_2$, $Rh(CO)(C_2H_4)$, $Rh(CO)H_x$) was also capable of catalyzing ethylene hydrogenation and dimerization. Moreover, despite the initially different ligand environment around the metal center, all these catalysts had exactly the same activity patterns at steady-state due to the common nature of intermediates formed[15,16].

CO and C_2H_4 ligands are quite ubiquitous in organometallic catalysis[17-19] in solution. Since we already explored their influence on reactivity in the heterogeneous gas phase catalysis[15,16], we decided to shift our focus to ligands not so common such as NO (nitrosyl). NO binding to metal sites on extended metal surfaces[20,21] and in a large number of organometallic compounds[22-24] has been a well-studied topic. Any kind of catalysis by organometallic complexes with NO ligands in liquid phase, however, remains a very obscure field. Only few examples exist in the literature of successfully employing $Rh(NO)_x$ complexes in catalysis. One of them is cyclohexene hydrogenation with 100% hydrogen in dichloromethane at room temperature by tris(triphenylphosphine)nitrosyl rhodium[25] The other one is CO_2 hydrogenation at 50 °C and 3 bar with equimolar CO_2/H_2 by a Rh(NO) complex with a chelating tridentate phosphine ligand[26]. The mechanism of these transformations is poorly understood, although in the latter case it is believed to involve Rh(NO) hydride intermediates[26].

For the first time, we demonstrate the pathway to selectively prepare the family of supported square planar $Rh(NO)_2$ complexes supported on HY 30, 15 and 2.6 and show that two different types of rhodium dinitrosyl species form on all supports; the ratio between type I and type II rhodium dinitrosyl species mildly depends on the degree of dealumination.

Also, we show the first of its kind unprecedented activity of single-site $Rh(NO)_2$/HY30 complexes in ethylene hydrogenation and dimerization. Activity in ethylene hydrogenation/dimerization and selectivity to products therefore can be tuned by subtly modifying coordination environment of supported $Rh(XO)_2$ species exemplifying the validity of truly molecular engineering approach to heterogeneous catalysis.

3.3 Experimental Methods

3.3.1 Reagents and Materials

Dicarbonylacetylacetonato rhodium (I) $Rh(CO)_2(acac)$ (acac = $C_5H_7O_2$) (Strem, 98% purity) was used as supplied. n-Pentane (Aldrich, 99% purity) and tetrahydrofuran (Aldrich, >99.9 %) were refluxed under N_2 in the presence of Na/benzophenone ketyl to remove traces of moisture and deoxygenated by sparging of dry N_2 prior to use. All glassware used in preparation steps was previously dried at 120°C. He, NO, H_2 and C_2H_4 (Airgas, all UHP grade) were additionally purified to their use by passage through oxygen/moisture traps (Agilent) capable of removing traces of O_2 and water to 15 and 25 ppb, respectively. CBV760, CBV720, and CBV600 dealuminated HY zeolites (Zeolyst International) with Si/Al atomic ratios of 30, 15, and 2.6, respectively, were calcined in flowing O_2 at 400°C for 5 h and then evacuated at 10^{-3} Torr and 400°C for 16 h. For simplicity, these zeolite supports are further denoted as HY30, HY15, and HY2.6, respectively. All treated supports were stored and handled in a glovebox (MBraun) filled with dry N_2. The residual water and O_2 concentrations in the glovebox were kept below 0.1 ppm.

3.3.2 Preparation of Supported Samples

The syntheses and sample transfers were performed with exclusion of air and moisture on a double-manifold Schlenk line and in a N_2-filled MBraun glove box. Supported samples were prepared by slurrying the $Rh(CO)_2(acac)$ precursor with a

corresponding powder support in n-pentane under N_2 for 24 h at room temperature, followed by overnight evacuation at 25°C to remove the solvent. In each case, the $Rh(CO)_2(acac)$ precursor was added in the amount needed to yield samples containing 1 wt% Rh. The Rh weight loading was verified by inductively coupled plasma-mass spectrometry (ICP-MS) analysis (Galbraith Laboratories Inc.).

Reaction between NO and HY30-supported $Rh(CO)_2$ complexes was performed in plug-flow pyrex reactor. All prepared samples were stored and handled in a glovebox filled with N_2 to prevent possible contamination and decomposition of supported species.

3.3.3 FTIR Spectroscopy

A Nicolet Nexus 470 spectrometer equipped with a MCT-B detector cooled by liquid nitrogen was used to collect spectra with a resolution of 2 cm^{-1}, averaging 64 scans per spectrum. Each powder sample was pressed into a self-supported wafer with a density of approximately 20 mg/cm^2 and mounted in a home-made cell connected to a gas distribution manifold. The cell design allowed for the treatment of samples at different temperatures, while various gases flowed through the cell.

3.3.4 Mass-Spectrometry Measurements

Mass spectrometry (MS) measurements were used to monitor ligand exchange reactions between surface species and different gases and to identify

the products released during such reactions. In a typical experiment, approximately 100 mg of the sample was loaded into a plug-flow micro reactor in a glovebox and the reactor was sealed to avoid air exposure. The reactor was subsequently connected to a gas distribution system equipped with mass flow controllers and an online Inficon Transpector 2 residual gas analyzer operating in a multi-ion detection mode. Before each experiment, the reactor was purged with He (100 ml/min) at 25 °C and atmospheric pressure for 1 h to stabilize the baseline mass spectrometer signal. When this procedure was completed, various feeds (as specified in the text) were introduced into the reactor at 25 °C and a flow rate of 100 ml/min. The feed and effluent compositions were routinely monitored with time on stream to detect CO (m/z= 28) and NO (m/z= 30).

The m/z values shown in brackets and listed in increasing order of their relative intensities and correspond to the most abundant lines in the fragmentation pattern of each species.

3.3.5 Catalytic Tests

Catalytic activity measurements of C2H4 hydrogenation were performed in a quartz single-pass fixed-bed reactor at atmospheric pressure and room temperature. The temperature inside the reactor was monitored by a thermocouple inside the reactor touching the catalyst bed. Samples in powder form (0.1 g) were loaded in a glovebox and the reactor was sealed to avoid air exposure. The total volumetric flow rate of the reactant mixture (608 Torr H2/ 76 Torr C2H4/balance N2) was held at 100 ml/min (1atm, 25°C), yielding a corresponding Gas Hourly Space Velocity (GHSV) of 6,000 h^{-1}. The feed and

the reaction products were analyzed with an on-line gas chromatograph (HP 7890 A, Agilent) equipped with TCD and FID detectors and two capillary columns. A Rt-Alumina column (50m, 0.53 mm ID, Restek) was used for the analysis of hydrocarbons, while a Carboxen 1010 Plot column (30m, 0.53 mm ID, Supelco) was used for the analysis of hydrogen. In the absence of a catalyst, there was no measurable conversion of C_2H_4.

3.4 Results and Discussion

3.4.1 Selective Synthesis and Characterization of Well Isolated Single-Site Rhodium Dinitrosyl Complexes Supported on HY Zeolite Supports

Exposure of $Rh(CO)_2$/HY30 prepared from the $Rh(CO)_2$(acac) precursor to pulses of a 1% NO/He mixture, significant changes were observed in the infrared spectra. Difference spectra shown in Fig. 3.1 demonstrate that the symmetric and asymmetric ν_{CO} bands (2117 and 2053 respectively) originating from the $Rh(CO)_2$ started to disappear after the first pulse of NO at room temperature:

Simultaneously, two strong bands at 1855 and 1779 cm^{-1} started to grow. It is obvious, that the growth of the latter two bands happens at the expense of the ν_{CO} bands of $Rh(CO)_2$/HY30. The ν_{CO} bands originating from $Rh(CO)_2$ surface species decreased in intensity during subsequent NO pulses and disappeared from the spectra after approximately 3 NO pulses, while the development of the 1855 and 1779 cm^{-1} bands was essentially complete at this point.

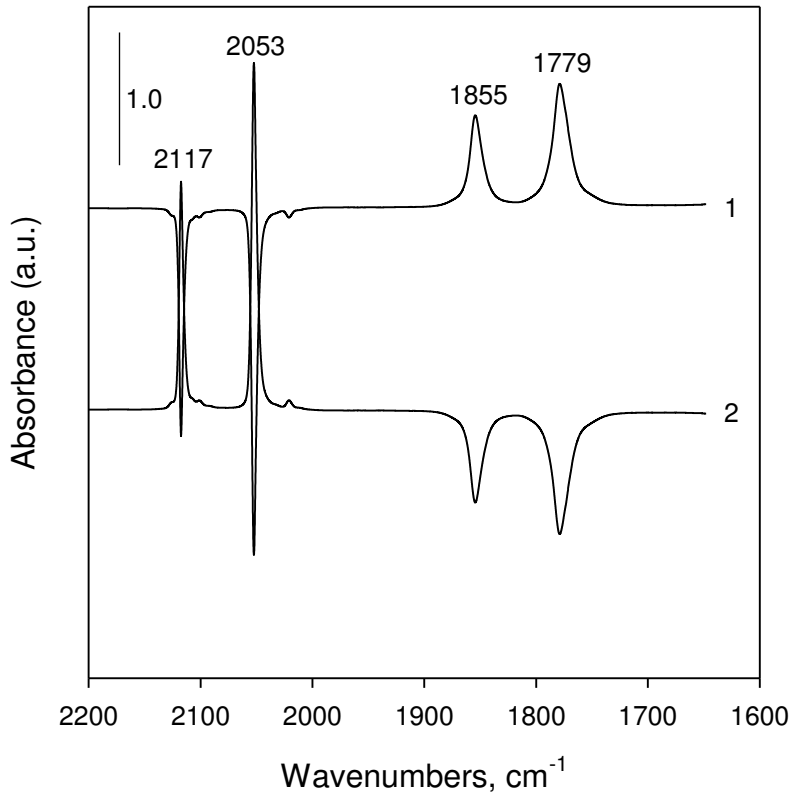

Fig. 3.1 Difference FTIR spectra illustrating changes in the ν_{CO} and ν_{NO} regions after (1) a pulse of NO over the $Rh(CO)_2$/HY30 sample (2) a subsequent pulse of CO.

CO and NO^+ ligands are known to be structurally similar[22]. A few literature examples from organometallic chemistry are known in which CO ligands of transition-metal organometallic complexes can be replaced with NO[27,28]. Therefore, the assumption that the disappearance of CO ligands on single-site $Rh(CO)_2$/HY30 took place because the CO ligands were replaced with NO ligands would be quite logical. Indeed, most known metal nitrosyl complexes demonstrate the IR vibrational signature in the 1525-1900 cm^{-1} region[24]. The newly formed 1855 and 1779 cm^{-1}, thus, can be assigned to some Rh nitrosyl complex or complexes formed in place of $Rh(CO)_2$/HY30.

The striking similarity between the signature of ν_{CO} and ν_{NO} bands, namely the higher-frequency band corresponding to the symmetric X-O bond vibration with the lower frequency counterpart corresponding to the asymmetric X-O vibration, leads to the conclusion that the Rh nitrosyl complex that was formed is structurally similar to the initial $Rh(CO)_2$/HY30 and can be denoted as $Rh(NO)_2$/HY30. The reaction that takes place is the complete ligand exchange reaction, well-described for organometallic molecular precursors:

$$Rh(CO)_2/HY30 + 2\,NO \rightarrow Rh(NO)_2/HY30 + 2\,CO$$

Two different types of transition metal nitrosyl complexes are known[29,30]: the one with linear NO in which the angle between N and O does not deviate significantly from 180º and the one with bent NO in which the significant deviation from 180º is observed. The former type complexes typically have the IR signature in the 1650-1900 cm^{-1} region, whereas the latter ones have the IR signature in the 1525-1690 cm^{-1} region.

This allows us to conclude with confidence that the $Rh(NO)_2$/HY30 complexes that are formed after NO exposure, have two essentially linear nitrosyl ligands coordinated to the square-planar rhodium atom. Moreover, these bands are similar to the previously described ν_{NO} bands of $Rh(NO)_2$ complexes (i.e., at 1862 and 1785 cm^{-1}) in ZSM-5 zeolites.[31,32] It strengthens and confirms the observation that the exposure of the mononuclear site-isolated $Rh(CO)_2$/HY30 complexes to gas-phase NO leads to the selective formation of $Rh(NO)_2$/HY30.

3.4.2 Reversibility of CO-NO Exchange for HY Zeolite Supported Single-Site Rhodium Complexes

Since the $Rh(NO)_2$/HY30 species were formed by CO/NO ligand exchange, it was interesting to see if the NO ligands could be further replaced with CO.

FTIR data (Figure 3.1) indicate that upon the first pulse of 1% CO/He gas mixture, the intensity of ν_{NO} bands immediately goes down concomitantly with the appearance and growth of two ν_{CO} bands of the supported $Rh(CO)_2$/HY30 species. The ν_{NO} bands disappear completely after approximately 3 minute of 1% CO/He pulses, and that is when the ν_{CO} bands of the supported $Rh(CO)_2$/HY30 species stop growing. Obviously, the following reaction takes place:

$$Rh(NO)_2/HY30 + 2\ NO \rightarrow Rh(CO)_2/HY30 + 2\ NO$$

This exchange was also monitored using Mass Spectroscopy. Pulses of 1% CO/He were interspersed with 1% NO/He pulses. The results obtained are presented in Figure 3.2. Pulse of NO on $Rh(CO)_2$/HY30 leads to a sharp spike CO (m/e=28) in the gas-phase. However, when the $Rh(NO)_2$ species were exposed to a pulse of CO, NO (m/e=30) appeared in the gas phase. As inferred from FTIR data, the $Rh(CO)_2$ species with characteristic ν_{CO} bands at 2117 and 2053 cm^{-1} were formed on the surface. Furthermore, the $Rh(NO)_2$-$Rh(CO)_2$ transformation cycle can be repeated several times without regions as evidenced by the absence of significant changes in the area and intensity of corresponding CO and NO Mass Spectroscopy peaks, suggesting that the facile substitution of CO/NO ligands is fully reversible and this process reaches completion fairly quickly.

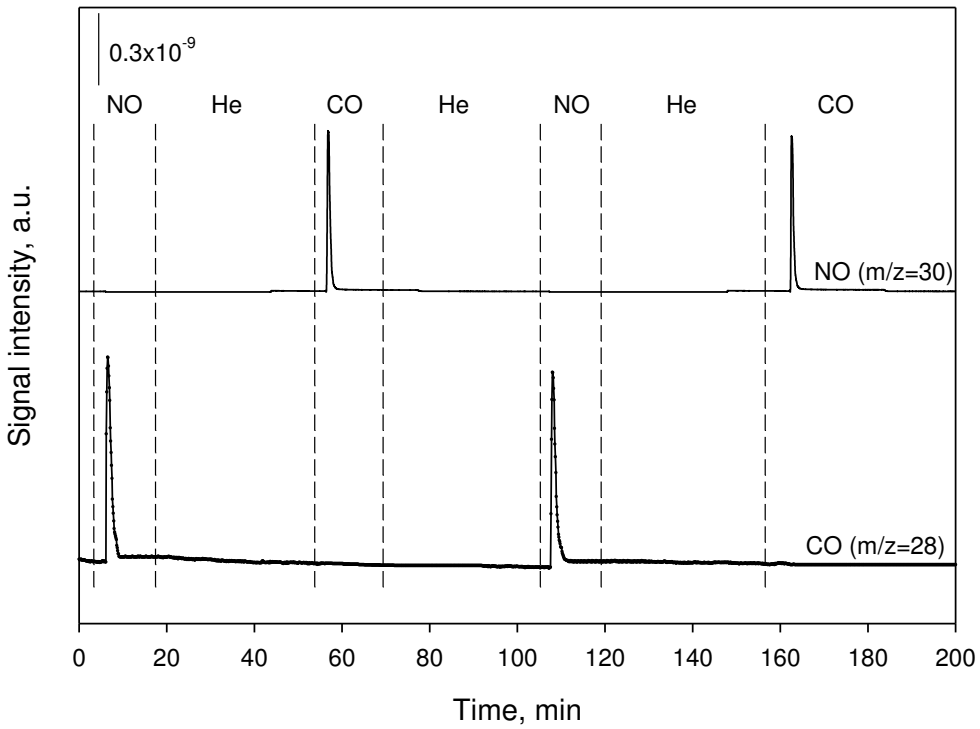

Fig. 3.2 Mass Spec experiment; 1%NO/He/1%CO pulses on $Rh(CO)_2$/HY30.

3.4.3 Formation of Rhodium Dinitrosyl Complexes on HY Zeolites with Different Si/Al Ratio

Since the $Rh(CO)_2$/HY30 produced $Rh(NO)_2$/HY30 in quantitative yield, it was of great interest to understand whether the same well-isolated single-site $Rh(NO)_2$ complexes could be selectively synthesized on HY zeolites high lower Si/Al ratio.

Exposure of $Rh(CO)_2$ supported on HY15 and HY2.6 to pulses of 1% NO/He in the FTIR cell led to the gradual decrease and disappearance of ν_{CO} bands of $Rh(CO)_2$ complexes (i.e., at 2117 and 2053 cm^{-1}) with concomitant growth of ν_{NO} bands of $Rh(NO)_2$ complexes (i.e. at 1862 and 1785 cm^{-1}). The disappearance of the CO bands

and growth of the NO bands happen pretty quickly, and in all three cases are complete after a few minutes. Evidently, the $Rh(NO)_2$ complexes that are produced on HY15 and HY2.6 supports have the same NO bands (1862 and 1785 cm^{-1}) as $Rh(NO)_2$/HY30. It proves identical rhodium dinitrosyl complexes with similar properties form in quantitative yield on three different zeolites upon reaction of $Rh(CO)_2$/HY with gas-phase NO.

It was previously shown by our group in the combined FTIR and DFT study that in fact, two different types of $Rh(CO)_2$ species with different ν_{CO} bands FTIR signatures and reactivity towards carbonyl ligand displacement with ethylene are present on the surface[33]. These two carbonyl types were denoted as type I (more reactive, 2117 and 2053 cm^{-1} ν_{CO} bands) and II (less reactive, 2113 and 2048 cm^{-1} ν_{CO} bands), the majority of species on HY30 being type I carbonyl, the relative fraction of type II species increasing with the degree of dealumination up to 50% on H2.6. The only difference between type I and II $Rh(CO)_2$ HY-supported species is the different types of oxygens in the vicinity of tetrahedral Al site that Rh coordinates to[33].

In an attempt to understand the nature of the formed $Rh(NO)_2$ species, deconvolution of the ν_{NO} region of those species on three different supports was undertaken . The resulting spectra are presented below (Figures 3.5, 3.6 and 3.7): Analogously, for $Rh(NO)_2$ supported on HY 30, 15 and 2.6 type I and II species can be found for $Rh(NO)_2$ species as well. Moreover, the N-Rh-N angle for $Rh(NO)_2$ square planar complexes can also be estimated for type I and II complexes on the basis of Isym/I asymm ν_{NO} ratio:

$I_{sym}/I_{asymm}=ctg(a^2/2)$ where a is the N-Rh-N angle

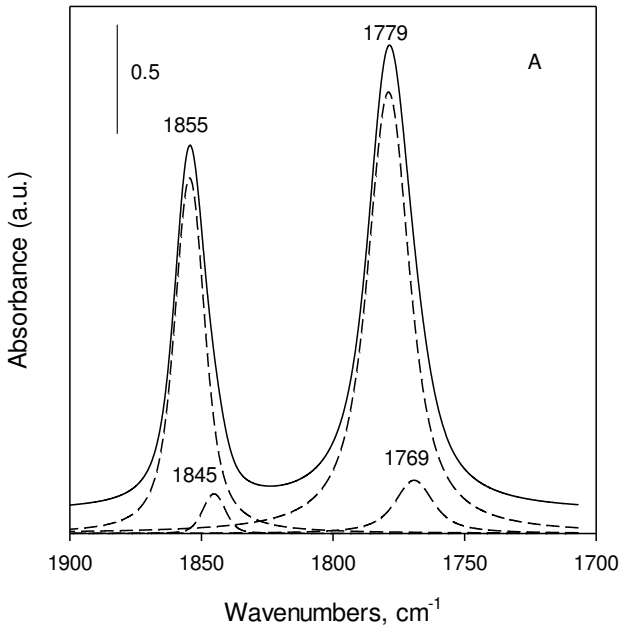

Fig. 3.3 Room-temperature FTIR spectra in the ν_{NO} region of (A) $Rh(NO)_2$/HY30 (solid line) and deconvolution results (dashed lines).

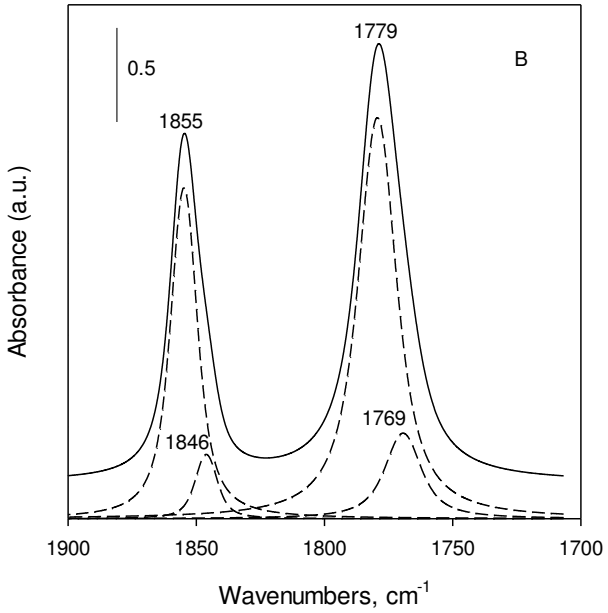

Fig. 3.4 Room-temperature FTIR spectra in the ν_{NO} region of (B) $Rh(NO)_2$/HY15 (solid line) and deconvolution results (dashed lines).

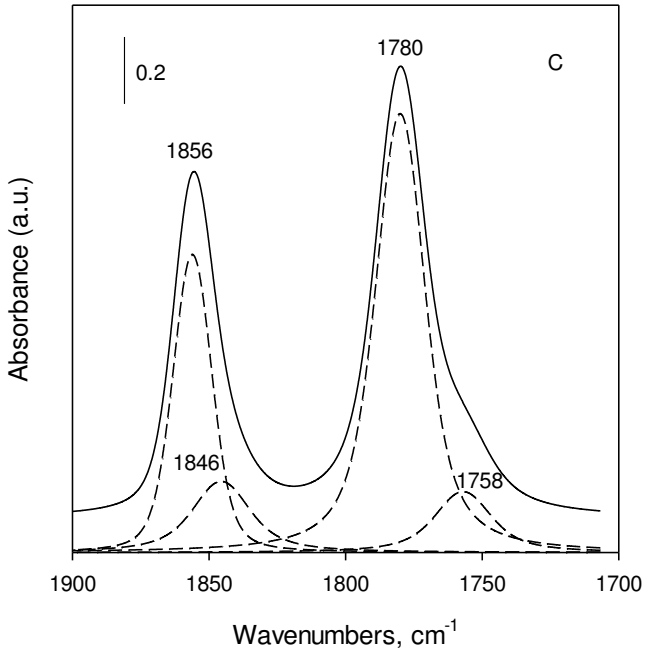

Fig. 3.5 Room-temperature FTIR spectra in the ν_{NO} region of (C) $Rh(NO)_2$/HY2.6 (solid line) and deconvolution results (dashed lines).

The summary of the results for the $Rh(NO)_2$ complexes formed on three different zeolites is presented in Table 3.1.

The relative amount of Type II species for $Rh(NO)_2$ increases with decreasing Si/Al ratio but not as drastically as for $Rh(CO)_2$.

On average, the angle between two NO ligands for $Rh(NO)_2$/HY is slightly larger (105°) than the corresponding angle between two CO ligands for $Rh(CO)_2$ (96°).

Table 3.1. Deconvolution parameters of ν_{NO} bands observed in FTIR spectra of various samples.

Sample	Band position, cm^{-1}	FWHM, cm^{-1}	Split $(\nu_s-\nu_{as})$,[a] cm^{-1}	N-Rh-N angle, deg	Relative fraction, %
$Rh(NO)_2$/HY30	1855	13.6	76	104	91
	1779	19.0			
	1845	10.0	76	106	9
	1769	17.2			
$Rh(NO)_2$/HY15	1855	12.4	76	104	85
	1779	18.0			
	1846	10.2	77	106	15
	1769	16.8			
$Rh(NO)_2$/HY2.6	1856	17.4	76	104	82
	1780	21.1			
	1846	23.2	88	106	18
	1758	24.2			

3.4.5 Interactions of $Rh(NO)_2$/HY30 with Hydrogen, Ethylene and Ethylene/Hydrogen Gas Mixtures

As reported elsewhere, $Rh(CO)_2$[15] does not interact with hydrogen at room temperature. Nitrosyl ligand NO^+ is isoelectronic with CO, and it is expected to behave in a similar manner. Indeed, pulses of 100% H_2 over $Rh(NO)_2$/HY30 do not lead to any changes in the spectra. Like $Rh(CO)_2$/HY30, $Rh(NO)_2$/HY30 does not interact with H_2 under ambient conditions (Figure 3.6).

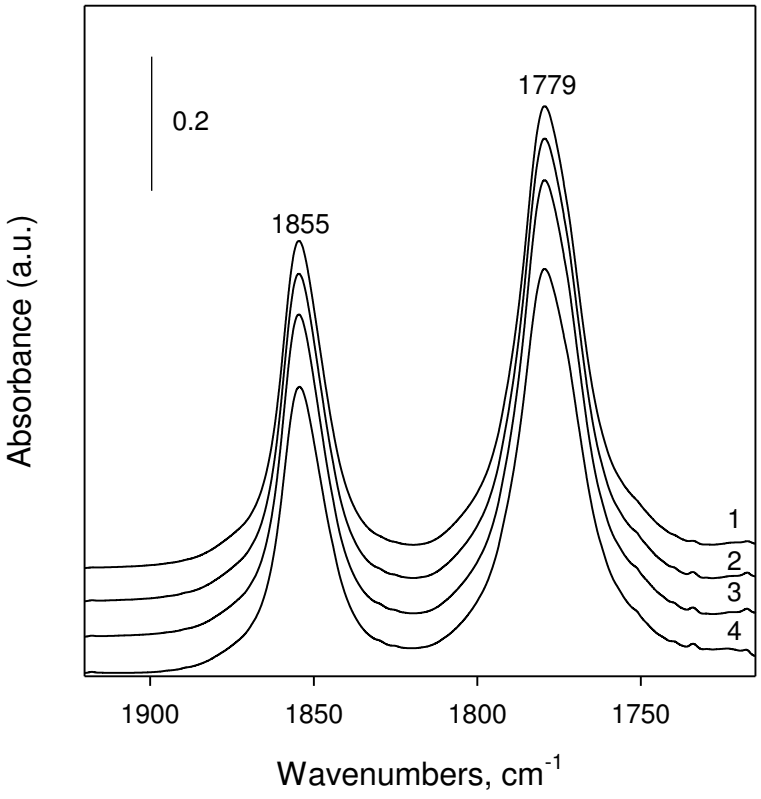

Fig. 3.6 FTIR spectra of $Rh(NO)_2$/HY30 exposed to (1) H_2 flow at 25°C for 1 min, (2) H_2 flow at 25°C for 5 min, (3) 45 psi of H_2 at 25°C, and (4) H_2 flow at 90°C.

Interaction of $Rh(CO)_2$/HY30 with gas-phase ethylene leads to the fast replacement of one CO ligand and formation of $Rh(CO)(C_2H_4)$/HY30 complex which is capable of activating H_2 at room temperature to produce $Rh(CO)H_x$/HY30. The perceived structural similarity of $Rh(CO)_2$/HY30 and $Rh(NO)_2$/HY30 prompted us to investigate the chemical interaction between $Rh(NO)_2$/HY30 and C_2H_4.

Upon exposure to gas phase C_2H_4, significant changes in the ν_{NO} region were observed (Figure 3.7).

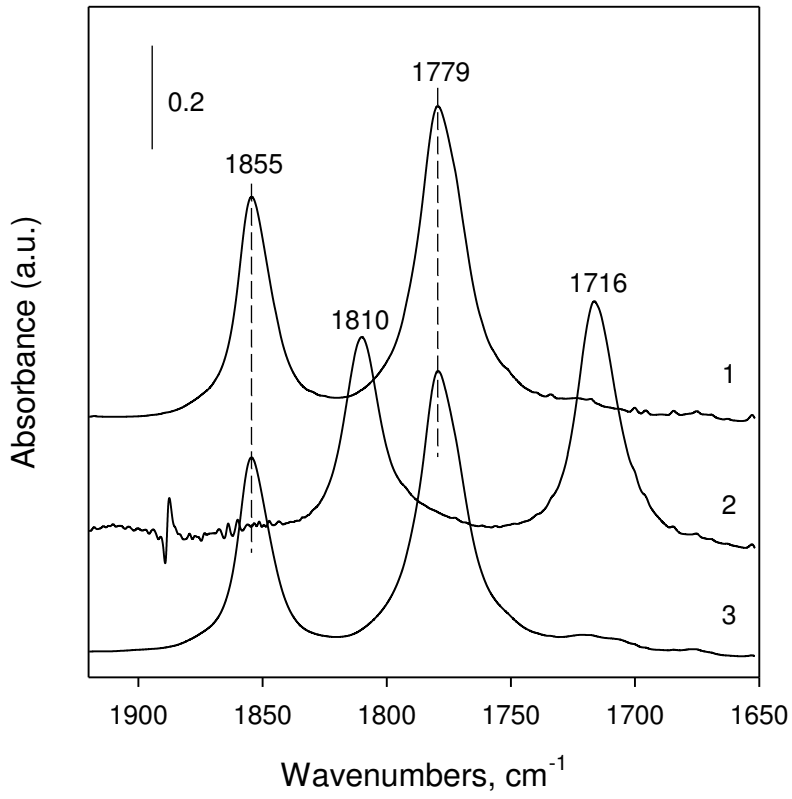

Fig. 3.7 FTIR spectra in the ν_{NO} region of $Rh(NO)_2$/HY30 recorded after sequential exposure to flows of (1) He, (2) C_2H_4, and (3) He at 25°C for 15 min.

The 1862 and 1785 cm^{-1} corresponding to the symmetric and asymmetric ν_{NO} shifted to 1810 and 1716 cm^{-1} respectively. Interestingly, as soon as C_2H_4 flow was stopped and replaced with ethylene, the 1862 and 1785 cm^{-1} bands of the $Rh(NO)_2$/HY30 starting complex reappeared immediately, with intensities closely matching the intensities of the $Rh(NO)_2$/HY30 that was reacted with gas phase ethylene.

There is a profound difference in reactivity of $Rh(NO)_2$/HY30 and $Rh(CO)_2$/HY30 towards ethylene. In the latter case, one of the two carbonyl ligands gets selectively replaced with ethylene. $Rh(NO)_2$/HY30, however, demonstrates a completely different behavior towards ethylene. This is a clear example of the subtle electronic differences of CO and NO ligands. Although they are isoelectronic and often considered similar in chemical behavior, analogous $Rh(NO)_2$/HY30 complex does not react with ethylene by replacing one of the NO ligands with ethylene. Instead, some complex with a different set of ν_{NO} bands is formed while ethylene is present in the gas phase. As soon as ethylene is replaced with He, the bands corresponding to well-defined $Rh(NO)_2$/HY30 of similar intensity return, indicating weak coordination of ethylene to $Rh(NO)_2$/HY30. This is quite characteristic of ethylene π-complexes[34]. Moreover, π-coordination of ethylene with its electron-donating properties is expected to shift ν_{NO} bands to lower wavenumbers due to the increase in backdonation from rhodium into the π* orbital of NO[35]. FTIR region characteristic for zeolite-supported rhodium-ethylene π-complexes is 3000 cm^{-1} and above. Removal of ethylene from the gas phase immediately restores $Rh(NO)_2$/HY30. The CH-stretch region 3000 cm^{-1} can be seen in difference spectra in Fig 3.8. Appearance of the 3015 cm^{-1} could mean pi-coordination of ethylene on rhodium.

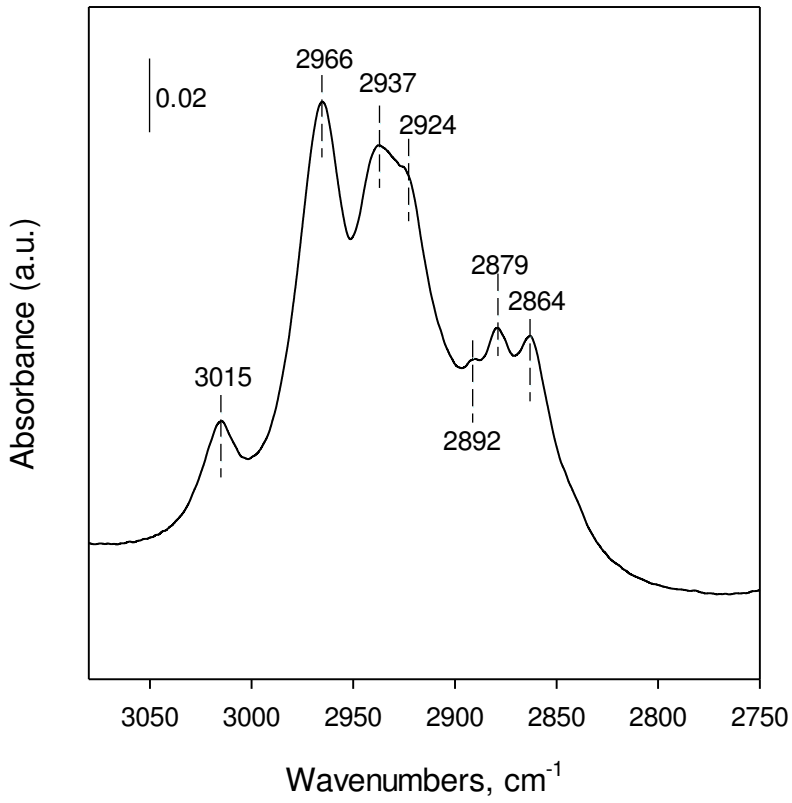

Fig. 3.8 Difference FTIR spectrum illustrating changes in the ν_{CH} region after exposure of $Rh(NO)_2$/HY30 to a C_2H_4 flow at 25°C for 15 min.

Taking into account the fact that $Rh(NO)_2$/HY30 is formally a 16-electron complex, it can coordinate one more 2-electron ligand (such as ethylene in the π-binding mode). Obviously, ethylene coordination is pretty weak, and flushing with inert gas immediately restores $Rh(NO)_2$/HY30.

The observed unusual behavior towards ethylene prompted us to investigate the possibility of ethylene hydrogenation by adding H_2 to the C_2H_4/He mix. There are a few literature examples that indicate that certain transition metal nitrosyl complexes can be used as liquid-phase hydrogenation catalysts. For example, Morris[25] et all demonstrated

that tris(triphenylphosphine)nitrosyl rhodium can catalyze cyclohexene hydrogenation by 1 atm of 100% hydrogen in dichloromethane at room temperature. The mechanism of this reaction was not studied. Jiang et al[26] used Rh(NO)(dcpe) complex with bent NO and chelating diphosphine for CO_2 hydrogenation at 50 C and 3 bar CO_2/H_2 mixture pressure. It showed moderate activity towards formic acid with a calculated TON 106 after 16 hours.

We added H_2 to the C_2H_4 flow and collected FTIR spectra in time for $Rh(NO)_2$/HY30. Significant changed were immediately noticeable upon addition of H_2 (Figure 3.9).

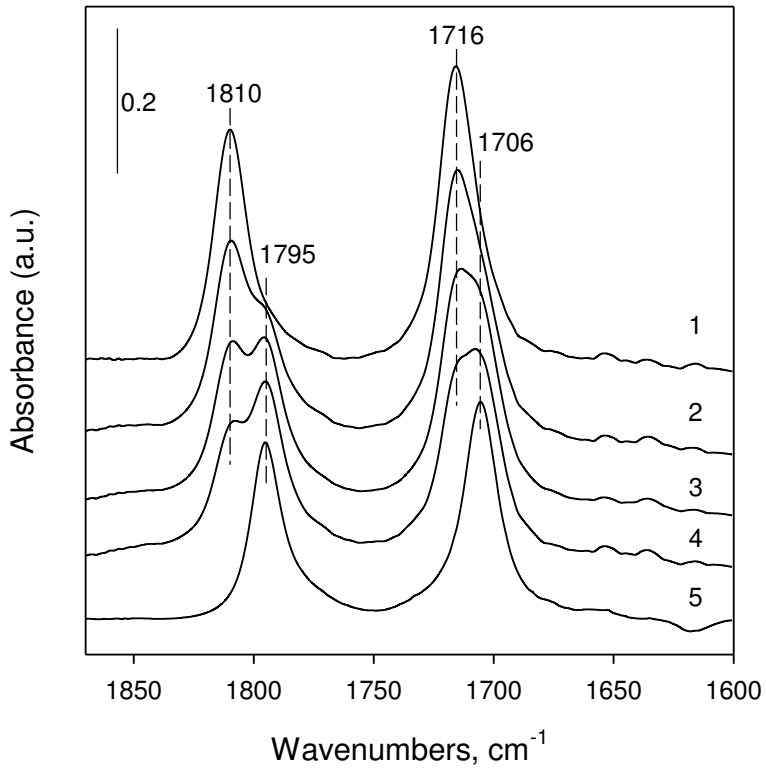

Fig. 3.9 FTIR spectra in the ν_{NO} region of $Rh(NO)_2$/HY30 after exposure to flows of (1) C_2H_4 and a 75%H_2/25%C_2H_4 mixture at 25°C for (2) 1 min, (3) 5 min, (4) 9 min, and (5) 60 min.

Peaks characteristic of $Rh(NO)_2(C_2H_4)$/HY30 started to decrease in intensity with the simultaneous appearance of two new peaks (shoulders) at 1795 and 1702 cm^{-1}. After approximately 60 minutes of reaction (flowing H_2/C_2H_4 mix), the intensity of the 1810 and 1715 cm^{-1} bands was close to zero while 1795 and 1702 cm^{-1} bands remained in the spectra. Interestingly, no Rh-H bands expected to appear[15] above 2100 cm^{-1} were observed during the reaction. Unlike $Rh(CO)_2$/HY30, $Rh(NO)_2$/HY30 does not form hydrides during C_2H_4/H_2 treatment. This once again signifies the general picture in which, despite a lot of similarity between CO and NO ligands, even such subtle electronic changes around the zeolite-anchored single rhodium site dramatically change the reactivity of this single site and pathways to activation of simple molecules like C_2H_4 and H_2.

The subsequent flow of He does not significantly affect the 1795 and 1702 cm^{-1} bands. Additionally, during the first few minutes of He flow after the reaction, a weak band at 3015 cm^{-1} is visible in the spectra. One possible explanation for the observed 3015 band is that during the reaction, ethylene might be weakly pi-coordinated to rhodium with the subsequent flow of He removing it[34].

The shift of ν_{NO} bands to lower frequencies during and after the reaction is indicative of presence of an electron-donating group or groups either on rhodium or NO ligand. Activation of hydrogen without formation of Rh-H can be understood in terms of hydrogen activation by NO ligand(s), as well as possible formation of $Rh(NO)_x(C_2H_5)_y$ species:

$$Rh(NO)_2 + H_2 \rightarrow Rh(NOH)_2$$

$$Rh(NOH) + C_2H_4 \rightarrow Rh(C_2H_4)(NOH) \rightarrow Rh(NO)(C_2H_5)$$

Indeed, there is spectroscopic evidence for the formation of surface ethyl species during reaction. Comparison of FTIR spectra during the reaction undoubtedly shows continuous formation of ethyl/alkyl species with characteristic ν_{CH} stretching frequencies: 2965, 2935, 2878, 2862[34]. To confirm the single-site nature of Rh/lack of clusterization after catalysis, pulses of 1%CO/He were administered onto the sample. These pulses led to immediate restoration of 2117 and 2053 cm^{-1} ν_{CO} bands of the $Rh(CO)_2$/HY30. These bands are uniquely sharp indicating the structural uniformity and lack of Rh aggregation during catalysis (see the following chapter).

3.4.6 Catalytic Ethylene Hydrogenation and Dimerization by HY30 Supported Single-Site $Rh(NO)_2$ Complex

As we demonstrated in previous chapters, $Rh(CO)_2$/HY30 is capable of performing continuous gas-phase catalysis, namely ethylene dimerization and hydrogenation at room temperature and total 1 atm pressure. In the view of FTIR results for $Rh(NO)_2$/HY30, proving unique reactivity towards C_2H_4/H_2, it was of great interest to determine whether the stable site-isolated HY30 supported $Rh(NO)_2$ complexes could catalyze ethylene hydrogenation (and possibly dimerization) in the gas phase at room temperature. We tested them in ethylene hydrogenation under similar conditions, and discovered they do in fact catalyze ethylene hydrogenation, with TOF higher than $Rh(CO)_2$/HY30 (at steady state TOF for ethane are 0.010 and 0.006 s^{-1} respectively) . It is the first unprecedented example of the supported transition metal complex with NO ligands capable of doing any kind of catalysis (Fig 3.10).

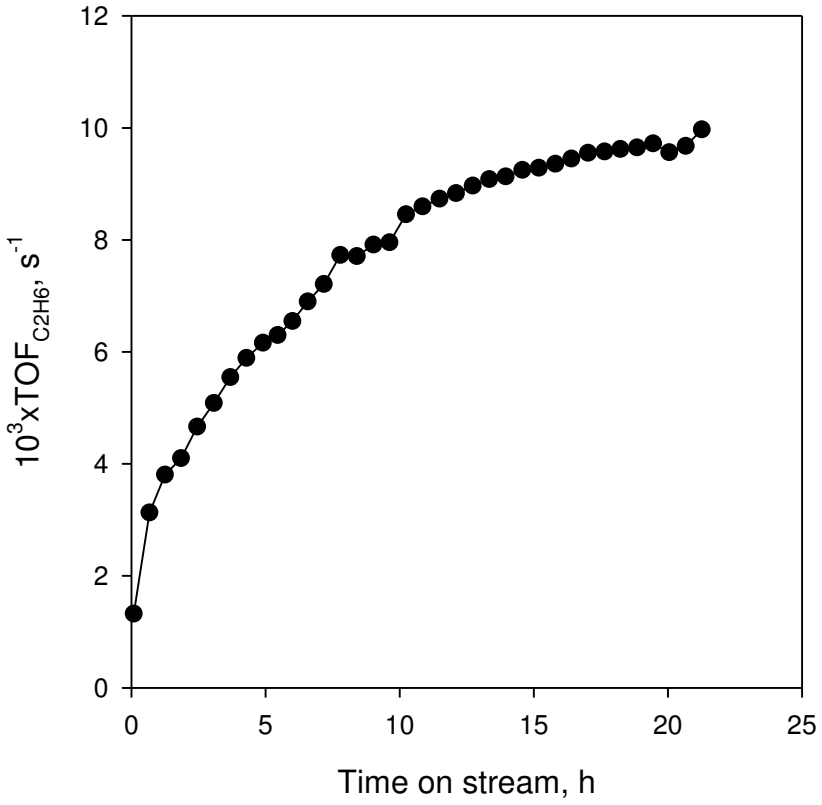

Fig. 3.10 Rates (TOF) for ethane formation with Time On Stream (TOS) for $Rh(NO)_2$/HY30 at 76 Torr of C_2H_4 and 608 Torr H_2 under ambient conditions.

Based on these data, it is clear that $Rh(NO)_2$/HY30 complexes are active catalysts for ethane production. After approximately 20 hours, the catalyst reaches steady state with no significant TOF drop afterwards. Surprisingly, ethane is one of a few products formed. Various n-butenes are also produced during catalysis, revealing intrinsic activity of rhodium dinitrosyl complexes for ethylene dimerization. Results of a typical catalytic experiment performed at 608 Torr of H_2 and 76 Torr of C_2H_4 at ambient conditions show rates of ethane, butene-1, cis-2-butene and trans-2-butene formation (Figure 3.11).

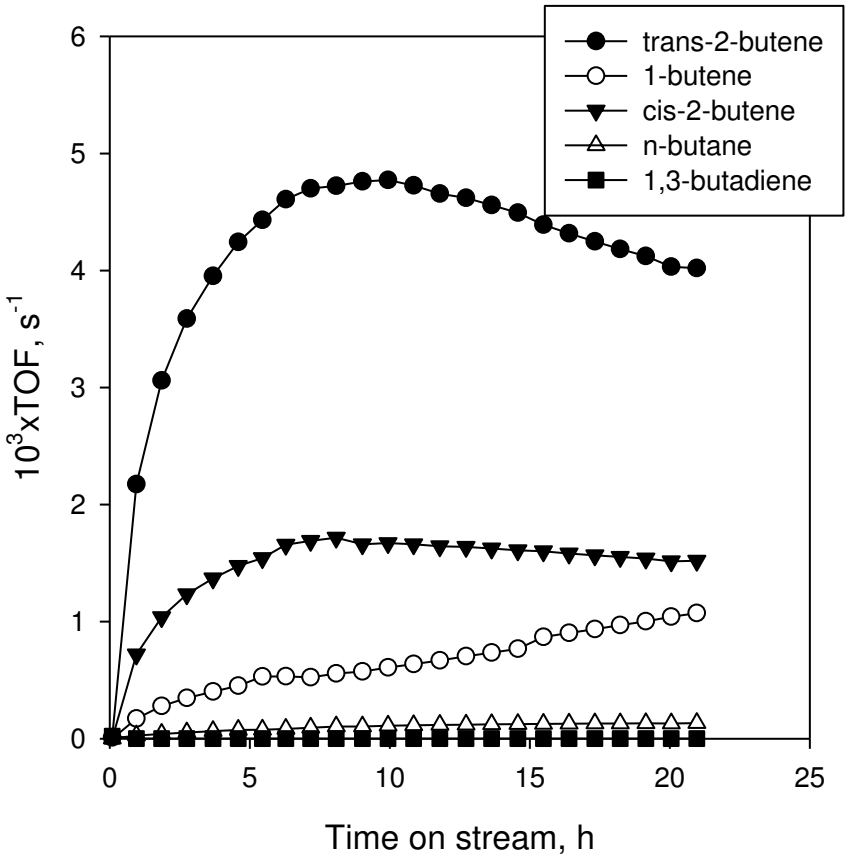

Fig. 3.11 Formation of C_4 hydrocarbons as a function of time over a $Rh(NO)_2$/HY30 catalyst. (Reaction temperature 25°C; feed composition: 76 Torr C_2H_4/608 Torr H_2/He balance).

The summary of selectivity and TOF for all products formed after 20 hours on stream is summarized in Table 3.2.

At steady state, the selectivity for ethane is 60%, whereas the selectivity sum for all C_4 products is 40%.

Table 3.2 Turn Over Frequencies (TOF) and Selectivity to C_2 and C_4 products after 20 h on stream.

Sample	C_2H_6, TOF*10^3, s^{-1}	C_2H_6, %	C_4, TOF*10^3, s^{-1}	n-butane, %	1-butene, %	Cis-2-butene, %	Trans-2-butene,%	Total C_4, %
$Rh(NO)_2$/HY30	10,0	60	6.7	1	6	9	24	40

Comparison with $Rh(CO)_2$/HY30, for which selectivity to ethane at steady-state is about 32% with n-butenes being the major species produced, reveals significant differences between these two structurally similar supported site-isolated molecular rhodium complexes. The origin of this difference most likely stems from different mechanisms of ethylene and hydrogen activation as was observed with FTIR spectroscopy.

Kinetic data and reaction orders were determined for both $Rh(CO)_2$/HY30 and $Rh(NO)_2$/HY30. These kinetic data indicate competitive adsorption of ethylene and hydrogen on a single site for ethane formation. The dependence on H_2 partial pressure for $Rh(NO)_2$/HY30 is somewhat lower compared to $Rh(CO)_2$/HY30 (0.45 and 0.7 respectively). Butene formation for both catalysts is highly dependent on ethylene partial pressure (about 1 in both cases). It is not surprising considering that in order to form a C-C bond, two ethylene molecules in one activated form or another have to come in proximity. The anomalously low ethylene partial pressure dependence for both catalysts for saturated n-butane formation means butenes that are formed, are further hydrogenated to butane via the similar mechanism as ethylene to ethane (hence identical orders).

Table 3.3 Reaction Orders in H_2 and C_2H_4 with respect to C_2 and C_4 products.

Sample	Product	Order H_2	Order C_2H_4
$Rh(NO)_2$/HY30	Ethane	0.69	0.43
	n-butane	1.07	0.39
	Trans-2-butene	0.80	1.19
	1-butene	0.38	1.28
	Cis-2-butene	0.64	1.13
$Rh(NO)_2$/HY30	Ethane	0.45	0.39
	n-butane	0.64	0.39
	Trans-2-butene	0.63	0.88
	1-butene	0.29	1.18
	Cis-2-butene	0.48	0.86

In previous chapters the mechanism of ethylene hydrogenation and dimerization on $Rh(CO)_2$/HY30 was described in detail. Surface-assisted dimerization and hydrogenation pathways apparently play a very important part in catalysis. The role of the support is to activate ethylene, while the role of metal on the surface is to activate hydrogen as well as ethylene, and then bring these species in proximity via various pathways. Unambiguous similarity of kinetic data for $Rh(CO)_2$/HY30 and $Rh(NO)_2$/HY30 points at the very

important similar roles of zeolite support in these catalytic properties (despite different mechanisms of ethylene and hydrogen activation by those complexes). The studies are now underway to further clarify this phenomenon.

Additionally, in order to confirm the lack of Rh reduction/aggregation during catalysis, STEM images were collected on the $Rh(NO)_2$/HY30 after 20 hours of catalysis. The images are presented in Figures 3.12 and 3.13.

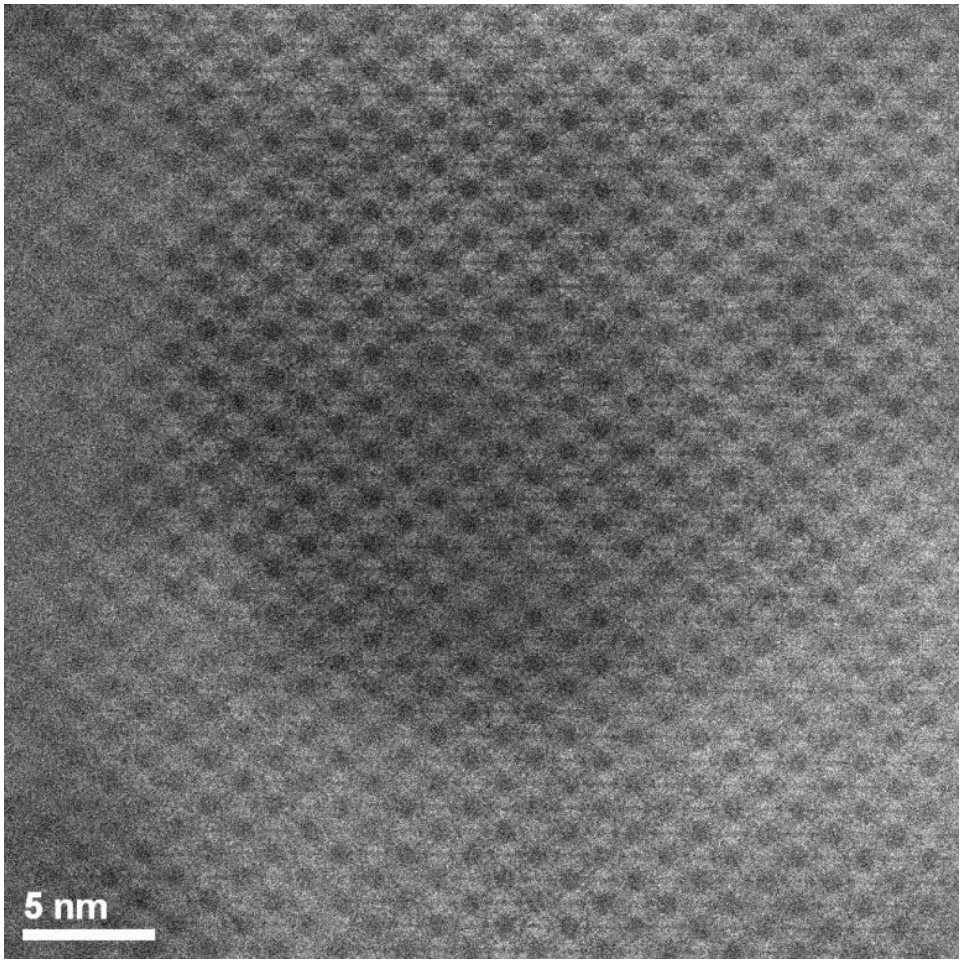

Fig. 3.12 High-angle annular dark-field (Z-contrast) STEM image of $Rh(NO)_2$/HY30 after 20 h catalysis in zeolite [110] projection. The image shows only individual Rh atoms as bright spots which are well dispersed and present in the absence of detectable rhodium clusters.

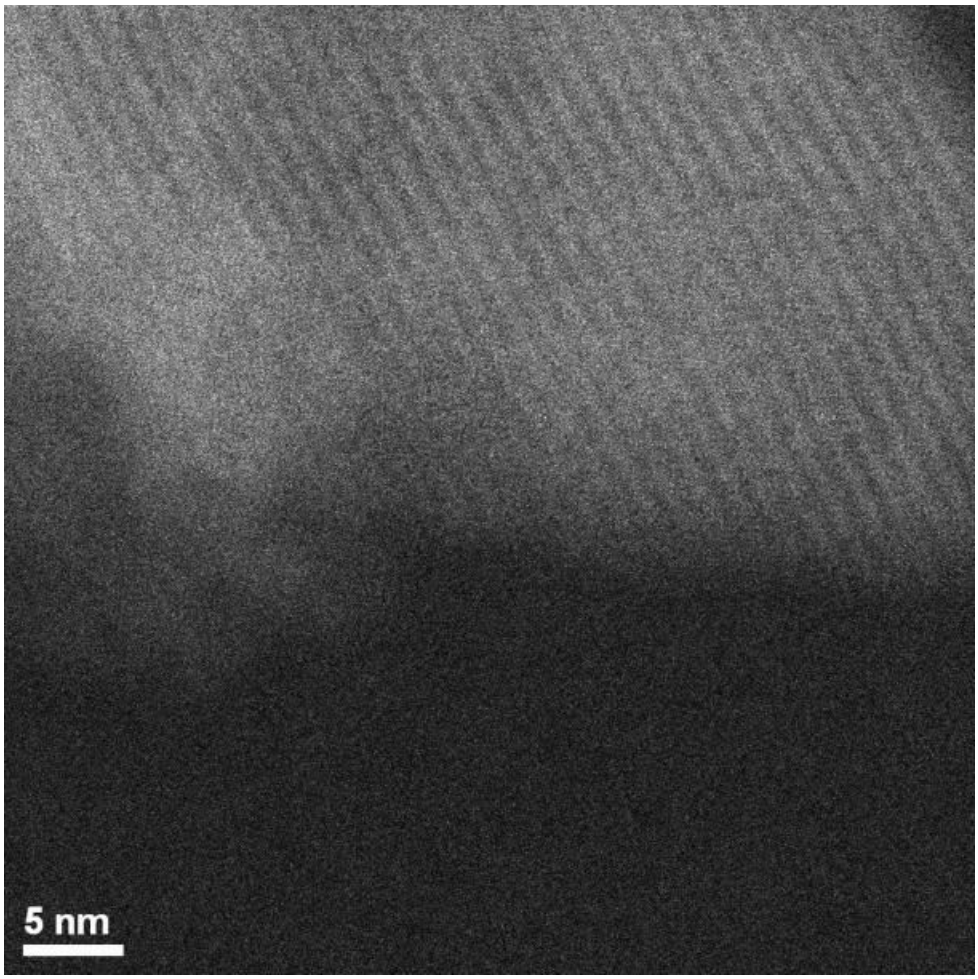

Fig. 3.13 High-angle annular dark-field (Z-contrast) STEM image of $Rh(NO)_2$/HY30 after 20 h catalysis. The image shows only individual Rh atoms as bright spots which are well dispersed and present in the absence of detectable rhodium clusters.

These HAADF-STEM images serve as another proof that Rh retains its single-site nature even after 20 hours catalysis and does not aggregate.

3.5 Conclusions

HY Zeolite-supported mononuclear $Rh(NO)_2$ were selectively prepared by a ligand exchange reaction of $Rh(CO)_2$ complexes supported on HY30, 15 and 2.6 with gas phase NO. These complexes display characteristic ν_{NO} bands at 1855 and 1779 cm^{-1}. Th CO/NO

exchange is fully reversible and complete. $Rh(NO)_2$/HY30 showed activity in ethylene hydrogenation and ethylene dimerization under ambient conditions. Compared to $Rh(CO)_2$/HY30, TOF for ethane formation was 1.5 times higher.

Hydrogen and ethylene activation pathways on $Rh(NO)_2$/HY30 differ from those on $Rh(CO)_2$/HY30. No spectroscopic evidence of Rh-H band presence was found. Rh remained site-isolated before, during and after catalysis

REFERENCES

Chapter 1

[1] J. Osborn, F. Jardine, J. Young, G. Wilkinson, Journal of American Chemical Society A (1966) 1711

[2] J. Osborn, G. Wilkinson, Inorganic Syntheses 10 (1967) 67.

[3] B. R. James, Homogeneous Hydrogenation; Wiley-Interscience, New York, 1973.

[4] J. E. Backvall, Journal of Organometallic Chemistry 652 (2002) 105.

[5] D. A. Evans, G. Fu, A. H. Hoveyda, Journal of American Chemical Society 110 (1988) 6917.

[6] I. Ojima, T. Kogure, Tetrahedron Letters 13 (1972) 5035.

[7] W. S. Knowles, Advanced Synthetic Catalysis 345 (2003) 3.

[8] D. Evans, J. Osborn, G. Wilkinson, Journal of American Chemical Society 33 (1968) 33 3133.

[9] M. Konkol, J. Okuda, Coordination Chemistry Reviews 252 (2008) 1577.

[10] P. Serna, B. Gates, Accounts of Chemical Research 47 (2014) 2612.

[11] O. S.Alexeev, B. Gates, Topics in Catalysis 10 (2000) 273.

[12] C. Copéret, M. Chabanas, R. P. Saint-Arroman, J.-M. Basset, Angewandte Chemie 42 (2003) 156.

[13] J.-M. Basset, J.-P. Candy, C. Coperet, F. Lefebvre, E. Quadrelli, Nanotechnology and Catalysis 2 (2004) 447.

[14] C. Coperet, J.-M. Basset, Advanced Synthetic Catalysis 349 (2007) 78.

[15] D. Soulivong, S/ Norsic, M. Taoufik, C. Coperet, J. Thivolle-Cazat, S. Chakka, J.-M. Basset, Journal of American Chemical Society 130 (2008) 5044.

[16] C. Rosier, G. Niccolai, J.-M. Basset, Journal of American Chemical Society 119 (1997 12408.

[17] V. Dufaud, J.-M. Basset, Angewandte Chemie. 37 (1998) 806.

[18] M. Taoufik, E. Le Roux, J. Thivolle-Cazat, J.-M. Basset , Angewandte Chemie 46 (2007) 7202.

[19] J.-M. Basset, C. Coperet, D. Soulivong, M. Taoufik, J.-T. Cazat, Accounts.of Chemical. Research 43 (2010) 323.

[20] V. Vidal, A. Théolier, J. Thivolle-Cazat, J.-M. Basset, Science 276 (1997) 99.

[21]. E. Le Roux, M. Taoufik, C. Copéret, A. De Mallmann, J. Thivolle-Cazat, J.-M. Basset, Angewandte Chemie 44 (2005) 6755.

[22] M. Ward, T. Harris, J. Schwartz, Journal of American Chemical Society Communications 8 (1980) 357.

[23] C. Foley, S. J. DeCanio, K Tau, K. Chao, J. H. Onuferko , C. B. Dybowski , B. Gates, Journal of American Chemical Society 105 (1983) 3074.

[24] S. Scott, A. Mills, C. Chao, J.-M. Basset, N. Millot, C. C. Santini, Journal of Molecular Catalysis A 204-205 (2003) 457.

[25] M. Rimoldi, A. Mezzetti, Inorganic Chemistry 53 (2014) 11974.

[26] F. Solymosi, A. Erdohelyi, T. Bansagi, Faraday Transactions 77 (1981) 2645.

[27] T. Yoshida, D. L. Thorn, T. Okano, J. A. Ibers, S. Otsuka, Journal of American Chemical Society 101 (1979) 4212.

[28] J. F. Goellner, B. C. Gates, G. N. Vayssilov, N. Rosch, Journal of American Chemical Society 122 (2000) 8056.

[29] P. Serna, B. Gates, Journal of Catalysis 308 (2013) 201.

[30] H. Miessner, I. Burkhardt, D. Gutschick, A. Zecchina, C. Morterra, G. Spoto, Faraday Transactions 85 (1989) 2312.

[31] I. Burkhardt, D. Gutschick, U. Lohse, H. Miessner, Journal of Chemical Society Chemical Communications 4 (1987) 291.

[32] S.Dinda, A. Govindasamy, A. Genest, N. Rösch, Journal of Physical Chemistry C 118 (2014) 25077.

[33] A. Vityuk, H. Aleksandrov, G. Vayssilov, S. Ma, O. Alexeev, M. Amirdis, Journal of Physical Chemistry C 118 (2014) 26772.

[34] A.Vityuk, O. Alexeev, M. Amiridis, Journal of Catalysis 311 (2014) 230.

[35] J. P. Perdew, Y. Wang, Physical Reviews B 45 (1992) 13244.

[36] G. Kresse, J. Hafner, Physical Reviews B 49 (1994) 14251.

[37] G. Kresse, J. Furthmüller, Computational Material Science 6 (1996) 15.

[38] D. Vanderbilt, Physical Reviews B 41 (1990) 7892.

[39] G. Kresse, J. Hafner, Journal of Physics Condensed Matter 6 (1994) 8245.

[40] Y. Jeanvoine, J. Angyan, G. Kresse, J. Hafner, Journal of Physical Chemistry B 102 (1998) 5573.

[41] C. Baerlocher, L. B. McCusker, Database of Zeolite Structures. http://www.iza-structure.org/databases/.

[42] K. Hadjiivanov, G. Vayssilov, Advances in Catalysis 47 (2002) 307.

[43] P.W.N.M. van Leeuwen, Homogeneous Catalysis: Understanding the Art; Kluwer, Dordrecht, 2004.

[44] X. Yuan, S. Bi, Y. Ding, L. Liu, M. Sun, Journal of Organometallic Chemistry 695 (2010) 1576.

[45] M. Bühl, M. Håkansson, A. H. Mahmoudkhani, L. Öhrström, Organometallics 19 (2000) 5589.

[46] L. Vaska, Journal of American Chemical Society 88 (1966) 4100.

[47] A. Liang, V. Bhirud, J. Ehresmann, P. Kletnieks, J. Haw, B. Gates, Journal of Physical Chemistry B 109 (2005) 24236.

[48] G. Vayssilov, N. Rösch, Journal of American Chemical Society 124 (2002) 3783.

[49] E. Ivanova, M. Mihaylov, F. Thibault-Starzyk, M. Daturi, K. Hadjiivanov, Journal of Catalysis 236 (2005) 168.

[50] E. Ivanova, M. Mihaylov, H. Aleksandrov, M. Daturi, F. Thibault-Starzyk, G. Vayssilov, N. Rösch, K. Hadjiivanov, Journal of Physical Chemistry C 111 (2007) 111, 10412-10418.

[51] P. Nachtigall, J. Sauer, Surface Science and Catalysis 168 (2007) 659.

[52] I. Voleská, P. Nachtigall, E. Ivanova, K. Hadjiivanov, R. Bulánek, Catalysis Today 243 (2015) 53.

[53] H. Aleksandrov, P. Petkov, G. Vayssilov, Energy Environmental Science 4 (2011) 1879.

[54] E. Ivanova, K. Hadjiivanov, Physical Chemistry Chemical Physics 5 (2003) 655.

[55] K. Hadjiivanov, E. Ivanova, L. Dimitrov, H. Knözinger, Journal of Molecular Structures 661 (2003) 459.

[56] G. Vayssilov, A. Hu, U. Birkenheuer, N. Rösch, Journal of Molecular Catalysis A 162 (2000) 135.

Chapter 2

[1] R.I. Wijngaarden, K.R. Westerterp, A. Kronberg, "Industrial Catalysis: Optimizing Catalysts and Processes", WILEY-VCH, Weinheim, 1998.

[2] C.H. Bartholomew, R.J. Farrauto, "Fundamentals of Industrial Catalytic Processes", WILEY-INTERSCIENCE, Hoboken, New Jersey, 2006.

[3] D.J. Adams, P.J. Dyson and S.J. Taverner, Chemistry in Alternative Reaction Media, John Wiley & Sons Ltd, Chichester, 2004.

[4] Shang-Tian Yang, Hesham El Enshasy, Nuttha Thongchul, Bioprocessing Technologies in Biorefinery for Sustainable Production of Fuels, Chemicals, and Polymers, John Wiley & Sons Inc, Hoboken, 2013

[5] H. Sugiyama, F. Uemura, N. Yoneda, T. Minami, T. Maejima, K. Hamato, Japan Patent 235250 (1997).

[6] D.J. Cole-Hamilton, Science 299 (2003) 1702.

[7] J.M. Fraile, J.I. Garcia, C.I. Herrerias, J.A.M. and E. Pires, Chemical Society Reviews 2009 (38) 695.

[8] A. Choplin, F. Quignard, Coordination Chemistry Reviews 178–180 (1998) 1679.

[9] G.A. Ozin, C. Gil, Chemical Reviews 89 (1989) 1749.

[10] S.M.C. Neiva, J.A.V. Santos, J.C. Moreira, Y. Gushikem, H. Vargas, D.W. Franco, Langmuir 9 (1993) 2982.

[11] J.C. Hicks, B.A. Mullis, C.W. Jones, Journal of American Chemical Society 129 (2007) 8426.

[12] J.F. Dıaz, K.J. Balkus, Journal of Chemical Materials 9 (1997) 61.

[13] P. Sutra, D. Brunel, Chemical Communications (1996) 2485.

[14] P. Hernan, C. del Pino, E. Ruiz-Hitzky, Chemical Materials 4 (1992) 49.

[15] A.M. Liu, K. Hidajat, S. Kawi, Journal of Molecular Catalysis A: Chemical 168 (2001) 303.

[16] H. Zhao, J. Peng, M. Cai, Catalysis Letters 142 (2012) 138.

[17] Y. I. Yermakov, B. N. Kuznetsov, V. A. Zakharov, "Catalysis by Supported Complexes", Elsevier, Amsterdam, 1981.

[18] H. C. Foley, S. J. DeCanio, K. D. Tau, K. J. Chao, J. H. Onuferko, Cecil Dybowski, B. C. Gates, Journal of the American Chemical Society 105 (1983) 3074.

[19] P. Dufour, C. Houtman, C.C. Santini, C. Ndez, J.M. Basset, L.Y. Hsuf, S.G. Shore, Journal of the American Chemical Society 114 (1992) 4248.

[20] M.D. Ward, J.J. Schwartz, Journal of Molecular Catalysis 11 (1981) 397.

[21] M.D. Ward, J.J. Schwartz, Journal of the American Chemical Society 103 (1981) 5253.

[22] S.L. Scott, M. Szpakowicz, A. Mills, C.C. Santini, Journal of the American Chemical Society 120 (1998) 1883.

[23] K. Khivantsev, A.D. Vityuk, O.S. Alexeev, M.D. Amiridis, Journal of Catalysis (2015) in press.

[24] A.D. Vityuk, O.S. Alexeev, M.D. Amiridis, Journal of Catalysis 311 (2013) 230.

[25] K. M. Minachev, Yu. S. Khodakov, B. M. Savchenko, V. K. Nesterov, Bulletin of the Academy of Sciences of the USSR 24 (1975) 1608.

[26] Z. V. Gryaznova, G. V. Tsitsishvili, N. N. Naskidashvili, Reaction Kinetics and Catalysis Letters 7 (1977) 59.

[27] J. A. van Bokhoven , A. M. J. van der Eerden , R. Prins, Journal of American Chemical Society 126 (2004) 4506.

[28] H. Van Bekkum, E. M. Flanigen, P. A. Jacobs, J. C. Jansen "Introduction to Zeolite Science and Practice, 2nd edition", Elsevier, Amsterdam, 2001.

[29] J. Lu, P. Serna, B.C. Gates, ACS Catalysis 1 (2011) 1549.

[30] D. Yardimci, P. Serna, B.C. Gates, ACS Catalysis 2 (2012) 2100.

[31] V.B. Kazansky, I.R. Subbotina, F.C. Jentoft, Journal of Catalysis 240 (2006) 60.

[32] J. Eheresmann, W. Wang, B. Herreros, D.-P. Luigi, T. N. Venkatraman, W. Song, J. B. Nicholas, J. F. Haw, Journal of American Chemical Society 124 (2002) 124 10868.

[33] R. A. van Santen, G. J. Kramer, Chemical Reviews 95 (1995) 637.

[34] I. Kiricsi, H. Forster, G. Tasi, J. B. Nagy, Chemical Reviews 99 (1999) 2085.

[35] P.Serna, B.C. Gates, Angewandte Chemie International Edition 123 (2011) 5642.

[36] L. R. Merte, G. Peng, W. Kudernatsch, S. Wendt, E. Lagsgaard, M. Mavrikakis, F. Besenbacher, Science 336 (2012) 889.

[37] A. Bakac, Dalton Transactions 13 (2006) 1589.

[38] R. Cramer, Journal of the American Chemical Society 87 (1965) 4717.

[39] C. Rosier, G.P. Niccolai, J.-M. Basset, Journal of the American Chemical Society 119 (1997) 12408.

[40] F. Bini, C. Rosier, R.P. Saint-Arroman, E. Neumann, C. Dablemont, A. de Mallmann, F. Lefebvre, G.P. Niccolai, J.-M. Basset, M. Crocker, J.K. Buijink, Organometallics 25 (2006) 3743.

[41] U. Romano, Gicrnale di Chimica Industriale 83 (2001) 30.

[42] S. Kowalak, R.C. Weiss, K.J. Balkus Jr, Journal of the Chemical Society Chemical Communications (1991) 57.

[43] D.E. De Vos, E.J.P. Feijen, R.A. Schoonheydt, P.A. Jacobs, Journal of the American Chemical Society 116 (1994) 4146.

[44] T. Joseph, D. Srinivas, C.S. Gopinath, A. Halligudi, Catalysis Letters 83 (2002) 209.

[45] K.K. Bania, R.C. Deka, Journal of Physical Chemistry C 117 (2013) 11663.

[46] J.F. Goellner, B.C. Gates, G.N. Vayssilov, N. Rosch, Journal of the American Chemical Society 122 (2000) 8056.

[47] J.T. Yates, T.M. Duncan, S.D. Worley, R.W. Vaughan, Journal of Chemical Physics 70 (1979) 1219.

[48] J.T. Yates, T.M. Duncan, R.W. Vaughan, Journal of Chemical Physics 71 (1979) 3908.

[49] R.R. Cavanagh, J.T. Yates, Journal of Chemical Physics 74 (1981) 4150.

[50] J. Evans, G.S. McNulty, Journal of Chemical Society Dalton Transactions (1984) 587.

[51] E.A. Wovchko, J.T. Yates Jr., Journal of the American Chemical Society 117 (1995) 12557.

[52] B.R. James, G. L. Rempel, Discussion of the Faraday Society 46 (1968) 48.

[53] S.H. Straws, D. Shriver, Inorganic Chemistry 17 (1978) 3069.

[54] S. Muthukumaru Pillai, M. Ravindranathan, S. Sivaram, Chemical Reviews 86 (1986) 353.

[55] J. N. Kondo, E. Yoda, M. Hara, F. Wakabayashi, K. Domen, Studies in Surface Science and Catalysis 130 (2000) 2933.

[56] S. Siegel, D. W. Ohrt, Journal of Chemical Society Chemical Communications 23 (1971) 1529.

[57] K. E. Janak, D. G. Churchill, G. Parkin, Chemical Communications 1 (2003) 22.

[58] M. Brookhart, J. M. DeSimone, B. E. Grant, M. J. Tanner, Macromolecules 28 (1995) 5378.

[59] Eric G. Derouane "Catalysts for Fine Chemical Synthesis Microporous and Mesoporous Solid Catalysts" John Wiley & Sons Ltd, 2006, 126.

[60] S. Namuangruk, P. Pantu, J. Limtrakul, A European Journal of Physical Chemistry and Chemical Physics 6 (2005) 1333.

[61] A. Forestière, H. Olivier-Bourbigou, L. Saussine, Oil & Gas Science and Technology Reviews 64 (2009) 649.

[62] A.W. Al-Sa'doun, Applied Catalysis A: General 105 (1993) 1.

[63] K. Ziegler, H. Martin, U.S. Patent 2,943,125 (1960).

[64] P. Serna, B. C. Gates, Journal of Catalys, 308 (2013) 201.

[65] A. Vityuk, H. A. Aleksandrov, G. N. Vayssilov, S. Ma, O. S. Alexeev, M. D. Amirdis, Journal of Physical Chemistry C 118 (2014) 26772.

[66] M. Kawai, M. Uda, M. Ichikawa, Journal of Physical Chemistry 89 (1985) 1654.

[67] M.A. Baltanas, J.H. Onuferko, S.T. McMillan, J.R. Katzers, Journal of Physical Chemestry 91 (1987) 3772.

[68] B.G. Frederick, G. Apai, T.N. Rhodins, Journal of the American Chemical Society 109 (1987) 4797.

[69] M.J. Remy, D. Stanica, G. Poncelet, E.J.P. Feijen, P.J. Grobet, J.A. Martens, P.A. Jacobs, Journal of Physical Chemistry 100 (1996) 12440.

[70] Q.L. Wang, G. Giannetto, M. Guisnet, Journal of Catalysis 130 (1991) 471.

[71] C.J.A. Mota, R.L. Martins, L. Nogueira, W.B. Kover, Journal of Chemical Society, Faraday Transactions 90 (1994) 2297.

[72] S. Li, S.-J. Huang, W. Shen, H. Zhang, H. Fang, A. Zheng, S.-B. Liu, F. Deng, Journal of Physical Chemistry C 112 (2008) 14486.

[73] V. Bolis, J.C. Vedrine, Journal of Chemical Society, Faraday Transactions 76 (1980) 1606.

[74] M. Kranenburg, Y.E.M. van der Burgt, P.C.J. Kamer, P.W.N.M. van Leeuwen, K. Goubitz, J. Fraanje, Organometallics 14 (1995) 3081.

[75] J. Klosin, C.R. Landis, Accounts of Chemical Research 40 (2007) 1251.

Chapter 3

[1] A.J. Liang, V.A. Bhirud, J.O. Ehresmann, P.W. Kletnieks, J.F. Haw, B.C. Gates, Journal of Physical Chemistry B 109 (2005) 24236.

[2] A. Uzun, V.A. Bhirud, P.W. Kletnieks, J.F. Haw, B. C. Gates, Journal of Physical Chemistry C 111 (2007) 15064.

[3] J. Lu, P. Serna, B.C. Gates, ACS Catalysis 1 (2011) 1549.

[4] M. Flytzani-Stefanopoulo, B. C. Gates, Annual Review of Chemical and Biomolecular Engineering 3 (2012) 545.

[5] J. R. Zoeller, V. H. Agreda, S. L. Cook, N. L . Lafferty, S. W. Polichnowski, D. M. Pond, Catalysis Today 13(1) (1992) 73.

[6] R. V. Kastrup, J. S. Merola, A. A. Oswald, Advances in Chemistry 196 (1982) 43.

[7] P. W. N. M. van Leeuwen, Homogeneous Catalysis: Understanding the Art Springer (2005)

[8] D. J. Cole-Hamilton, Science 299 (2003) 1702.

[9] D.E. De Vos, M. Dams, B.F. Sels, P.A. Jacobs, Chemical Reviews 102 (2002) 3615.

[10] D.C Bailey, S.H. Langer, Chemical Reviews 81 (1981) 109.

[11] J.C. Fierro-Gonzalez, S. Kuba, Y. Hao, B.C. Gates, Journal of Physical Chemistry B 110 (2006) 13326.

[12] M.D. Ward, J.J. Schwartz, Journal of the American Chemical Society 103 (1981) 5253.

[13] S.L. Scott, M. Szpakowicz, A. Mills, C.C. Santini, Journal of the American Chemical Society 120 (1998) 1883.

[14] R. Cramer, Journal of the American Chemical Society 87 (1965) 4717.

[15] K. Khivantsev, A.D. Vityuk, O.S. Alexeev, M.D. Amiridis, Journal of Catalysis (2015) in press.

[16] A.D. Vityuk, O.S. Alexeev, M.D. Amiridis, Journal of Catalysis 311 (2013) 230.

[17] G.A. Ozin, C. Gil, Chemical Reviews 89 (1989) 1749.

[18] Y. I. Yermakov, B. N. Kuznetsov, V. A. Zakharov, "Catalysis by Supported Complexes", Elsevier, Amsterdam, 1981.

[19] J. F. Hartwig, Organotransition metal chemistry - from bonding to catalysis. University Science Books, 2009.

[20] L. J. Farrugia, Proceedings of the NATO Advanced Research Workshop on The Synergy Between Dynamics and Reactivity at Clusters and Surfaces, NATO ASI Series, Drymen, Scotalnd, 2004.

[21] M. Shelef, Nitric Oxide: Surface Reactions and Removal from Auto Exhaust, Marcel Dekker, Inc, 1975.

[22] T. W. Hayton , P. Legzdins , W. B. Sharp, Chemical Reviews 102 (2002) 935.

[23] J. L.C. Thomas, C. W. Bauschlicher, Jr., M. B. Hall, Journal of Physical Chemistr: A 101 (1997) 8530.

[24] J. H. Enemark, R. D. Feltham, Coordination Chemistry Reviews 13 (1974) 339.

[25] J. P. Collman, N. W. Hoffman, D. E. Morris, Journal of the American Chemical Society 91 (1969) 5659.

[26] F. Zoua, J. M. Coleb, T. G. J. Jones, L. Jiang, Applied Organometallic Chemistry 26 (2012) 546.

[27] S. Ye , W. Zhou , M. Abe , T. Nishida , L. Cui ,K. Uosaki , M. Osawa, Y. Sasaki, Journal of American Chemical Society 126 (2004) 7434.

[28] A. Cotton, G. Wilkinson, C. A. Murillo “Advanced Inorganic Chemistry”, Wiley Interscience, 1999.

[29] B. L. Haymore , J. C. Huffman , N. E. Butler, Inorganic Chemistry 22 (1983) 168.

[30] M. P. Mingos, Inorganic Chemistry 12 (1973) 1209.

[31] E. Ivanova, M. Mihaylov, F. Thibault-Starzyk, M. Daturi, K. Hadjiivanov, Journal of Catalysis 236 (2005) 168.

[32] E. Ivanova, M. Mihaylov, H. A. Aleksandrov, M. Daturi, F. Thibault-Starzyk, G. V. Vayssilov, N. Rösch, K. Hadjiivanov, Journal of Physical Chemistry C 111 (2007) 10412.

[33] A. Vityuk, H. A. Aleksandrov, G. N. Vayssilov, S. Ma, O. S. Alexeev, M. D. Amirdis, Journal of Physical Chemistry C 118 (2014) 26772.

[34] B. Enderle, B.C. Gates, Journal of Molecular Catalysis A 204–205 (2003) 473.

[35] P.S. Braterman "Reactions of Coordinated Ligands, Volume 2", Plenum Press, New York, 1989.